12-2019

Evolution of the Book Cliffs Dryland Escarpment in Central Utah - Establishing Rates and Testing Models of Escarpment Retreat

Nicholas R. McCarroll
Utah State University

EVOLUTION OF THE BOOK CLIFFS DRYLAND ESCARPMENT IN CENTRAL UTAH – ESTABLISHING RATES AND TESTING MODELS OF ESCARPMENT RETREAT

by

Nicholas R. McCarroll

A thesis submitted in partial fulfillment
of the requirements for the degree

of

MASTER OF SCIENCE

in

Geology

Approved:

_____	_____
Joel Pederson, Ph.D. Major Professor	Tammy Rittenour, Ph.D. Committee Member
_____	_____
Patrick Belmont, Ph.D. Committee Member	Richard S. Inouye, Ph.D. Vice Provost for Graduate Studies

UTAH STATE UNIVERSITY
Logan, Utah

2019

ABSTRACT

Evolution of the Book Cliffs Dryland Escarpment in Central Utah - Establishing Rates and Testing Models of Escarpment Retreat

by

Nicholas Reilly McCarroll, Master of Science

Utah State University, 2019

Major Professor: Dr. Joel L. Pederson
Department: Geology

Since the earliest explorations, geologists have invoked escarpment retreat as a substantial part of landscape evolution of the Colorado Plateau. However, despite the advent of multiple geochronometers and the many studies establishing rates of vertical incision for the rivers that drain the Colorado Plateau, only a couple studies have quantified escarpment retreat, and indeed for cliff retreat the world over. Likewise, the mechanisms driving escarpment retreat have been debated since the 1940's. Initial investigations focused on autogenic variations in erosion processes as the primary control of retreat, whereas subsequent studies focused on the role of climate as a forcing mechanism of escarpment evolution.

This thesis consists of two related studies conducted along the Book Cliffs of central Utah. The first study is of remnant talus flatirons and piedmont terrace deposits along the Book Cliffs between the Horse Canyon alluvial fan and Price River. This study

uses mapping and optically stimulated luminescence to build a chronostratigraphy of four generations of deposits. Results indicate deposition occurred at major climatic transitions or times of climatic instabilities along with pulses of transient incision propagating up cliff drainages which we propose is related to the base level fall of the Price River. These findings do not match an autogenic model of retreat nor the classic assumption that erosion and deposition occur at the height of glacial epochs. Therefore, we suggest escarpment evolution is governed largely by top-down climate-forcing of sediment production, or at least preservation, from the cliff face rather than in response to glacial maximum conditions or local erosional processes on the toeslope.

The second study uses computational terrain analysis to constrain rates of escarpment retreat, the geometric relationships between vertical incision and lateral retreat, and patterns of piedmont drainage steepness. Through a novel profile-area-integration approach combined with the geochronology of Chapter 2, rates of cliff retreat and toe-slope incision where calculated to 1 -3 m/ky and ~0.5 m/ky respectively. To our knowledge these are the best-constrained rates of dryland escarpment retreat in the world. They indicate that escarpment retreat outpaces vertical toe slope incision up to a 20:1 ratio. These results confirm early conceptual estimates of lateral retreat and for the first time empirically show that cliffs move laterally faster than vertical incision. Furthermore, channel steepness analysis reveals the presence of knickpoints propagating up Book Cliff drainages and a decrease in channel steepness of piedmont trunk drainages from north to south across the study area. These observations further confirm the presence of a wave transient incision propagating up from the Price River as well as suggesting that for escarpment drainages, steepness is controlled by the amount and caliber of sediment.

(152) pages

PUBLIC ABSTRACT

Evolution of the Book Cliffs Dryland Escarpment in Central Utah - Establishing Rates and Testing Models of Escarpment Retreat

Nicholas Reilly McCarroll

Since the earliest explorations of the Colorado Plateau, geologists have suspected that cliffs are retreating back laterally. Clarence Dutton envisioned “the beds thus dissolving edge wise until after the lapse of millions of centuries their terminal cliffs stand a hundred miles or more back from their original position” when he wrote about the landscape in 1882. While many geologic studies have determined how fast rivers cut down through the Plateau, only a few studies have calculated how quickly cliffs retreat laterally, and geologists have been arguing since the 1940’s what exactly drives cliffs to retreat in the first place. We study the Book Cliffs in central Utah, and in particular remnant landforms and deposits related to a 120,000-year history of erosion and deposition, which we date by optically stimulated luminescence methods. Our dataset shows that deposits along the Book Cliffs are preserved especially during times of climate instability, which suggests that escarpment retreat locally is driven by climatic disturbances. This disproves older hypotheses suggesting escarpments retreat in response to local factors regardless of shifts in climate, and it is consistent with the few other well-studied escarpment records globally. We also constrain the rates of cliff retreat via a new measurement approach and luminescence age control, showing that the Book Cliffs have retreated at 1-3 meters per thousand years while local toeslope drainages have incised at about 0.5 meters per thousand years, which confirms that cliffs of shallow-dipping, layered rock retreat laterally faster than streams lower the landscape vertically.

ACKNOWLEDGEMENTS

I would like to acknowledge the people and organizations who helped to make this investigation into cliff retreat possible. First, I would like to thank the Society for Sedimentary Geology, the Colorado Scientific Society, the Geologic Society of America, and the Utah State Geology Department for helping fund my work through various research grants. Without funding from these sources, I wouldn't have been able to figure out how quickly the Book Cliffs are retreating or why they are in the first place. Thanks to all of my fellow grad-students for helping me out with the odd tasks related to a master's thesis. Special thanks to Ellen Imler and Hollie Richards for keeping me sane when something logistical fell apart during my time at USU. Much appreciation needs to be given to the USU luminescence laboratory staff, Carlie Ideker and Michelle Nelson, without them I couldn't have gotten all my samples finished in the timely manner that I did, nor have listened to some real awesome podcasts. I also would like to thank my committee members Tammy Rittenour and Patrick Belmont for helping me through the processes of planning and writing a masters proposal and thesis.

I want to thanks my parents Todd and Judy McCarroll for their constant support during my time at USU. Without their guidance and love, a little boy from Lehman, PA wouldn't have even found his way out to Utah to finally become the "scientist" he always wanted to become. Thanks to my brothers Andrew and Will who always keep me on my toes and are always ready to help me out. I would also like to thank my longtime girlfriend Mary Evans for her support grammatically and otherwise, as well as her constant love. Finally, and most importantly I want to thank the man with the most awesome mustache who got me out to Utah in the first place, my advisor Joel Pederson. I

want to thank Joel for being such an awesome mentor whose Book Cliff project is one of the coolest things I have ever been able to work on. Joel your passion for geomorphology and awesome geology is infectious and I couldn't ask for a better role model who just so happens to be always up for a pickup game of Chinese Checkers. Thanks for always having your door open to one of my many questions no matter how small, as well as guiding me through the rapids of a crafting a thesis as well as applying for PhD programs on the side. As I move on to Kansas State to work on a PhD I will always look back at my time at USU fondly and the people I met as part of my extended family. I will especially miss Fritter Friday along with all the other awesome events I was able to be a part of. Thanks again everyone who helped me make this project what it is and I hope one day my path will lead me back to G.K. Gilbert's old stomping ground.

-Nicholas Reilly McCarroll

CONTENTS

Page

LIST OF TABLES

LIST OF EQUATIONS

LIST OF FIGURES

CHAPTER 1

INTRODUCTION

Lateral retreat of escarpments has been invoked as a primary mode of erosion in dryland landscapes. Rates and drivers of lateral cliff retreat are poorly understood and have only been quantified in a few choice locations globally. Along the Book Cliffs of central Utah, a sequence of toeslope colluvial deposits that produce talus flatirons provide a record of cliff retreat. Such flatirons have been used in other dryland settings to constrain escarpment evolution and retreat rates. Numerical dating by optically stimulated luminescence (OSL) methods and computational terrain analysis allow us to address questions about the rates, timing, patterns, and controls of escarpment evolution along the Book Cliffs.

This Thesis consists of two related studies along a 20 km-long reach of the Book Cliffs between Price and Green River, Utah. The northern boundary of the study reach is the Horse Canyon alluvial fan and the southern end is marked by the Price River. Chapter 2 develops a chronostratigraphy of colluvial and piedmont deposits along the Book Cliffs through OSL dating and field observations to test two endmember models of escarpment retreat. Results indicate there are four generations of talus flatirons and piedmont alluvial terrace deposits preserved along the Book Cliffs escarpment, dating to 123 – 117 ka, 95 – 75 ka, 62-48 ka, and 13 - 1 ka, which correspond to periods of high climate variability or the transitions from glacial-to-interglacial conditions. The correlation of depositional ages to these specific climate events supports the idea that sediment production along the cliff

is a top-down climate-controlled processes. However, escarpment evolution is in response to climatic disturbances and not exclusively during glacial maxima as previous research suggested. Systematic differences in deposition age in relation to upstream distance reveals the presence of transient incision that we propose is due to periodic aggradation and incision of the Price River.

Chapter 3 presents a computational terrain analysis of topographic profiles and drainages along the Book Cliff study area. Forty-six talus-flatiron landforms are projected and compared to neighboring gully profiles to discriminate lateral and vertical distances of erosion through a novel profile-area-integration approach and to calculate rates of retreat based on the chronology presented in Chapter 2. Our measurements are in line with early, unconstrained, observation based, estimates of retreat rates in the Colorado Plateau as well as rates from similar studies in the drylands of Spain. Results also confirm the geometric prediction that lateral cliff retreat proceeds several times faster than vertical incision of toeslopes. Finally, patterns of drainage steepness reveal transient incision working its way up cliff drainages that further confirms transience controlled by periodic aggradation and incision of the Price River.

CHAPTER 2

QUATERNARY CHRONOSTRATIGRAPHY OF PIEDMONT AND COLLUVIAL DEPOSITS ALONG THE BOOK CLIFFS, UTAH

ABSTRACT

The mechanisms driving escarpment retreat have been debated since the 1940's. Initial investigations focused on autogenic variations in erosion processes, whereas subsequent studies focused on the role of climate as a forcing mechanism of escarpment evolution. These two schools of thought provide conceptual models of escarpment retreat, which can be tested along a section of the Book Cliffs in central Utah. Colluvial deposits and piedmont terraces were mapped and targeted for optically stimulated luminescence (OSL) dating to test these conceptual models.

Mapping indicates four generations of talus flatirons and piedmont alluvial terrace deposits preserved along the Book Cliffs escarpment. OSL age control indicate four age clusters 123 - 117 ka, 90 -75 ka, 62 - 48 ka, and 13 - 1 ka, that correspond to transitional climate conditions during the last 100 ky glacial cycle. The ages cluster in relation to glacial-interglacial transitions and periods of climatic instability, which supports the concept of climate-driven sediment production along the cliff in response climatic disturbances, though not coinciding with glacial maxima as previous researchers assumed (Bull and Schick, 1979; Gerson and Grossman, 1987; Schmidt: 1996). Analysis of our chronology also reveals a decrease in deposit age with increasing distance from the Price River. This pattern suggests the presence of transient incision related to the baselevel fall of Price River, which we propose is related to periodic aggradation and incision of the river.

This record at the Book Cliffs does not correlate to those of the Ebro Basin, Spain and The Negev Desert, Israel, but they all share the feature of preserved deposits corresponding in age to times of climate instability. Thus, we suggest escarpment evolution is governed largely by top-down climate-forcing of sediment production, or at least preservation, from the cliff face rather than in response to glacial maximum conditions or local erosional processes on the toeslope.

INTRODUCTION

Drylands cover approximately a third of the world's land surface and are home to roughly 30 percent of the world's population (Reynolds et al. 2007). Drylands are especially sensitive to shifts in climate and can take millennia to regain geomorphic equilibrium after such shifts (Bull, 1991). Therefore, understanding their evolution under a changing climate is a critical research need. In semiarid and arid landscapes, classical geologists, such as Clarence Dutton, have long suggested that the lateral retreat of cliffs is one of the primary mechanisms of erosion (Bryan, 1940; King, 1953). While escarpment retreat has been recognized as an important component of landscape evolution, the forcing mechanisms and the role climate changes play are still debated. Key to understanding dryland evolution are new geochronology techniques, especially as applied to remnant sediment records at toeslopes, also known as talus flatirons. Cliff retreat and the linked creation of talus flatirons in dryland environments has been a topic of inquiry within the geomorphic community since the 1940's. However, chronologies of escarpment retreat are sparse across the world, especially in the southwestern United States.

Initial investigations focused on autogenic variations in erosional processes independent of climate variations as playing a dominant role in cliff retreat (Bryan 1940; Koons 1955). In this conceptual model, baselevel fall drives cliff evolution via gully erosion undermining the cliff face and resulting in failure, retreat, and deposition of new toeslope material (Bryan 1940; Carter, 1981; Mills, 1981; Ward et al., 2011). Subsequent studies changed their focus to understanding the role of climate as a forcing mechanism of escarpment sediment production and transport (e.g. Bull and Schick 1979; Gerson and Grossman, 1987; Schmidt 1996). Important in this model is how fluctuations in climate disturbed vegetation patterns as well as controlled rates of weathering through wet-dry and freeze-thaw cycles, resulting in greater sediment production (Schumm and Chorley,1966; Schmidt, 1996). Given such an increase in sediment transport from the cliff face, deposition of new toeslope material and cliff retreat would be expected to occur in response to climate cooling or disturbances. Indeed, climate changes over the Pleistocene and Holocene have been invoked as the primary forcing mechanism of sediment production, storage, and transport along escarpments (Schmidt, 1996; Clapp et al. 2000; Enzel et al., 2012, Sheehan and Ward, 2018). Yet, climate histories are not synchronous or of the same magnitude globally, thus global geomorphic records may still correlate poorly with each other

This contrast in prior conceptual models, between top-down climate influences versus bottom-up baselevel drivers, reviewed fully below, will be tested in this investigation along the Book Cliffs of central Utah. We address this through the study of remnant colluvium and piedmont alluvial terraces with optically-stimulated luminescence (OSL) geochronology. Our Book Cliffs study area is marked by the presence of four generations

of talus flatirons, providing opportunities to understand a ~120 ky history of escarpment evolution

BACKGROUND

The Book Cliff escarpment features landforms and associated deposits along its toeslope liked to lateral cliff retreat. These talus remnants, or talus flatirons, connect cliffs and piedmont landscape components. A talus flatiron is a bedrock slope armored with colluvial material that has been separated from the cliff face by a combination of gullying and subsequent lateral retreat of the escarpment (King, 1953; Koons, 1955). These geomorphic features are commonly observed in arid to semi-arid settings as the southwestern United States, Israel, Africa, Brazil and Spain (Schumm and Chorley, 1966; Pinheiro and Neto, 2017). The lack of talus along certain cliffs in the Colorado Plateau has been attributed to the rapid mechanical weathering of especially sandstone talus by freeze-thaw processes (Schumm and Chorley, 1966). However, talus and talus remnants are preserved along some cliffs. It is in these setting that a record of sediment production and cliff retreat are preserved and can be used to test hypotheses related to the driving mechanisms of cliff retreat (Bryan, 1940; Koons, 1955; Schmidt, 1996).

Previous research on dryland escarpment evolution

Previous studies in Israel and Spain, as well as more local work in the Colorado Plateau, have focused on dryland landscape evolution related to hillslope processes. The following review organizes previous ideas into models of escarpment evolution that can be distilled and tested for this study.

Hyper-arid Negev, Israel

In the Nahal Yael Basin, early workers focused on the hypothesis that sediment production is greater in arid landscapes during wet climate phases (Bull and Schick, 1979; Gerson and Grossman 1987). From field observations, Bull and Schick (1979) and Gerson and Grossman (1987) suggested that during wetter climates, more colluvium is generated due to increased physical weathering of source rock through wetting and drying cycles. Increased cohesion via vegetation keeps colluvium stored on slopes. Once the climate shifts to arid conditions, sediment generation stops and vegetation density decreases. Subsequent gully and debris-flow dissection along the toeslope propagates up to the cliff face, leading to the final separation and the creation of a talus flatiron (Gerson and Grossman, 1987).

Clapp et al. (2000) revisited the Nahal Yael with the aid of cosmogonic radio-nuclide (CNR) dating methods to determine hillslope sedimentation rates, identify significant sediment sources, and test if the landscape is in steady state. They found that modern sediment yield is 53-86% greater than the long-term rate of bedrock erosion estimated from ^{10}Be and ^{26}Al. Clapp et al. (2000) proposed that the mining of older stores of sediment makes up the difference in the sediment budget. To better understand the origin of stored sediment they estimated a depositional age of terraces. They assumed terraces in the area were deposited rapidly and integrate nuclide production over the depth of the terrace (2m), and estimated deposition of alluvial terraces occurred ca. 11 ka. They proposed this age estimation is consistent with the late Pleistocene-Holocene stripping of stored hillslope deposits in response to climate change as proposed by Bull and Schick (1979).

Enzel et al. (2012) returned to the Nahal Yael catchment utilizing new climate proxy data and new interpretations of soil profiles that indicate Negev has stayed hyper-arid since at least 50 ka, calling into question Bull and Schick's climate-forcing hypothesis. Their newer OSL and CRN ages indicated valley aggradation occurred, 35 to 20 ka, largely during the last glacial maximum (Enzel et al., 2012). They propose that sediment generation at the time was cause by increased wet-dry cycle physical weathering, via frequent high intensity storms. Once the period of increased extreme storm frequency and increased sediment production ended, hillslope sediment was transported into drainages via gully erosion and debris flows by less frequent precipitation events leading to valley filling. Once the sediment supply was exhausted, streams incised back down though valley deposits to bedrock.

Like these studies in the Nahal Yael Basin, Gerson and Grossman (1987) explored how talus slopes act as indicators of environmental changes in Makhtesh Ramon, farther north in the central Negev Desert. Through field observations of geomorphic relationships between colluvium and piedmont deposits. They proposed a model that talus deposits were formed during semi-arid glacial periods due to increased frost cracking and wet-dry cycles. Subsequent arid and hyper-arid interglacial periods were dominated by dissection and stripping of talus deposits via gullying in their conceptual model.

Boroda et al. (2011) revisited the Makhtesh Ramon with OSL and CRN dating techniques and soil profile analysis to test the Gerson and Grossman model. OSL ages of dust matrix within talus flatirons cluster between 114 – 70 ka and 75-43 ka and are used as minimum age constraints. Cosmogenic exposure ages from flatirons apexes were

calculated to be approximately 610 ka and 170 ka respectively. Boroda et al.'s (2013) modeling suggests that the younger generation of talus flatirons were abandoned and surface stabilization occurred 170 ka and the older flatirons saw abandonment and surface stabilization 497 ka. These ages indicate that the talus sequences do not follow the temporal scale of orbital-climate cycles or glacial-interglacial cycles. Soil-profile analyses indicate the taluses were deposited under continuous hyper-arid conditions. High variability in cosmogenic inheritance values were interpreted as reflecting the stochastic nature of sediment production and transport in Makhtesh Ramon (Boroda et al., 2013). In contrast to older work, but like Enzel et al. (2012), they conclude that the deposition of talus and sediment transport in the hyper-arid Negev relates to random, high-intensity storms rather than landscape responses to glacial or interglacial climate modes or changes.

Spain

Significant chronostratigraphic work has been conducted in watersheds in middle and northern Spain investigating geomorphic controls on escarpment retreat and sediment production. Gutierrez et al. (1998) dated a set of flatirons in Ebro Basin south of Zaragoza, northeast Spain, using archeologic affiliation and radiocarbon dating. Depositional ages of three generations of talus flatirons are 35.5 ka BP, 27.9 ka BP, and 2.5-2.9 ka BP They proposed that minor but rapid perturbations in climate, such as Dansgaard–Oeschger events, and that not just glacial epochs can trigger the formation of talus in semiarid landscape through increased freeze-thaw and wet-dry cycles, which trigger rock fall and debris flow events. In order to explain why every climate fluctuation is not represented by a corresponding flatiron sequences Gutierrez et al. (1998) proposed

that specific environmental and climatic conditions are needed preserve flatirons, if transport or talus weathering is too great flatiron sequences are not preserved.

Gutiérrez et al. (2010) produced improved OSL and radiocarbon age control on four sets of talus flatirons mapped across three Tertiary basins of Spain (Ebro, Tajo, and Duero basins). The geochronology reveals four age clusters: 55.2-47.4 ka, 42.2-36.4 ka, 33.2-23.8 ka, and 2.6-2.4 ka, which correlate to documented wet periods associated with Heinrich Events. Thus, they interpret that aggradation of slopes occurred when water availability was higher (Gutiérrez et al., 2010). They suggest that increased vegetation inhibited incision. Subsequently dryer conditions lead to vegetation loss, the loss of cohesion, and gullying removed sediment forming flatirons.

Roque et al. (2013) used flatirons in the most northern portion of the basin at the base of the Spanish Pyrenees as a record of the influence of both climate variation and human settlement. Two sets of flatirons and piedmont terraces were described and dated using a combination of OSL, radiocarbon, and archeological artifacts (Roque et al., 2013). Ages for the older set of flatirons correspond with the LGM (25 – 19 ka), and only partly overlap with one of the age clusters of Gutiérrez et al. (2010) despite similar geographic region. The younger inset deposits were again found to be ~2 ka and were interpreted to correspond to when the Romans removed stabilizing vegetation locally to create more arable land. This removal of vegetation triggered incision of pre-existing colluvial slopes. The chronostratigraphic results from Spanish flatirons suggest a more complicated relationship between climate and cliff evolution and not a simple glacial versus interglacial signal.

Southwestern United States

The earliest investigations into escarpment retreat took place in the southwestern United States. Initial hypotheses hinged upon the concept that large rocky talus can armor the toe slope below an escarpment (Bryan, 1940; Koons, 1955). Bryan (1940), later refined by Mills (1981), suggested a simple conceptual model, "Gully Gravure" where weathering resistant-armor causes differential erosion locally and eventually leads to a topographic inversion. The colluvial mantle eventually becomes elevated topography while the bare slopes incise, creating flatiron remnants (Bryan 1940; Mills 1981). Likewise, Koons (1955) proposed that once talus below an escarpment is removed, erosion through rilling and sheet wash erode the bare rock slope undercutting the cliff face. This leads to random threshold failure of the cliff face and deposition of new talus first occupying what was the deepest-gullied areas of the toeslope irrespective of climate. Both Bryan (1940) and Koons (1955) together describe escarpment evolution governed by internal thresholds, localized erosion on the toeslopes leading to random failure of the cliff face independent of climate conditions.

The earliest geomorphic work around the Book Cliffs study area was conducted by Carter (1981), investigating pediment formation and assuming baselevel as the control. Carter (1981) identified five sets of pediments capped by debris flow deposits. Based on field observations of the distribution and morphology of pediments, Carter (1981) concluded that one regional baselevel fall propagating up from the Price River opposed to his alternative hypothesis of local stream piracy, explained the distribution of the pediments across the landscape.

Working in the southwest, Schmidt (1996) proposed that climate, not local processes, is the primary driver of escarpment evolution. Schmidt examined several escarpments, including those in Grand Canyon and the Henry Mountains. However, he focused on the Book Cliffs most intensely due to the widespread presence of flatirons. He proposed a conceptual model that was extremely similar to those proposed by the earlier work of Bull and Schick (1979) and Gerson and Grossman (1987). In Schmidt's model, when climate is wetter, increased talus deposition and preservation occurs due to increase physical weathering of the cliff face as well as increased sediment storage due to vegetation cover. Once the climate shifts to dryer conditions and vegetation density and sediment production decrease, gully dissection of toeslope talus occurs more readily, leading eventually to abandonment and separation from the escarpment.

More recent work by Ward et al. (2011) with the Book Cliffs in mind applies rules-based modeling, using the CHILD model of Tucker et al. (2001). Ward et al. recognize the influence that shifts in climate can have, modeling was conducted using constant climatic conditions for simplicity. Ward et al. focuses on toeslope gullying as the key modulator of escarpment evolution, like Bryan (1940) and Koons (1955) in the absence of changes in climate. Their modeling of talus production and removal is governed by two factors. The first factor is that the system is internally limited by bare-rock toeslope erosion by random gullying from baselevel fall. A slowly eroding bedrock plinth can cause an escarpment to become eventually buried by its own debris (Ward et al. 2011). The second factor is the rate at which armoring talus is removed on toeslopes via in-situ weathering, with slowly weathering talus armor limiting gullying.

In the Coal Cliffs of central Utah only 50 km southwest of our study area, Sheehan and Ward (2018) utilize ^{36}Cl surface-exposure dating on sandstone boulders to test hypotheses related to cliff retreat. Thirty-three boulder ages were produced, which range between 46-4 ka, with most clustering around 30-20 ka. This clustering of ages leads them to accept that increased deposition of talus was in response to the wetter/cooler conditions of the Last Glacial Maxima and talus dissection began as the transition into interglacial conditions began. However, two main issues arise when considering their chronology. First, ages that are reported are exposure not depositional ages and second, in situ weathering of boulders is an issue within the results that they do not take it into account, which will cause overestimate

Although Grand Canyon is 350 km to the south of the Book Cliffs, the chronostratigraphic record of hillslope deposits is well documented. Anders et al. (2005) explored records of hillslope sediment production and transport in eastern Grand Canyon tributary basins, presenting a chronology with OSL, U-series, and CRN ages on piedmont hillslope deposits that grade into or overlie Colorado River terrace deposits. Five piedmont deposits were mapped, however only four were targeted for age control and produced age clusters of 109-92ka, 50-30 ka, 12-7 ka, and 5-4 ka indicating periods of deposition. Additional work in the eastern Grand Canyon by DeJong (2007) examined some of the same drainage basins in more detail and with additional OSL geochronology, refining five periods of escarpment toeslope and upper tributary aggradation to: 100-90 ka (S4), 77-55 ka (S3o), 50-35 ka (S3y), 26-22 ka (S2o) and 14-7 ka (S2y). He suggests aggradation of deposits primarily occurs both during cooler glacial periods as well as

during times of climatic instability during interglacial periods. Whereas sediment reworking primarily occurring during dry or climatically stable interglacial periods.

RESEARCH DESIGN AND STUDY AREA

End-member conceptual models

The previous review of global research can be synthesized into end-member conceptual models useful in a research design for understanding the mechanisms controlling escarpment evolution. The work of Bryan (1940), Koons, (1955), Mills (1981), and Ward et al. (2010) assume cliff retreat is driven by local erosional processes at the toe of the escarpment. Variably armored or unarmored toeslopes are attacked by gullying driven by baselevel erosion propagating up drainages (Step 1 of Figure 2.1. A). Once incision undercuts the cliffs, mass-wasting failures are triggered and the cliff retreats, armoring slopes and gully bottoms with new material (Step 2). The neighboring less-armored slopes erode away and eventually, topographic inversion occurs where former gullies collecting talus become flatiron hilltops (Step 3).

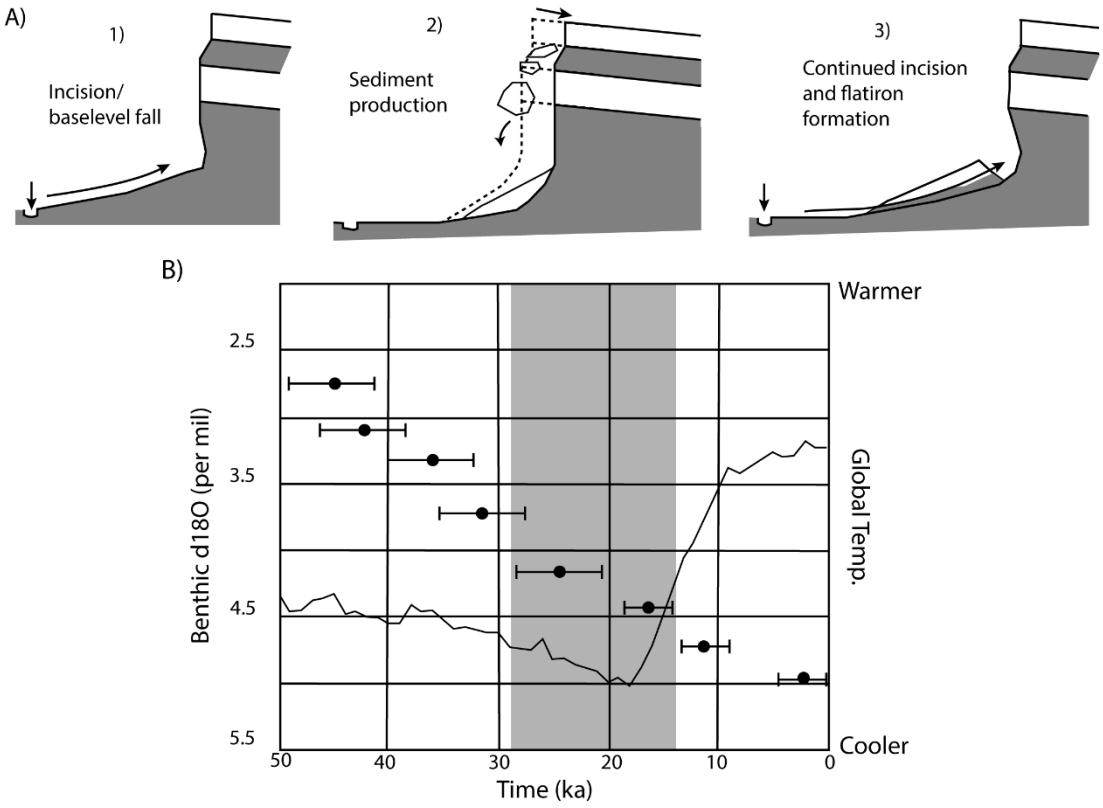

Figure 2.1. A) Conceptual model of autogenic cliff retreat in three steps: 1) Baselevel fall drives erosion and causes undercutting; 2) Threshold cliff failure and deposition of new talus on shale plinth; 3) Gullying result in abandonment and topographic inversion of armored talus slope in response to following baselevel fall. B) Predicted age distribution of piedmont and colluvial deposits plotted with global oxygen isotope climate record, black line (Lisiecki and Raymo, 2005) Ages do not cluster in relation to climate due to deposition being governed by internal stochastic variations.

This autogenic conceptual model predicts a spread of ages that do not exhibit clustering behavior over time (Figure. 2.1B). Ages from colluvium would instead reflect the stochastic nature of rock falls. On the other hand, if the retreat is governed by a master baselevel fall event, then piedmont alluvial and talus ages would vary in relation to when that signal propagated bottom-up to the cliff face and triggered retreat and cliff-slope mechanical failure. This would express itself as an age gradient with older alluvial-

terrace deposits closer to local baselevel and younger piedmont and colluvial ages upslope due to head ward migrating erosion.

The second endmember conceptual model proposes that escarpment retreat is a top-down progression of processes driven by changes in climate (Bull and Schick, 1979; Gerson and Grossman, 1987; Schmidt: 1996; Boroda et al., 2011; Enzel et al., 2012). The climate-controlled processes include weathering and sediment production, transport and deposition of talus, and vegetation affecting rooting, cohesion, infiltration, and runoff. The rates of physical weathering of sandstone are highly influenced by moisture as well as temperature, as these factors control freeze-thaw action and wetting-drying cycles (Schumm and Chorley, 1966). Increases in physical weathering lead to fracturing and mass failure during glacial maxima (Figure 2.2.A Step 1). Following deposition, a transition from wetter to drier climate decreases vegetation density as well as sediment production. This triggers fluxes of toeslope sediment that prograde onto the piedmont (Figure 2.2.A Step 2). Gullying and incision of talus out-stripping cliff sediment production eventually leads to flatiron formation (Figure 2.2.A Step 3).

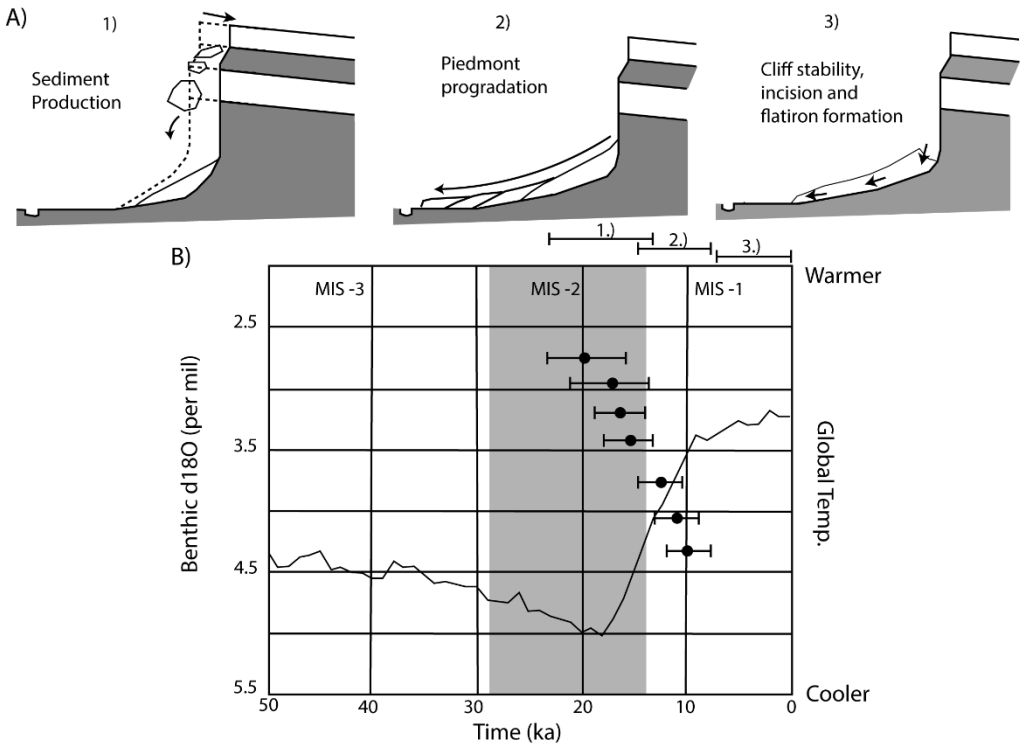

Figure 2.2. A) Conceptual model of climate driven cliff retreat in three steeps: 1) High weathering period, lateral retreat, and deposition of talus; 2) Transport of material onto piedmont by alluvial processes as well as debris flows; 3) Disturbance and high sediment transport rates cause gullying and the creation of flatirons. B) Predicted age distribution of piedmont and colluvial deposits plotted with oxygen isotope climate record, black line (Lisiecki and Raymo, 2005). Ages express clustering in relation to climate to deposition being governed by top-down climate control processes.

In this classic "Bull-model" there is a top-down chain of processes; weathering and sediment production from the cliffs, stabilization of sediment via vegetation, progradation onto piedmont and subsequent removal by gullying and incision when sediment production is low and stabilizing vegetation is lost. The expected patterns of talus flatiron ages would correlate to and cluster around glacial maxima and the transition from glacial to interglacial climate phases (Figure 2.2.B). However, in the case of Boroda et al. (2011) and Enzel et al. (2013) ages would correspond to periods of increased

frequency of large storms in the hyper arid Negev. Furthermore, talus deposits would be systematically older than downslope piedmont material reworked during and after climate transitions, inasmuch as mass-wasting events outpace more incremental sediment reworking across the piedmont. This model also predicts that there would be a distinct physical distribution of flatirons across the landscape, with correlatable generations of flatirons aligned parallel to the modern cliff face.

Study area setting

The Book Cliffs extend ~400 km from central Utah to Grand Junction, Colorado where the escarpment terminates (Figure 2.3.). The cliffs range from 300 m high in the south and 600 m in height at the north end of study area. The slope form is mainly controlled by lithology, which is the same across the study transect. The base of the Book Cliffs is composed of the easily erodible Cretaceous Mancos Shale. This unit forms the primary plinth of the escarpment. This shale is overlain by the Mesa Verde Group, which is composed in ascending order of the Star Point Sandstone and Black Hawk Fm. and the Castlegate Sandstone member of the Price River Formation, which holds up the top of the cliff (Figure 2.4.) (Richardson, 1909; Fisher et al., 1960) The escarpment is situated between the Laramide structural dome of the San Rafael Swell to the southwest and the Uinta Basin to the northeast (Richardson, 1909; Fisher et al., 1960). The down-dip limb of the structural dome crosses the Book Cliffs and the beds of the cliffs gently dip to the northeast toward the Uinta Basin.

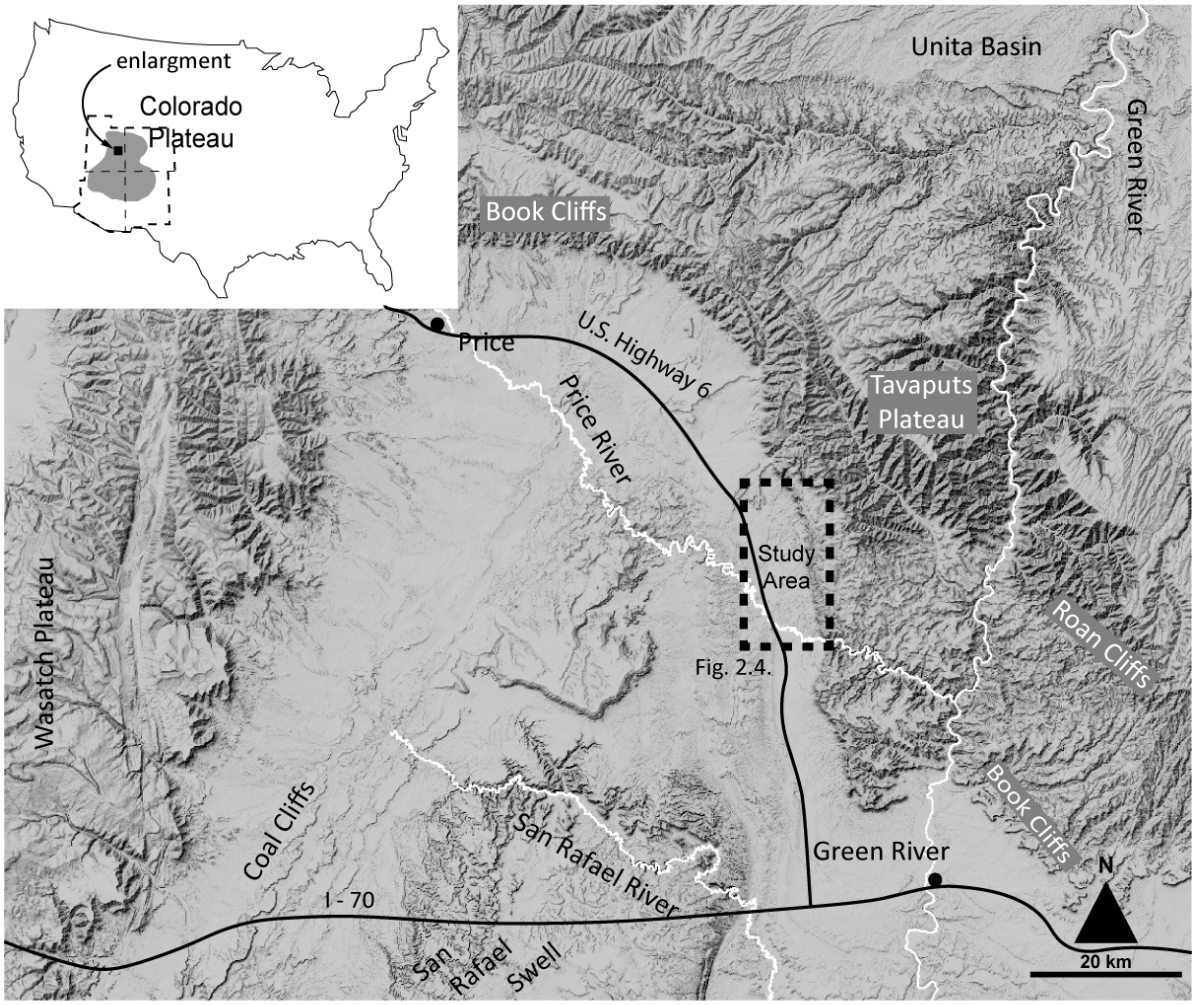

Figure 2.3. Regional map of Utah section of Book Cliffs. Major regional rivers are denoted with a white line, the study section of the Book Cliffs is denoted Figure 2.6.

Figure 2.4. C2 flatiron and C1 apron. Visible basal strath of colluvial deposits on Mancos Shale (K_{ms}) denoted by white lines. The lower sandstone unit of the cliffs is the Black Hawk Formation (K_{bh}). Inset image is to illustrate target OSL sample facies, but image is not from this particular flatiron.

The 20-km long study transect of the Book Cliffs is southeast of Price, Utah (Figure 2.3). This section of the escarpment has a uniform aspect and lithology. The northern boundary is marked by an alluvial fan that extends out of Horse Canyon. The southern end of the study area is where the path of the Price River cuts through the Book Cliffs on its way east to the meet the Green River. Although set in a canyon, the modern Price River channel flows through its own alluvium. Elevation of the study area and the

cliff distance from baselevel decrease along the study transect from north to south. These gradients can be leveraged to test in more detail the conceptual models of escarpment retreat.

Geologic mapping

Geologic mapping was conducted by Joel Pederson in two focus areas of the toeslope and proximal piedmont (Figure 2.3). Generations of colluvial – alluvial flatiron and terrace deposits were distinguished and correlated based upon landscape position. Field mapping was conducted using the National Agriculture Imagery Program 2016 aerial photographs of 1 m pixel resolution. Field mapping iterated with digital mapping on-screen with the aid of Google Earth. Final products are at 1:12k scale and presented in the result section of this chapter.

Luminescence geochronology

Twelve sediment samples were collected for luminescence dating and combined with nine prior OSL results in the study region. All three main units of talus and piedmont sediments have at least four samples, two colluvial and two piedmont, samples collected at different positions across the study area where naturally exposed and accessible, with a total of 14 samples (Figure 2.5). An OSL age represents that last time a grain was exposed to light at the surface before it was deposited and buried by subsequent depositional episode or rockfall. Sampling targets were sand lenses in colluvial diamicton and alluvial deposits, sediment was horizontally extracted in steel pipes and representative samples of the surrounding material was collected for dose rate and water content. We preferentially sampled sand lenses with primary sedimentary

structures and no evidence of bioturbation or other post depositional disturbances– qualities indicative of transport allowing sediment exposure to light without significant post-depositional mixing (Nelson et al. 2015). Ages are complete with at least 15 accepted aliquots and are reported to 1-sigma standard error.

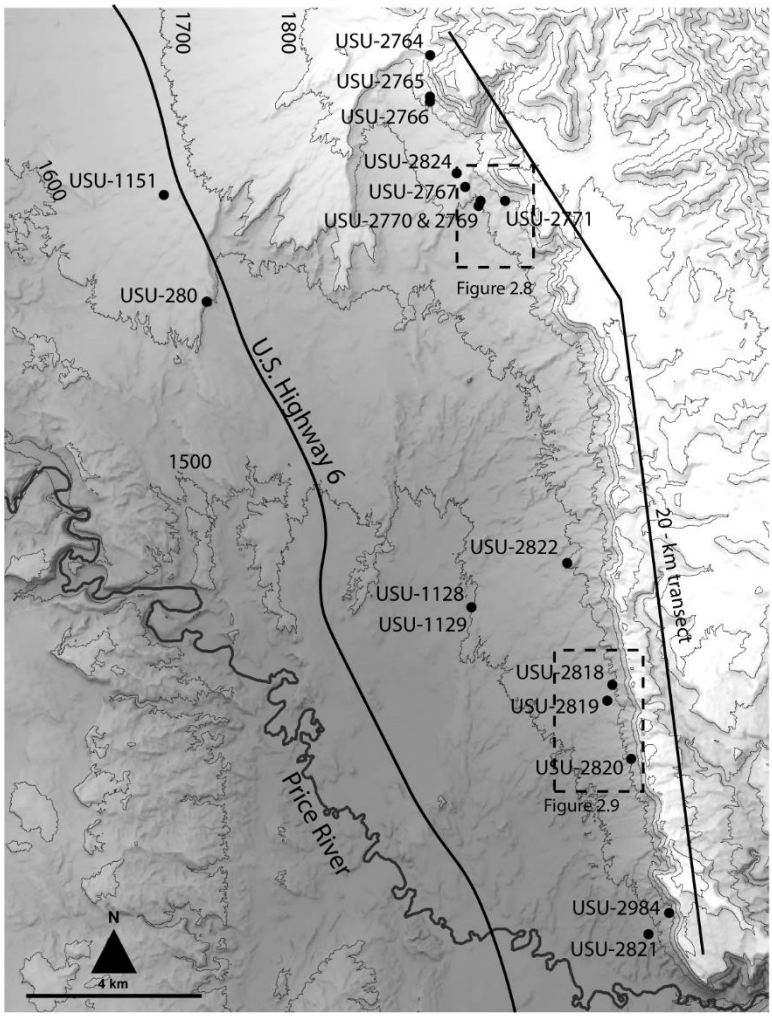

Figure 2.5. Location of luminescence sample sites within 20-km study transect and are labeled by sample lab number. Note the gradient in distance between the Book Cliffs and the local baselevel control of the Price River. USU 257, 1132, 1151, 1152, and 1173 are not shown here due to being collected outside of the 20-km transect. 100-meter contour lines have been placed to illustrate the elevation gradient within the study area.

Samples were processed and analyzed at the Utah State University Luminescence Lab following the single-aliquot regenerative-dose (SAR) protocol of Murray and Wintle (2000). The environmental dose rate was calculated from elemental concentrations of radio-isotopes in the sediments surrounding each sample using the conversion factors of Guérin et al. (2011). Depositional ages were calculated by dividing the equivalent dose by the dose rate and using the central age model of Galbraith and Roberts (2012) or the minimum age model.

RESULTS

Quaternary stratigraphy and sedimentology

Observations in the study area indicate there are four generations of deposits, with three correlatable landforms within the study area. These three generations of connected colluvial (C) and piedmont (P) deposits were mapped in two focus areas of the study transect. Deposits exhibit a sequential and vertically nested arrangement with C1 and P1 being the youngest inset deposits, whereas P4 is the highest in the landscape (Figure 2.6.). Although P4 and P3 deposits are distinct and mappable on the Horse Canyon fan at the north edge of the study area, within the lower-relief mapping transect, they could not be consistently distinguished and are grouped as generation 4/3 deposits.

Toeslope boulder-gravel of flatirons grade into alluvial-piedmont pebble gravel with increasing distance from the cliff. Generation 4/3 deposits are the thickest, up to 20 m in the Horse Canyon Fan, and generation 1 deposits are the thinnest, ~5m at the most. All C-P deposits are the thickest at the base of the toeslope and proximal piedmont transition, and they are thinner at the talus tip and down slope across the piedmont. Along

the study transect C/P 2 is by far the most common and well preserved, followed by the younger C/P 1. C/P 4/3 deposits are better preserved in the north and become increasingly rare to the south. Colluvial and piedmont deposits of each generation exhibit similar sedimentary characteristics and configuration across the field area (Figure 2.7).

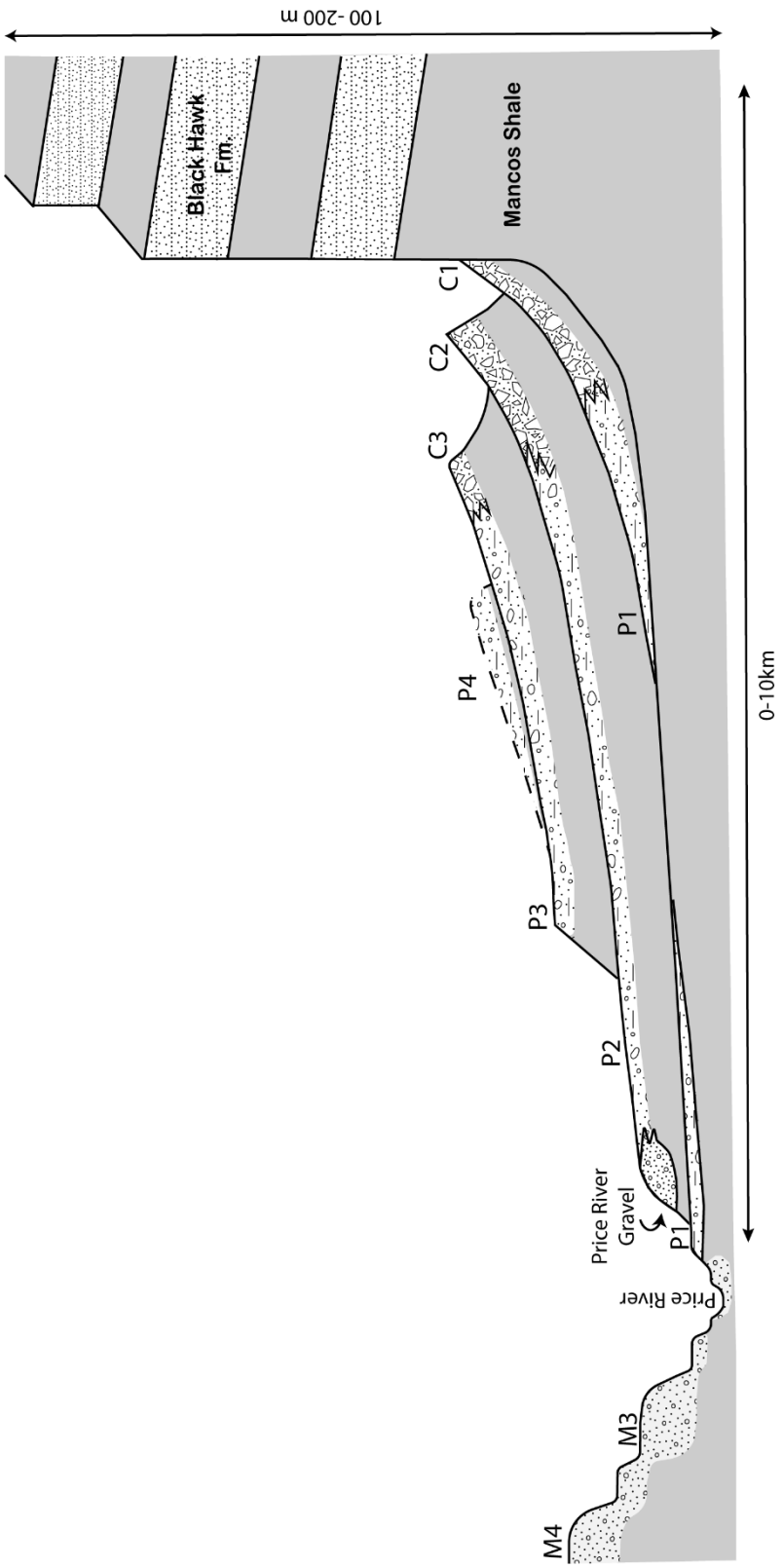

Figure 2.6. Schematic cross section illustrating the spatial relationships between the cliffs and flatiron colluvial and piedmont deposits.

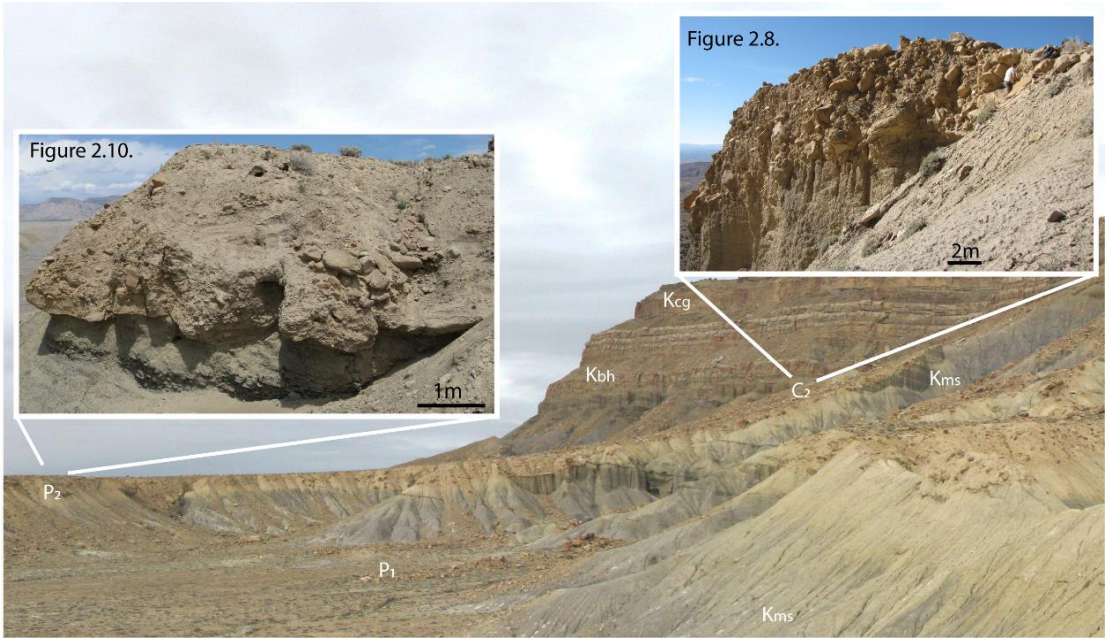

Figure 2.7. Example of colluvial and piedmont deposits in the southern section of the study transect looking north. Bedrock units are the Mancos Shale (Kms), Black Hawk (K_{bh}) and Castlegate (K_{cg}) sandstones. Note the transition between colluvium (C2) and continual traceable (P2) piedmont deposits. Inset images are representative of sedimentology of deposits shown. Example images are not from the locations in the picture but from analogous deposits elsewhere along the Book Cliffs.

C1 talus is commonly still attached to and currently in the process of being separated from the cliff via gully erosion (Figures 2.4, 2.6). In most places, the C1 may be still receiving rock-fall material from the cliff. Yet, the toe of C1 is incised by gullies and stands as a terrace of increasing height downslope. C1 deposits are common and cover broad toeslopes between older flatirons. P1 deposits are rarer and expressed as small terraces on the sides of streams and gullies and commonly converge with active alluvium and modern washes with increasing distance from the toeslope of the cliff (Figure 2.6).

C2 deposits are well-developed flatirons that are separated from the cliff and the most prominent in the landscape (Figure 2.6, Figure 2.8, Figure 2.9). The P2 is likewise the most extensive alluvial terrace in the landscape, reaching all across the field area and interfingering with Price River terrace deposits (Figure 2.6 and 2.7).

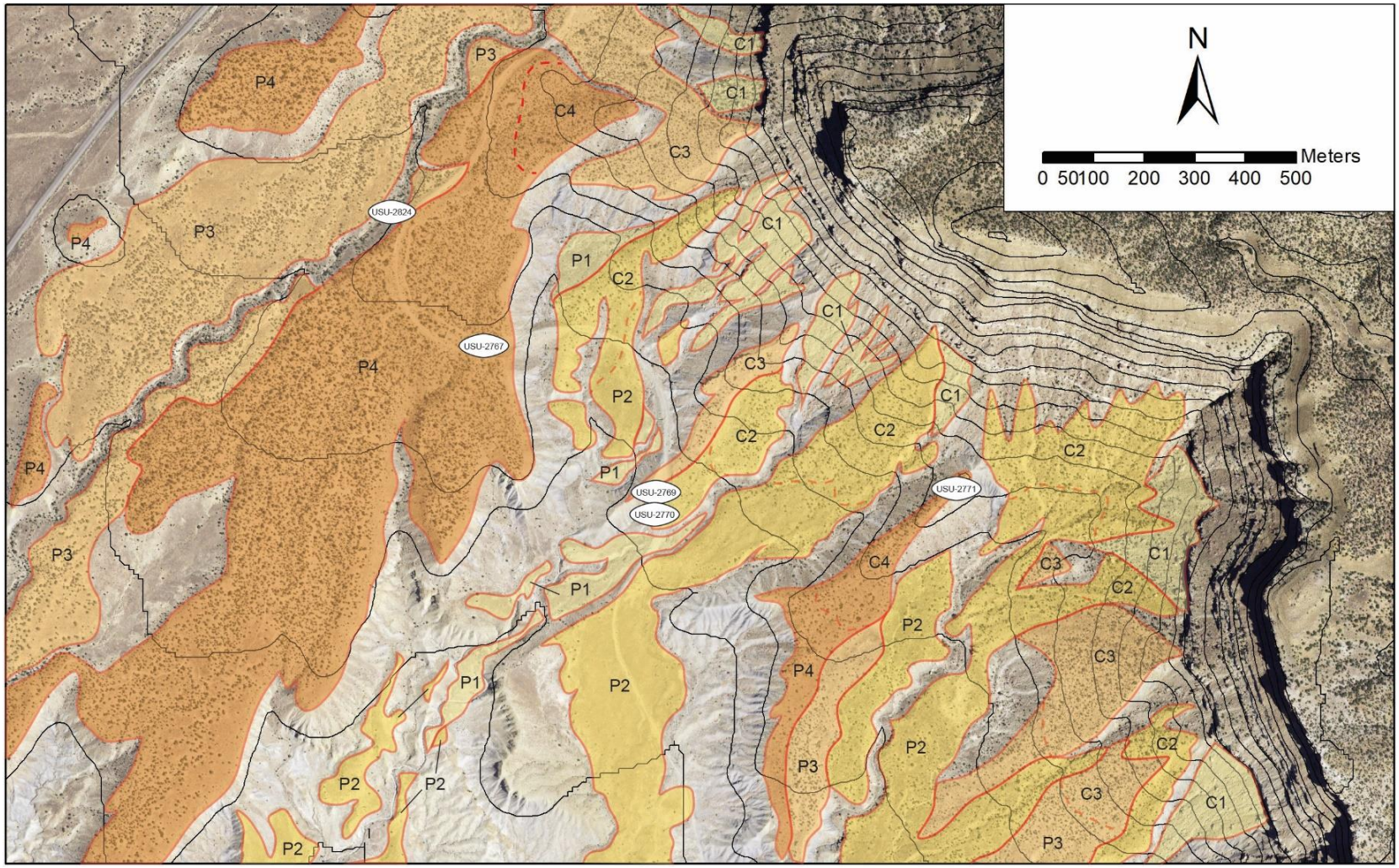

Fig. 2.8. Mapped deposits at most northern section of the study transect (Figure 2.5.). Contour interval is 20 meters, and map scale is 1:12,000.

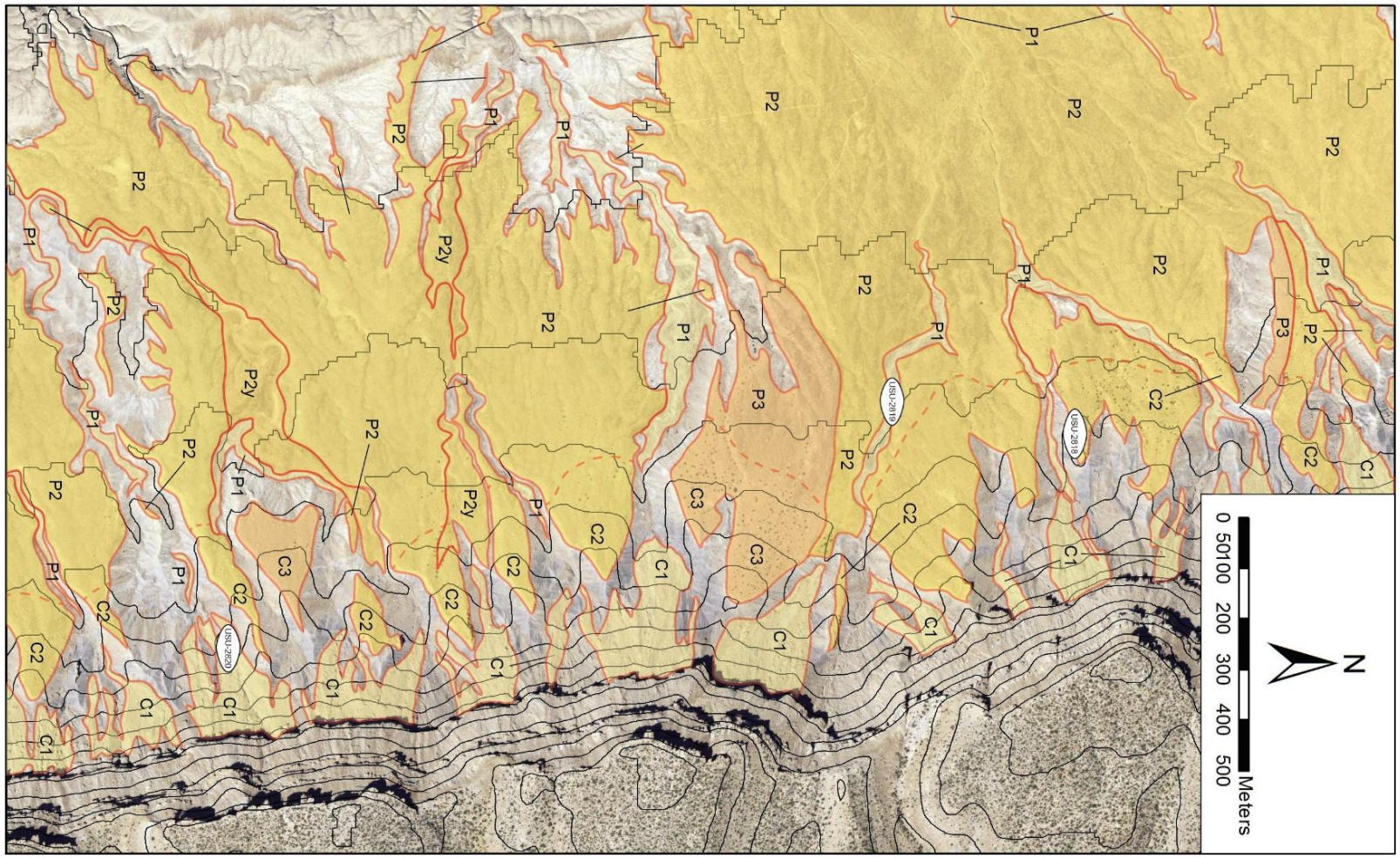

Fig. 2.9. Mapped deposits in southern section of the study transect (Figure 2.5). Contour interval is 20 meters, and map scale is 1:12,000.

C4/3 and P4/3 are less plentiful within the study transect. C4/3 deposits form flatirons in the northern study transect, but are increasingly rare toward the southern end of the study area and preserved deposits are mostly piedmont alluvium with proximal talus being eroded away. P4/3 can be observed south of the Price River, outside this study area, indicating a wider spatial distribution. Distinct P4 deposits are observed prominently on the Horse Canyon fan at the north edge of the study area (Figure 2.6). These P4 deposits converge with P3 midway down the Horse Canyon fan, with P4 not distinctly preserved west of U.S. highway 6 (Figure 2.5). Thus, in most places, P3 and P4 deposits significantly overlap in elevation and have similar surface characteristics, making them difficult to separate them in the field.

Sedimentologically, the colluvial deposits of the study area are composed of lenticular beds of matrix-supported, boulder-cobble and cobble-boulder gravel interbedded with clast-supported, boulder-cobble gravel (Figure 2.10 and 2.11). These poorly sorted, angular diamictons are interpreted as rock fall, rock avalanche and debris flow deposits. Medium – thin, lenticular beds of planar and ripple-laminated sand and silt are found locally around the margins of boulders and large cobbles or in rare lenses interbedded with the diamicton. These are interpreted as slopewash and gully deposits, and were the primary target of OSL sampling. Deposit strath (contact) with Mancos Shale is irregular.

Figure 2.10. C2 example. 10 m thick deposit consists matrix-supported gravel interbedded with clast-supported gravels. Lenses of laminated and/or rippled sands can be found locally around margins of larger cobbles and boulders were target of OSL tube sampling.

Figure 2.11. Example of C3-P3 toeslope deposits. Deposit consists of alternating beds of clast-supported gravels and matrix-supported gravels that are ~0.5-2m thick. Within clast-supported deposits, sand lenses exhibit ripples, laminations, and cross beds.

Piedmont alluvial deposits of the study area change in character with distance downslope. Cliff proximal piedmont at the toe of talus are characterized by lenticular beds of clast-supported, cobble-boulder to pebble-cobble gravels interbedded with matrix-supported, cobble-boulder and pebble-cobble gravels. (Figures 2.11 and 2.12). These thicker, more matrix supported, boulder diamicton are interpreted as debris flow deposits reworking talus at the lower toeslope, which results in the distinct talus-debris flow break in slope commonly observed (Figure 2.7). The transition across the upper-mid piedmont to distal deposits are moderately sorted, with sorting increasing and grain size decreasing across the piedmont away from the cliff. Clasts are sub-angular to rounded, commonly imbricated, and are interpreted as alluvial deposits interbedded with minor debris-flow deposits. Contact with Mancos Shale is slightly wavy, but mostly planar in places. Pebbly-sand interbeds become more common downslope, sand-pebble and pebble-gravel beds being the most common type of alluvial deposit and were the target of Luminescence sampling (Figures 2.12 and 2.13).

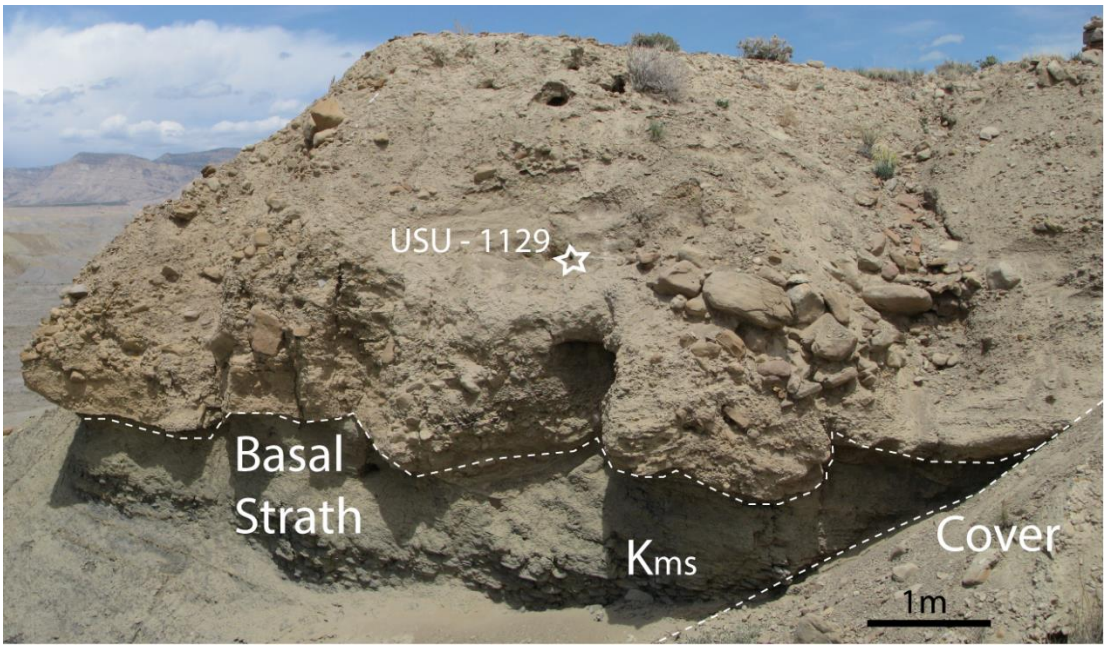

Figure 2.12. Example of P2 deposit. Deposit is ~4 m thick and is composed of alternating packages of clast-supported gravel interbedded with pebbly-sandy. Note the OSL sample location of USU – 1129.

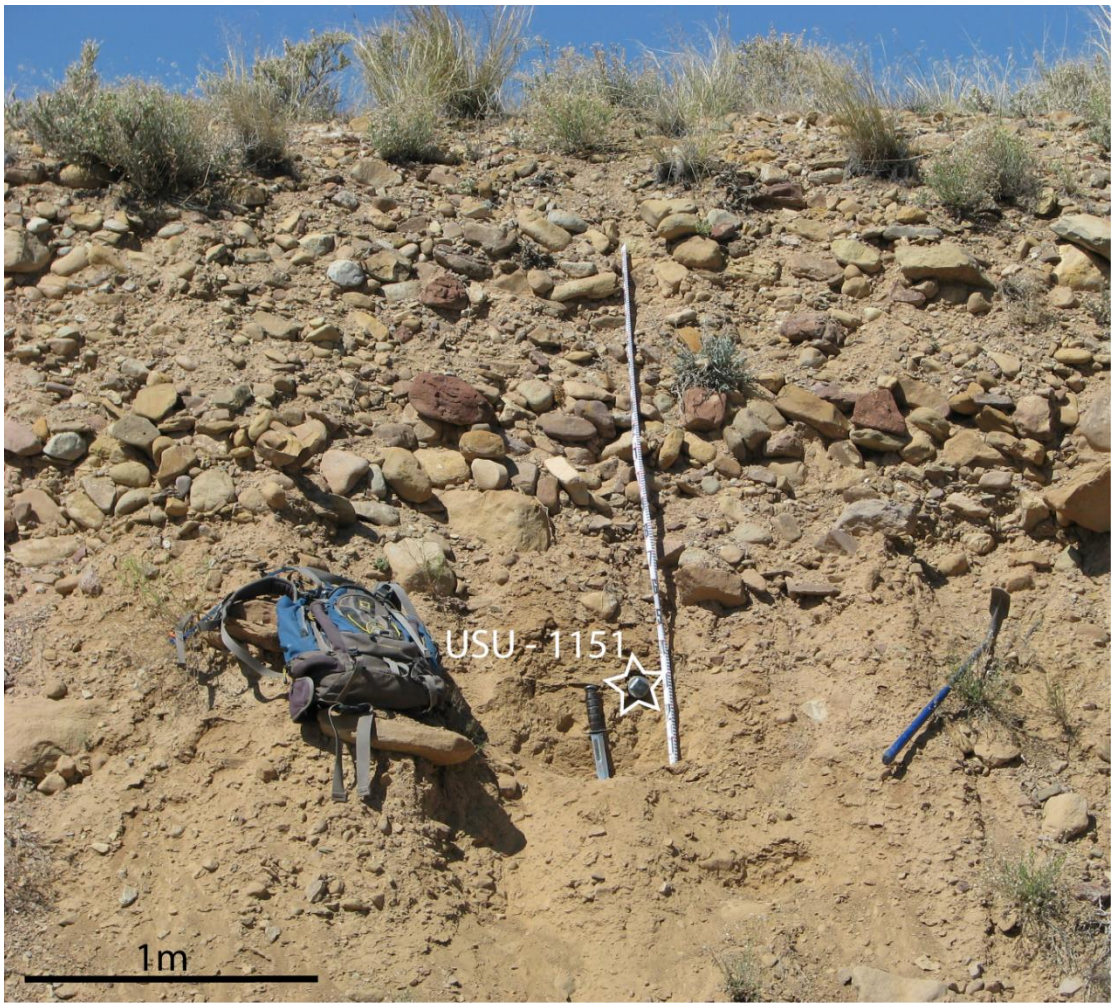

Figure 2.13. P3 example on the Horse Canyon Fan. Deposit composed of alternating beds of clast-supported gravel and pebbly-sand. Note imbrication and the location of OSL sample USU – 2768.

Chronostratigraphy of Book Cliff deposits

Geochronology efforts targeted the three sets of mappable deposits discussed in the previous section. A total of 14 samples were collected during the course of this research and complied with another nine finished samples collected in the area prior to this project, totaling 25 OSL ages (Table 2.1). Five of the previously collected samples are from outside of the study transect, with two from the adjacent Horse Canyon fan, two

from the Book Cliff piedmont south of the study area, and two from colluvium of the Book Cliffs north of Green River, UT. Sixteen luminescence samples were collected from piedmont deposits due to their accessibility and plentiful sand lenses, while nine samples are from rarer sand lenses in colluvium (See Appendix A for more sample information). All samples are complete with 15 to 34 accepted aliquots.

TABLE 2.1. PLEISTOCENE LUMINESCENCE CHRONOLOGY

Deposit*	USU #	# Aliquots (total)	Dose Rate (Gy/ka)			Equivalent dose (Gy)#			OSL age (ka)$			Model
C1	USU-2766	20 (37)	1.85	±	0.08	2.91	±	0.4	1.6	±	0.2	CAM
C1	USU-2820	15 (30)	1.98	±	0.08	8.28	±	2.6	4.2	±	0.8	MAM
P1	USU-2824	17 (33)	1.39	±	0.06	8.41	±	1.2	5.7	±	0.6	CAM
P1	USU-2819	18 (29)	1.69	±	0.07	10.0	±	2.7	5.9	±	0.9	MAM
C1	USU-2984	12 (22)	2.56	±	0.11	27.5	±	2.2	10.7	±	1.0	CAM
C2	USU-2765	17 (25)	2.39	±	0.10	105.9	±	8.3	44.3	±	4.0	CAM
P2	USU-1132	26 (66)	2.14	±	0.12	99.5	±	14.0	47.2	±	5.1	CAM
P2	USU-2770	17 (19)	2.22	±	0.09	106.6	±	9.6	48.0	±	4.5	CAM
P2	USU-2769	17 (22)	1.67	±	0.07	80.9	±	5.9	48.1	±	4.3	CAM
P2	USU-1128	25 (53)	1.82	±	0.10	99.9	±	8.3	55.8	±	5.1	CAM
C2	USU-2818	18 (21)	1.58	±	0.06	91.4	±	4.9	58.3	±	5.0	CAM
P2	USU-1173	23 (67)	1.80	±	0.10	104.1	±	13.7	58.8	±	6.2	CAM
P2	USU-1129	20 (32)	1.88	±	0.10	112.5	±	16.2	61.0	±	6.6	CAM
P2+	USU-2821	20 (24)	1.58	±	0.07	107.9	±	12.9	69.1	±	6.7	CAM
M3	USU-1130	16 (33)	1.45	±	0.06	112.9	±	14.9	78.1	±	8.3	CAM
M3	USU-1131	34 (52)	1.55	±	0.07	88.5	±	8.23	57.1	±	5.4	CAM
C3	USU-2764	16 (21)	1.78	±	0.07	134.7	±	15.6	75.6	±	7.5	CAM
C3	USU-258	28 (33)	2.92	±	0.12	231.0	±	19.1	79.1	±	7.2	CAM
P3	USU-280	26 (45)	2.85	±	0.15	252.9	±	22.2	84.3	±	8.0	CAM
P3	USU-257	20 (25)	2.65	±	0.11	227.0	±	78.0	85.8	±	8.0	CAM
P3	USU-1151	18 (37)	3.21	±	0.17	258.7	±	22.1	85.9	±	9.1	CAM
P3	USU-1152	21 (34)	2.10	±	0.08	189.3	±	23.8	90.3	±	9.8	CAM
C4	USU-2771	18 (23)	1.79	±	0.07	211.3	±	19.1	115.9	±	10.8	CAM
P4	USU-2767	15 (22)	1.70	±	0.07	213.3	±	20.7	118.5	±	11.1	CAM
P4	USU-2822	16 (23)	1.65	±	0.07	203.2	±	28.8	119.2	±	12.8	CAM

*Organized by stratigraphic position, plus age results with in map units

Equivalent dose (DE) calculated using the CAM or MAM model of Galbraith and Roberts (2012) Reported with 2σ errors.

$ Age analysis using the single-aliquot regenerative-dose procedure of Murray and Wintle (2000) on 1-mm small aliquot of quartz sand. Reported with 1σ errors. See Appendix A for 2σ errors.

+ all samples use 5+/-2% H2O in the dose rate calculation

Three C1 samples and two P1 samples range in age from 10.7 ± 1.0 to 1.6 ± 0.2 ka with a mean age of 5.6 ± 0.5 ka. Seven P2 samples along with two C2 samples yield an age range of 69.1± 6.7 to 44.3 ± 4.0 ka with an outlier age of 69.1± 6.7 ka. The average age of generation 2 deposits is 54 ± 2.5 ka. Two samples from a the M3 Price River terrace, which generation 2 piedmonts grade to, were determined to be 57.1 ± 7.1 and 78.1 ± 12.2 ka respectively. Three C3 and three P3 yield ages between to 90.3 ± 9.2 to 75.6 ± 7.5 ka with a mean age of 83.4 ± 4.7ka. Two P4 and one C4 yield ages 115.9 ± 10.8 to 119.2 ± 12.8 ka with a mean age of 117± 9.4.

Mean central ages for deposit-generations were calculated by taking the average of the individual OSL central ages. Then the mean error for each generation was calculated using the following equation (Bennett, 1962) :

$$E = \frac{1}{n^2}\sum \sigma_n^2 \qquad \text{Eq. 2.1}$$

Where E is the mean generation standard error, n is the number of error values, and σ is two-sigma error of the individual OSL ages. This equation is generally used to calculate the mean of the variance of a set of variables. We use Eq. 1.1 to calculate the mean of the standard errors by substituting in the OSL 2-sigma standard error for variance (Appendix A).

Luminescence ages for each generation of deposit do cluster, but not very distinctly (Figure 2.14). Furthermore, there is no detectable pattern of age difference between piedmont versus colluvial deposits, such as one being systematically older or younger than the other. Generation 1 and 4 deposits clearly exhibit distinct age clusters with distinct 20 ky long periods absent of ages in relation to generation 2 and 3. C/P4

ages are much older than the main population of C/P3 despite the difficulty in distinguishing them in the field. In fact, we intended to sample C/P3 in the case of a couple samples, yet results indicate a remnant-buried P4 deposit instead. Generation 2 and 3 underlie distinct, separate sets of piedmont-colluvial landforms, especially in the northern part of the study area. Yet, generations 2 and 3 are temporally less distinct in age with only a subtle dip in the probability distribution function at ~70 ka, suggesting deposition of these deposits occurred over an extended episode of Pleistocene time with a less-distinct break (Figure 2.11 and 2.14). If the outlier USU-2821, 70.5 ± 9.7 ka, were to be removed, there would be a more distinct, ~10 ky, gap across MIS 4 time.

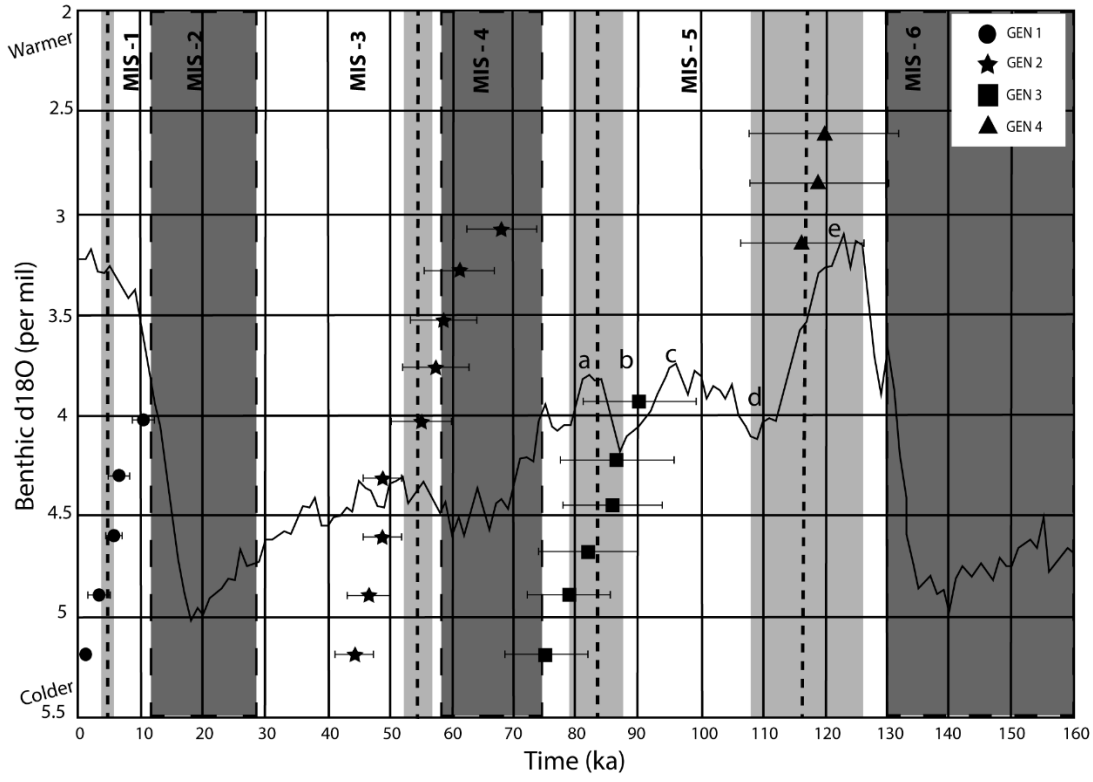

Figure 2.14. OSL ages of deposit with 1σ errors overlain on global oxygen isotope climate record (Lisiecki and Raymo, 2005). Marine Isotope stages with glacial periods denoted by the dark gray in background. The mean age of each generation is denoted with a dashed line and the mean error with light gray boxes.

The five OSL ages from C/P1 deposits span the Holocene. Even though age control on this deposit is sparse, it is consistent with ongoing dissection and transport of C1 deposits primarily formed in the early Holocene, with the 1.4 ka C1 age suggesting that the deposit can still receive new colluvium from the escarpment in places.

The spread of age results for both C/P3 and C/P2 deposits suggest each formed in an episode spanning ~20 ky window. However, strictly speaking, generation 3 and 2 deposits may also be interpreted as a single, longer episode of deposit preservation. Taken all together, the pattern across the past ~130 ky broadly suggests depositional activity occurs periodically with a weak beat of ~40 ky (Fig. 2.14), consistent with obliquity orbital forcing.

We plot age results by distance of the sample along drainage lines from the local baselevel of the Price River to explore the possible signature of age patterns up and down the piedmont and of transient incision. Generation 4/3 and 1 deposits have too few data for this analysis, however we still plot the ages of these deposits. Generation 2 deposits, the most robust data set, show the tread of deposits being generally younger the farther they are from the Price River (Figure 2.15). If the old outlier age is removed, sampled only 1-2 km from the Price River, the variation in age is less distinct and spans only ~10 ky. The oldest ages are in the south end of the study area while deposits in the north, far from the Price River ~15 km away are younger. Although not enough data to be significant, generation 1 deposits in the northern portion of the study transect are likewise younger than deposits in the southern part. These tentative results are consistent with Price River baselevel fall causing transient incision over millennia up the piedmont, abandoning the P2 terrace deposit on the way. This is opposite the top-down model

prediction of progradation of sediment downslope across the piedmont. Instead, it may help account for some of the variation in ages from given generations of deposits.

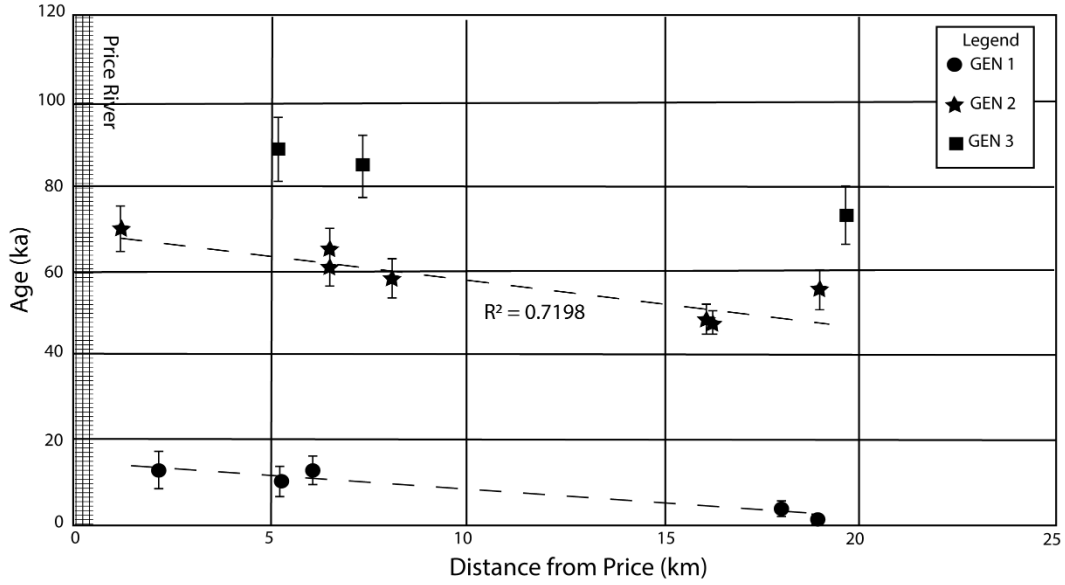

Figure 2.15. Distance from the Price River baselevel up tributary drainages to sample location versus age ± 1σ error for the 16 sample within the study transect. Least-squares best fit (dashed line) illustrates P2 deposit ages are younger in the north and older in the south, closer to the Price River.

DISCUSSION

Correlation to other Pleistocene chronostratigraphic records in region

North of the study transect, Carter (1981) documented five sets of correlatable pediments, whereas we have documented four generations of piedmont deposits. This suggests that the number of preserved distinct deposits decreases. Within our study transect P4 and P3 deposits are readily observed in the north and are completely absent in the south. If true, the fewer number of preserved deposit-generations in our study area may be the result of closer proximity to the Price River baselevel, or alternatively to

decreasing elevation and the linked vegetation and climate difference. Increased distance from baselevel (<12 km) and increased elevation and denser, shrub forest vegetation to the north could be shielding older deposits from erosion and increasing preservation potential in Carter's study area.

Sheehan and Ward's (2018) single, preserved generation of relict talus along the nearby Coal Cliffs was estimated to be 30-20 ka in age, and it should presumably correspond to generation 1 or 2 Book Cliff deposits. However, C/P1 (5.6 ± 0.5 ka) occurs after the Coal Cliff age cluster and C/P2 (54 ± 2.5 ka) occurs significantly before. This suggests the peak timing of deposition along the Coal Cliffs was not contemporaneous with the activity along the Book Cliffs. However, Sheehan and Ward's CRN age model did not consider *in situ* weathering rate. Furthermore, the distribution and geomorphology of the Coal Cliff deposits suggest they were once a continuous apron like our generation 2 suggesting both formed under similar circumstances. OSL geochronology, which resolves actual deposit age, in the Coal Cliffs would help to better understand how it relates to the Book Cliffs record.

Although not a study of hillslopes, Pederson et al. (2013b) produced a chronostratigraphy for the past ~115 ky for a set of six terraces along the Green River at Crystal Geyser. This study area is just 40 km south of the Book Cliffs for comparison to our Price River terrace and four sets of alluvial piedmont records, which span roughly the same time. The Crystal Geyser deposits date to 144 -103 ka, 99.4 - 96.8 ka, ~60 ka, and 41.8 ka, with a younger, undated terrace preserved.

The M3 Price River terraces at 57.1 ± 7.1 to 78.1 ± 12.2 ka may represent a period of time that overlaps with the ~60 ka Crystal Geyser terrace. However, further age

control on Price River terraces will be needed to make a definitive conclusion that the Price and Green River terrace ages due indeed temporally correlate. When we compare our piedmont-hillslope deposit ages to those of the Green River terraces a very general overlap can be observed. Our piedmont-hillslope ages of the C/P4 (115.9 ± 10.8 to 119.2 ± 12.8 ka) and C/P2 (69.1± 6.7 to 44.3 ± 4.0 ka) overlap with the younger end of the 144 -103 ka terrace and the individual ~60 ka and 41.8 ka Crystal Geyser terraces. However, there is no terrace at Crystal Geyser that corresponds with our C/P3 (90.3 ± 9.2 to 75.6 ± 7.5 ka) or C/P1 (10.7 ± 1.0 to 1.6 ± 0.2).

In the deposits of eastern Grand Canyon, DeJong's (2007) geochronology of Lava Chuar Creek indicates several periods of tributary aggradation: 100-90 ka, 61-35 ka, and 14-7 ka. This record seemingly overlaps our chronology of generations 3, 2 and 1, respectively. This correlation between the two records separated by 350 km would be expected if hillslopes regionally are responding to the common forcing mechanism of climate. The weak correlation between our record and that of Crystal Geyser and stronger correlation of the tributary record in the eastern Grand Canyon suggests that our piedmont-hillslope records follows the regional trend of mainstem trunk river terraces not matching those of local tributaries and hillslopes observed elsewhere (Anders et al., 2005; DeJong, 2007).

Potential paleoclimate controls

When examining our deposit ages in relation to paleoclimate, several key patterns can be observed. First, no deposit-generations correspond the middle of glacial epochs. Second, both C/P1 and C/P2 correspond to glacial-interglacial transitions with ongoing deposition extending afterward in the interglacial (Figure 2.13). Third, the C/P3 dates to

interglacial and intermediate-climate conditions of MIS-5 a/b. Fourth, the poorly constrained C/P4 may have formed during or after the interglacial period of MIS – 5 d/e more sampling will need to be performed to provide better resolution (Figure 2.14 and 2.16).

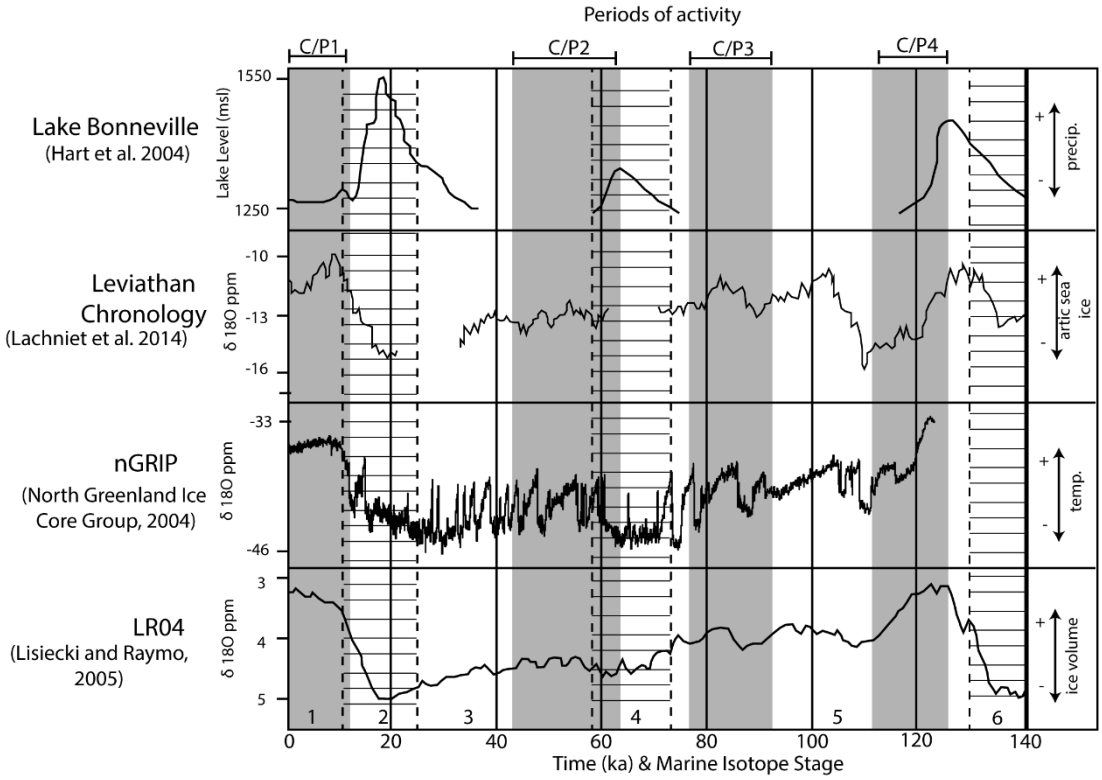

Figure 2.16. Global and regional climate proxies plotted for the last 140 ky. Shaded areas represent Book Cliff deposit ages (denoted with C/P1, C/P2, C/P3, and C/P4) and hashed areas are global glacial periods.

In order to better understand the age clustering of generation 2 and 3 deposits, we need to understand the Paleoclimate conditions during those times, MIS-3 and MIS-5. Global climate during MIS-3 was generally cooler compared to the present, on average 4 to 8 ^{o}C cooler (Kissel et al., 1999). Within MIS 3 there are several fluctuations in the global

oxygen ratio record that suggest this period was not one of total climatic stability but experienced several short period perturbations of 1-5 thousand years in length (Figure 2.16). These abrupt warming and cooling phases are known as Dansgaard-Oeschger events (DO), with temperature changes in the Northern Hemisphere over only a few decades of time (Kissel et al., 1999; Bond et al., 1999; Anderson et al., 2004). Likewise, global climate during the older MIS 5, was generally cooler, except the period of MIS 5e. MIS 5 was time of general climate instability as seen in the global oxygen isotope record (LR04) (Figure 2.15) (Lisiecki and Raymo, 2004). This instability can be seen as brief temperature perturbations of a few thousand years as seen in the speleothem of Leviathan (Lachniet et al., 2014).

Regionally several records suggest climate fluctuations that could drive escarpment evolution. The cave speleothem record of the Leviathan Chronology, of Nevada, records indicate variation in climate during MIS 3, which resulted in ground water fluctuating several meters over relatively short periods of time (Lachniet et al., 2014). It is also known that Bonneville saw swings in lake level during the later parts of MIS-3 which suggest significant fluctuations in water inputs in the Bonneville basin drainages (Balch et al. 2005). These swings could lead to pulses of increased sediment production at times of higher precipitation in the area.

Deposits preserved along the Book Cliffs appear to correspond to regional climate transitions from glacial to interglacial in the region. In other locations in the greater Rocky Mountains, landscape activity is marked by the presence of glacial landforms, however the lower drylands of the Book Cliffs and central Colorado Plateau are different. The relatively short climate oscillations seen in the global and regional records of MIS-3 could be a likely

explanation for the sub population of ages in generation 2 ages. Like MIS-3, the interglacial and intermediate climate of MIS-5 is marked by many millennial-scale oscillations in climate and general climate instability that would be able drive the evolution of the Book Cliff escarpment through similar processes. Generation 4 deposits also occur during MIS-5 and may have been deposited in response to the climate instability of that time. However, if you assume the maximum error on these ages, these deposits may have been generated in relation to the transition out the glacial period of MIS-6 into the interglacial of MIS-5 like generations 1 and 2.

Role of transient incision

Our geochronology, comparison to regional records, and examination of paleoclimate indicates that erosion and sedimentation along the Book Cliffs is behaving more like the climate end-member conceptual model, and less like the autogenic model. The autogenic conceptual model predicts predicted random age distribution for deposits, which is not seen in our data. However, the rough gradient in piedmont-deposit age with drainage distance from Price River (Figure 2.15) is consistent with transient incision. Pederson et al. (2013b) proposed that a regional wave of transient incision along the Green River is currently hung up in the Desolation Canyon-Book Cliffs region. A single regional incision pulse propagating up the Price River on time scales of ~100's of thousands of years would result in enhanced incision in areas draining to the Price River. There may be geomorphic evidence in the study area for differential baselevel fall over longer timescales preserved by individual terraces, as proposed by Pederson et al. (2013b). P3 and P4 deposits are relatively close in elevation and landscape position to each other, only separated by several meters, suggesting that between there was only

modest baselevel fall over the 119 to 80 ka timeframe. In contrast, P3 and P2 as well as P2 and P1 deposits are separated by 10's of meters in elevation, suggesting that since P3 time there has been faster baselevel fall.

Furthermore, when considering climatic variations superimposed onto this larger incision signal, the age gradients observed in distinct generations of deposits can be explained. Focusing in on P2 deposits, their downslope end interfinger with Price River terrace gravels. As the Price River proceeded through cycles of aggradation and then incision, a pulse of incision would migrate up tributaries along the piedmont. As this erosional pulse travels up drainages, like a waterfall or knickzone working its way up a bedrock stream, it would leave behind in its wake a terrace deposit. This terrace formation moving up tributaries would account for the older ages near the Price River and younger farther up tributary streams, at least as apparently seen in the best-dated P2 deposits (Fig 2.15).

Revised conceptual model of escarpment evolution

Neither end-member conceptual model expressed above perfectly fits as an explanation for the evolution of the Book Cliffs. Although we suggest that the Book Cliffs are behaving closer to the climate end-member conceptual model, that model does not explain all the trends seen in the data. Here we propose a hybrid conceptual model including roles for climate and local transient incision.

The Book Cliffs record can be simplified into a two-step model of escarpment evolution (Figure 2.16). First, mass movements and sedimentation is triggered by glacial-interglacial transitions or periods of climate instability. Increase sediment shedding from

the escarpment and retreat, resulting from increased freeze-thaw or wetting-and-drying leads to deposition of new talus which is reworked and delivered out onto the piedmont through debris flow and alluvial processes for an extended time, accounting for generation 4, 3, and 2 deposits in the study area (Figure 2.17). During times of relative climate stability and cooling, the colluvial sediment supply may significantly decrease as weathering and mass-failures wane, or erosional processes may increase due to greater wetness. Regardless, this allows erosional processes to take over along the piedmont, leading to incision. Top-down gully incision on the toe slope separates the talus from the cliff face, creating flatirons. This is consistent with the gaps in the Book Cliffs record between generations 3 and 2 as well as 2 and 1, which correspond partly to global glacial epochs. Meanwhile, if the Price River begins to incise, it will send transient incision up tributary streams. Together the top-down and bottom-up incision can result in the formation of the continuous, abandoned piedmont terrace-flatiron landforms found in the study area.

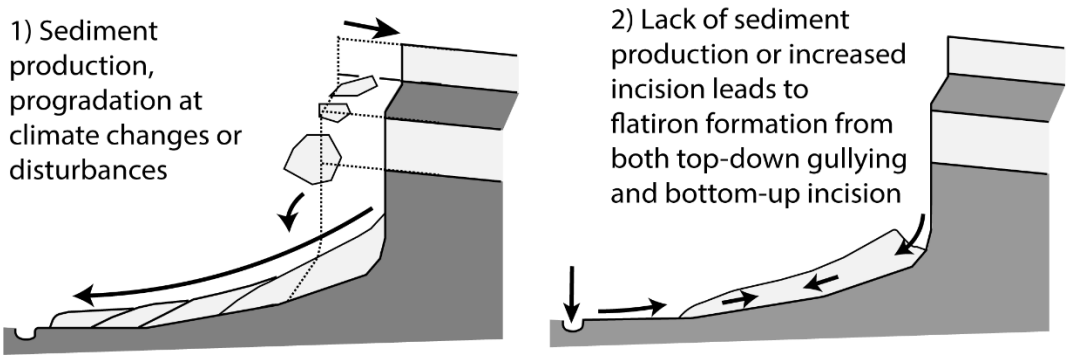

Figure 2.17. New conceptual model of cliff retreat and sediment production for the Book Cliffs.

Implications of new model globally

When considering our results in the context of other work globally. it appears that escarpment evolution is governed broadly by climate disturbances triggering sedimentation. While the Book Cliffs record does not temporally correlate with those published from Spain and Israel, they all share the feature of activity being triggered by climate disturbances. In Spain, escarpments appear to be sensitive to the short, millennial-scale climate oscillations of Dansgaard–Oeschger and Heinrich events (Gutierrez et al., 1998; Gutierrez et al., 2010 Roque et al., 2013). In Israel, escarpments in the hyper-arid Negev preserve deposits from extreme storms (Enzel et al., 2012; Boroda et al., 2011). Along the Book Cliffs, we suggest mass-wasting is triggered by climate instability such as the transitions from glacial to interglacial periods. Unlike hypothesized by earlier workers (Bull and Schick, 1979; Gerson and Grossman, 1987; Schmidt, 1996), escarpments globally do not follow a simple response to glacial versus interglacial climate modes The Book Cliffs record also shows that distance from local baselevel can influence the number of piedmont deposits preserved and also drive patterns of incision that complicate local records.

REFERENCES

Anders, Matt D., Joel L. Pederson, Tammy M. Rittenour, Warren D. Sharp, John C. Gosse, Karl E. Karlstrom, Laura J. Crossey, Ronald J. Goble, Lisa Stockli, and Guang Yang. "Pleistocene Geomorphology and Geochronology of Eastern Grand Canyon: Linkages of Landscape Components during Climate Changes." *Quaternary Science Reviews* 24, no. 23–24 (2005): 2428–2448.

Anderson, N. John, and Melanie J. Leng. "Increased Aridity during the Early Holocene in West Greenland Inferred from Stable Isotopes in Laminated-Lake Sediments." *Quaternary Science Reviews* 23, no. 7–8 (2004): 841–849.

Balch, Deborah P., Andrew S. Cohen, Douglas W. Schnurrenberger, Brian J. Haskell, Blas L. Valero Garces, J. Warren Beck, Hai Cheng, and R. Lawrence Edwards. "Ecosystem and Paleohydrological Response to Quaternary Climate Change in the Bonneville Basin, Utah." *Palaeogeography, Palaeoclimatology, Palaeoecology* 221, no. 1–2 (2005): 99–122.

Bennett, George. "Probability Inequalities for the Sum of Independent Random Variables." *Journal of the American Statistical Association* 57, no. 297 (1962): 33–45.

Bond, Gerard C., William Showers, Mary Elliot, Michael Evans, Rusty Lotti, Irka Hajdas, Georges Bonani, and Sigfus Johnson. "The North Atlantic's 1-2 Kyr Climate Rhythm: Relation to Heinrich Events, Dansgaard/Oeschger Cycles and the Little Ice Age." *Geophysical Monograph-American Geophysical Union* 112 (1999): 35–58.

Boroda, R., R. Amit, A. Matmon, R. Finkel, N. Porat, Y. Enzel, Y. Eyal, and ASTER Team. "Quaternary-Scale Evolution of Sequences of Talus Flatirons in the Hyperarid Negev." *Geomorphology* 127, no. 1–2 (2011): 41–52.

Bryan, Kirk. "Gully Gravure-a Method of Slope Retreat." *Journal of Geomorphology*, no. 3 (1940): 89–107.

Bull, William B., and Asher P. Schick. "Impact of Climatic Change on an Arid Watershed: Nahal Yael, Southern Israel." *Quaternary Research* 11, no. 2 (1979): 153–171.

Carter, Thomas Edward. "Pediment Development along the Book Cliffs, Utah." Doctoral dissertation, Colorado State University, 1981.

Clapp, Erik M., Paul R. Bierman, Asher P. Schick, Judith Lekach, Yehouda Enzel, and Marc Caffee. "Sediment Yield Exceeds Sediment Production in Arid Region Drainage Basins." *Geology* 28, no. 11 (2000): 995–998.

Cole, Kenneth L., and Larry Mayer. “Use of Packrat Middens to Determine Rates of Cliff Retreat in the Eastern Grand Canyon, Arizona.” *Geology* 10, no. 11 (1982): 597–599.

DeJong, Benjamin D. “Effects of Quaternary Climate Change on Tributary Sedimentation and Geomorphology in Eastern Grand Canyon.” Master’s Thesis, Utah State University, 2007.

Enzel, Yehouda, Rivka Amit, Tamir Grodek, Avner Ayalon, Judith Lekach, Naomi Porat, Paul Bierman, Joel D. Blum, and Yigal Erel. “Late Quaternary Weathering, Erosion, and Deposition in Nahal Yael, Israel: An ‘Impact of Climatic Change on an Arid Watershed’?” *Bulletin* 124, no. 5–6 (2012): 705–722.

Fisher, D. Jerome, Charles Edgar Erdmann, and John Bernard Reeside. *Cretaceous and Tertiary Formations of the Book Cliffs, Carbon, Emery, and Grand Counties, Utah, and Garfield and Mesa Counties, Colorado*. US Government Printing Office, 1960.

Galbraith, Rex F., and Richard G. Roberts. “Statistical Aspects of Equivalent Dose and Error Calculation and Display in OSL Dating: An Overview and Some Recommendations.” *Quaternary Geochronology* 11 (2012): 1–27.

Gerson, Ran, and Sari Grossman. “Geomorphic Activity on Escarpments and Associated Fluvial Systems in Hot Deserts.” *Climate, History, Periodicity, Predictability,* 1987, 300–322.

Guérin, Guillaume, Norbert Mercier, and Grzegorz Adamiec. “Dose-Rate Conversion Factors: Update.” *Ancient TL* 29, no. 1 (2011): 5–8.

Gutiérrez, Mateo, Pedro Lucha, Francisco Gutiérrez, Ana Moreno, Jesús Guerrero, Angel Martín-Serrano, Francisco Nozal, Gloria Desir, Cinta Marín, and Jaime Bonachea. “Are Talus Flatiron Sequences in Spain Climate-Controlled Landforms?” *Zeitschrift Für Geomorphologie* 54, no. 2 (2010): 243–252.

Gutiérrez, Mateo, Carlos Sancho, and Tomás Arauzo. “Scarp Retreat Rates in Semiarid Environments from Talus Flatirons (Ebro Basin, NE Spain).” *Geomorphology* 25, no. 1–2 (1998): 111–121.

Hart, William S., Jay Quade, David B. Madsen, Darrell S. Kaufman, and Charles G. Oviatt. “The 87Sr/86Sr Ratios of Lacustrine Carbonates and Lake-Level History of the Bonneville Paleolake System.” *Geological Society of America Bulletin* 116, no. 9–10 (2004): 1107–1119.

King, Lester C. “Canons of Landscape Evolution.” *Geological Society of America Bulletin* 64, no. 7 (1953): 721–752.

Kissel, C., C. Laj, L. Labeyrie, T. Dokken, A. Voelker, and D. Blamart. “Rapid Climatic Variations during Marine Isotopic Stage 3: Magnetic Analysis of Sediments from Nordic

Seas and North Atlantic." *Earth and Planetary Science Letters* 171, no. 3 (1999): 489–502.

Koons, Edwin Donaldson. "Cliff Retreat in the Southwestern United States." *American Journal of Science* 253, no. 1 (1955): 44–52.

Lachniet, Matthew S., Rhawn F. Denniston, Yemane Asmerom, and Victor J. Polyak. "Orbital Control of Western North America Atmospheric Circulation and Climate over Two Glacial Cycles." *Nature Communications* 5, no. 1 (May 2, 2014): 1–8.

Lisiecki, Lorraine E., and Maureen E. Raymo. "A Pliocene-Pleistocene Stack of 57 Globally Distributed Benthic Δ18O Records." *Paleoceanography* 20, no. 1 (2005).

Mills, Hugh H. "Boulder Deposits and the Retreat of Mountain Slopes, or," Gully Gravure" Revisited." *The Journal of Geology* 89, no. 5 (1981): 649–660.

Murray, Andrew S., and Ann G. Wintle. "Luminescence Dating of Quartz Using an Improved Single-Aliquot Regenerative-Dose Protocol." *Radiation Measurements* 32, no. 1 (2000): 57–73.

Nelson, Michelle S., Harrison J. Gray, Jack A. Johnson, Tammy M. Rittenour, James K. Feathers, and Shannon A. Mahan. "User Guide for Luminescence Sampling in Archaeological and Geological Contexts." *Advances in Archaeological Practice* 3, no. 2 (2015): 166–177.

Pederson, Joel L., W. Scott Cragun, Alan J. Hidy, Tammy M. Rittenour, and John C. Gosse. "Colorado River Chronostratigraphy at Lee's Ferry, Arizona, and the Colorado Plateau Bull's-Eye of Incision." *Geology* 41, no. 4 (2013): 427–430.

Pinheiro, Marcos Roberto, and José Pereira de Queiroz Neto. "From the Semiarid Landscapes of Southwestern USA to the Wet Tropical Zone of Southeastern Brazil: Reflections on the Development of Cuestas, Pediments, and Talus." *Earth-Science Reviews* 172 (2017): 27–42.

Reynolds, James F., D. Mark Stafford Smith, Eric F. Lambin, B. L. Turner, Michael Mortimore, Simon PJ Batterbury, Thomas E. Downing, Hadi Dowlatabadi, Roberto J. Fernández, and Jeffrey E. Herrick. "Global Desertification: Building a Science for Dryland Development." *Science* 316, no. 5826 (2007): 847–851.

Richardson, George Burr. "Reconnaissance of the Book Cliffs Coal Field, between Grand River, Colorado and Sunnyside, Utah." Goverment Print. U.S. Geological Survey, 1909.

Roqué, Carles, Rogelio Linares, Mario Zarroca, Joan Rosell, Xavier M. Pellicer, and Francisco Gutiérrez. "Chronology and Paleoenvironmental Interpretation of Talus

Flatiron Sequences in a Sub-Humid Mountainous Area: Tremp Depression, Spanish Pyrenees." *Earth Surface Processes and Landforms* 38, no. 13 (2013): 1513–1522.

Schmidt, Karl-Heinz. "Talus and Pediment Flatirons-Indicators of Climatic Change on Scarp Slopes on the Colorado Plateau, USA." *Zeitschrift Fur Geomorphologie Supplementband*, 1996, 135–58.

Schumm, Stanely Alfred, and R.J. Chorely. "Talus Weathering and Scarp Recession in the Colorado Plateaus." *US Geological Survey*, 1966, 11–36.

Sheehan, Christopher E., and Dylan J. Ward. "Late Pleistocene Talus Flatiron Formation below the Coal Cliffs Cuesta, Utah, USA." *Earth Surface Processes and Landforms* 43, no. 9 (2018): 1973–1992.

CHAPTER 3

A GEOMETRIC AND TERRAIN ANAYLSIS FOR CLIFF RETREAT OF THE BOOK CLIFFS, UTAH

ABSTRACT

Since the earliest explorations, geologists have invoked escarpment retreat as substantial part of landscape evolution of the Colorado Plateau. Geometry dictates that the lateral component of erosion is faster than vertical assuming that dryland escarpments, as controlled by sub-horizontal layered strata, maintain about the same relief and profile over geologic time. However, despite the advent of multiple geochronometers and the many studies establishing rates of vertical incision for the rivers that drain the Colorado Plateau, only a couple studies have quantified escarpment retreat, and indeed there are only a few well constrained rates of cliff retreat measured the world over. We apply empirical approaches to quantify escarpment retreat through the study of remnant colluvial slopes, aka. talus flatirons. The study area along the Book Cliffs of central Utah is marked by three distinct generations of talus flatirons constrained by 23 OSL dates to depositional episodes spanning the past 120 ky. Our terrain analysis involves projection of 46 paleo-landforms and discrimination of lateral and vertical distances of erosion through a novel profile-area-integration approach. Results confirm the geometric expectation that lateral cliff retreat proceeds several times faster than vertical incision of toeslopes (~2 m/ky vs. ~0.5 m/ky, respectively). The ratio of lateral retreat to vertical incision for the best-preserved C2 deposits ranges between 20:1 to 1:1. We also show that lateral retreat amount or rate does not correlate with distance from baselevel, and that the amount of vertical incision at toeslopes actually increases with

distance from baselevel. Our measurements are similar to early estimates of retreat rates in the Colorado Plateau made without age control, as well as rates from similar studies in Spain. Finally, steepness analysis reveals evidence of transient incision, with knickzones currently working their way up piedmont drainages.

INTRODUCTION

The most common metrics used to quantify the rate of landscape evolution are rates of vertical uplift, vertical incision by rivers, or overall denudation of landscapes. However, vertical changes in a landscape are only part of the story. Lateral components of mass removal, including valley widening and escarpment retreat are rarely quantified. To fully understand the evolution of landscapes, one must understand how quickly the landscape changes in both the vertical and lateral dimensions. This may be particularly critical for drylands, which comprise a significant portion of the land surface of the world. Classical theory suggests that the lateral retreat of cliffs is the primary mode of erosion in landscapes such as a Southwestern U.S., South Africa, and elsewhere (Dutton, 1882; Bryan, 1940; King, 1953). Despite the advent of multiple geochronometers over past decades, only a handful of well constrained rates of lateral retreat have been calculated the world over.

The Colorado Plateau in western North America is one of the best-studied erosional drylands. Focusing on rates of erosion, studies have established rates of vertical incision for the rivers that drain the Plateau (e.g. Lucchitta et al 2000; Pederson et al., 2006; Cook et al., 2009; Darling et al., 2012; Pederson et al., 2013a, b; Aslan et al., 2014; Jochems et al., 2015). Since the earliest explorations, geologists have invoked escarpment retreat as substantial part of the landscape evolution of the Colorado Plateau.

Clarence Dutton envisioned “the beds thus dissolving edge wise until after the lapse of millions of centuries their terminal cliffs stand a hundred miles or more back from their original position” when he wrote about this landscape in 1882. However, only two studies have measured lateral retreat in the southwest United States, and they are hampered by short records or indirect age control (Cole and Mayer, 1982; Sheehan and Ward, 2018).

Here we apply geometric and empirical approaches to quantify escarpment retreat through the study of remnant colluvial slopes, also known as talus flatirons. Our study area, the Book Cliffs of central Utah, is marked by the presence of four distinct generations of talus flatirons dated by optically stimulated luminescence (OSL), providing opportunities to quantify rates of escarpment retreat as well as understand the lateral and vertical components of landscape evolution. Initial results indicate that lateral retreat can be several times faster than vertical incision, confirming geometric expectations, and that this landscape has evidence for transient incision, like elsewhere in the region.

BACKGROUND

Lester King (1953) characterized escarpments as composed of three parts, a near vertical erosional face, a toeslope were talus is deposited, and piedmont marked by sediment transport. The toeslope area is the link between cliff sediment sources and piedmont transport systems, and it holds a record of processes directly below the escarpment. Key landforms in the toeslope along the Book Cliffs are remnant colluvial slopes, also known as talus flatirons. A talus flatiron is a bedrock slope mantled by colluvium, which has been separated from the cliff face by a combination of gullying and

subsequent lateral retreat of the escarpment (King, 1953; Koons, 1955). These geomorphic features are commonly observed in arid to semi-arid settings such as the southwestern United States, Israel, Africa, and Spain (Schumm and Chorley, 1966; Gerson and Grossman, 1987; Pinheiro and Neto, 2017). Talus flatirons are not preserved in all Colorado Plateau landscapes. This absence of talus has been attributed to the rapid mechanical weathering of especially sandstone clasts by freeze-thaw processes (Schumm and Chorley, 1966). Another requirement for the presence of relict talus is a significant cliff sediment source (Schumm and Chorely, 1966; Ward et al., 2011). Where tall cliffs exist and talus remnants are preserved, is a record of sediment production and cliff retreat can be preserved (Bryan, 1940; Koons, 1955; Schmidt, 1996).

Previous studies quantifying lateral retreat

When Schmidt (1996) was examining the Book Cliffs to determine the role of climate forcing on cliff retreat he also estimated rates of retreat over the Pleistocene. First, he simplified the cliff geometry by assuming the rocks of the cliffs were horizontal. Second, he assumed the timing of the two youngest talus were deposited during glacial-interglacial transitions. Therefore, the youngest generation of talus was assumed to be 12 ka in age, and the next oldest was 60 ka. He projected the surface of the flatiron using polynomial curves to approximate where the paleo-cliff face was. He then measured retreat distance from the top of the modern cliff face laterally to the projected curve. Schmidt (1996) estimated cliff-retreat rates of 2-3.5 m/ky.

Sheehan and Ward (2018) conducted a study using ^{36}Cl surface-exposure dating to understand rates and styles of erosion along, the Coal Cliffs, only ~50 km southwest of our Book Cliffs study area. This smaller, cuesta escarpment is composed of Cretaceous

sedimentary rocks that are stratigraphically just below those that form the Book Cliffs. Sheehan and Ward (2018) document a set of talus flatirons along the base of the Coal Cliffs with exposure ages ranging from 46 to 4 ka, with most ages clustering between 30-20 ka. They estimated rates of lateral cliff retreat by projecting best fit, second-order polynomial equations to flatiron-tread elevation profiles. The distance between the top bench of the modern cliff face and the projected polynomial profile was used as the distance of retreat, and rates were estimated between 3.2 – 18.1 m/ky. This range of retreat values is rapid compared to other records, which may be the result of using a short record with only one generation of talus as well as ignoring *in situ* weathering in their exposure-age calculation.

Farther south in Grand Canyon, Cole and Mayer (1982) attempted to use preserved and ^{14}C-dated packrat middens (nests) to estimate rates of cliff retreat below the Kaibab Plateau canyon rim. They note that active packrat middens are most commonly found within the first five meters of a cave entrances and quickly diminish in frequency farther from the entrance. Fifty-three middens collected from seven caverns were reported to range from 23 - 14 ka B.P. with most being between 20 – 15 ka B.P (Cole, 1981). Using a probabilistic relationship between midden position relation to the cave entrance and the radiocarbon ages, Cole and Mayer (1982) estimated rates of retreat of 0.18 – 0.72 m/ky for the Redwall Limestone cliff in eastern Grand Canyon. This method of cliff retreat is problematic for two reasons. First, like the Coal Cliffs this is a short record with retreat possibly accomplished by a single failure event. Second, retreat was calculated in this case by an indirect, probabilistic estimation of the original distance between the midden and cave opening.

Outside of the southwestern U.S., in the hyper-arid Negev Desert of Israel, Boroda et al. (2011) revisited the study area where Gerson and Grossman (1987) initially postulated a relation between climate cycles and escarpment evolution. Boroda et al. (2011) used OSL and cosmogenic ^{10}Be dating techniques, along with soil-profile analysis. The flatirons in the area were grouped into three sets by distance from the escarpments. They projected fitted polynomial profiles off of flatiron-trend profiles for the two closet sets of flatirons. They measured retreat via a horizontal distance from the top of the mesa escarpment to the projected profile and calculated 30m and 160m for the two sets of flatirons. Exposure ages of ~170ka and ~610 ka were used to calculate retreat rate and cliff retreat rates of 0.006-0.012 m/ky were calculated. Boroda et al. (2011) concluded that the calculated retreat rates are not able to account for the distances from the apex of the talus remnants to the cliffs alone, and Boroda et al. (2011) propose the talus flatirons themselves retreat away from the cliffs producing the majority of the retreat distance for the cliff as seen today.

Gutierrez et al. (1998) made estimations of escarpment retreat rates by projecting elevation profiles of two of three sets of flatirons along the toeslope of escarpments in the semiarid Ebro Depression, northeast Spain. Flatiron sediments were dated using a combination of archeological association and radiocarbon dating of charcoal found within deposits. Ages of 2.9 – 2.5 ka BP and 27 ka BP were found for the two analyzed flatiron sets. Flatiron elevation profiles were fitted with 2-D log-functions using regression analysis, and a horizontal line was projected from the top of the modern scarp to the projected surface to measure lateral distance. In combination with their age control, these profile measurements result in retreat rates of 0.9m/ky – 1 m/ky.

Elorza and Martinez (2001) returned to Ebro Depression, northeast Spain where Gutierrez et al. (1998) estimated rates of retreat on two sets of flatirons. Sediments from three sets of flatirons were dated using radiocarbon dating and yielded ages of 1 ka BP, 3.5 ka BP, and 28 ka BP. Flatiron elevation profiles were fitted with 2-D log-functions using regression analysis. A horizontal line was projected from the top of the modern cliff to the projected curve to measure lateral retreat distances. With their age control and these profile measurements result, retreat rates between generation of flatirons were calculated to 0.5 m/ky between the 2nd and 3rd set of flatirons and 10.5 m/ky between the 1st and 3rd set of flatirons. The large retreat rate is the result of using the youngest, partially attached flatiron in retreat rate calculations.

Lateral retreat and denudation

Rock strength and dip of the rock have been considered primary controls when considering patterns of erosion in cliff-bench landscapes like the Book Cliffs (Forte et al., 2016) as well as weathering and erosion rates on the plinth (Ward et al., 2011). Forte et al. (2016) modeled the effects of rock strength and structural dip on landscape evolution in such settings using a modified version of the CHILD model of Tucker et al. (2001). The modeling assumes that cliff retreat is driven by bottom-up, stream power processes driven by a constant uplift or baselevel fall, while they prescribed hillslope processes as simple linear diffusion. Forte et al. (2016) found the dip of the rock controls the pattern of erosion intensity and localization in a landscape. Increasing rock dip shifts the location where scarp retreat begins, from where a drainage exits a canyon towards the center of the catchment. The modeling of Forte et al. (2016) shows that increases in dip control the direction of retreat and tend to increase the localization of erosion into cliff bands and knickzones, and

that these elements erode faster than low benches do, even under simple constant baselevel fall. Therefore, in moderately inclined rocks lateral retreat should be significantly faster than vertical denudation. This modeling does not consider top-down changes in sediment production and transport processes (Chapter 2). Yet, faster erosion of cliff bands versus benches has been empirically recognized in recent studies (Riley et al. 2019; Darling et al., in press).

In the case of the Book Cliffs, the geometric relationships of an idealized system in topographic equilibrium can be used for a baseline prediction of how vertical incision and lateral retreat compare (Figure 3.1). With equilibrium topography, for every amount of vertical incision there is a corresponding amount of lateral retreat. Four key measurements can be obtained: incision between T_0 and T_1 (z), lateral retreat between T_0 and T_1 (x), bedrock dip angle (α), and the gradient of toeslope drainages (β) where incision is measured (Figure 3.1). Using the values of z, α, and β, one can calculate the amount of lateral retreat, x, that corresponds to the incision, z. First, we divide z into z_1 and z_2 to form right triangles and utilize the tangent of α and β to solve for x.

$$x = \frac{z_1}{\tan\alpha} = \frac{z_2}{tan\beta} \qquad \text{Eq. 3.1}$$

Since z is the sum of z_1 and z_2, we can reorganize this to:

$$x = \frac{z}{(\tan\alpha + \tan\beta)} \qquad \text{Eq. 3.2}$$

Equation 2 can be used with measured angles of bedrock dip and toeslope gradient to predict how much lateral retreat should occur for a given amount of vertical incision over time (Figure 3.2). For example, with the Book Cliffs, bedrock dip $\alpha = 5^o$ and an average

toeslope stream-gully gradient $\beta = 3^{o}$. Then with vertical incision z = 10 m, the predicted lateral retreat (x) is 71 meters, a ~7:1 geometric ratio of retreat to denudation.

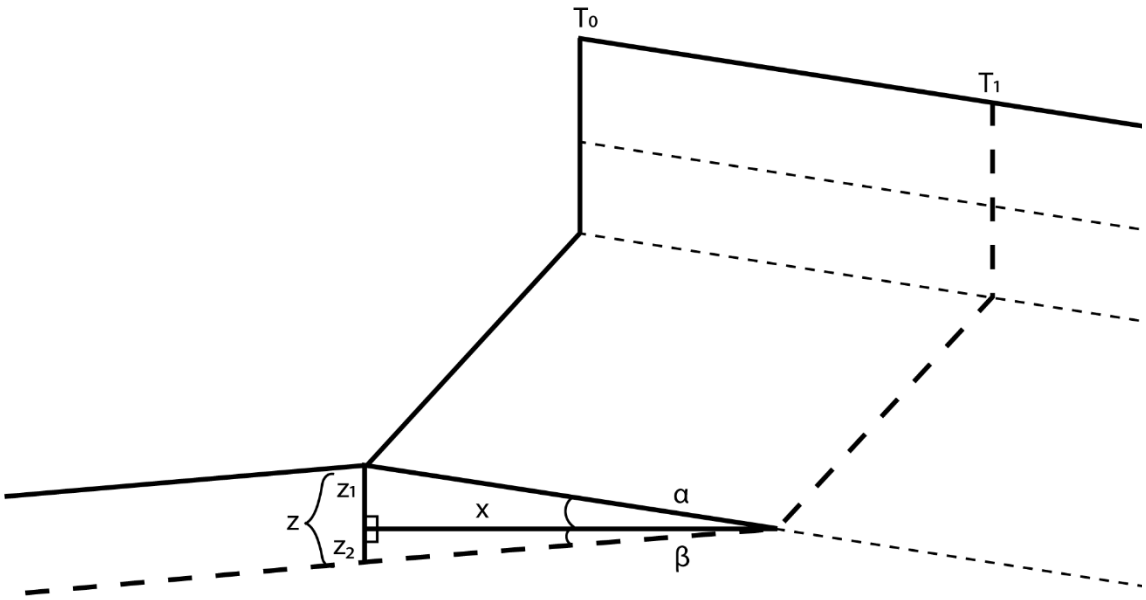

Figure 3.1. Schematic of cliff retreat assuming the profile of the cliff is maintained as an equilibrium form. Geometric relations are denoted for idealized lateral retreat and vertical denudation calculations.

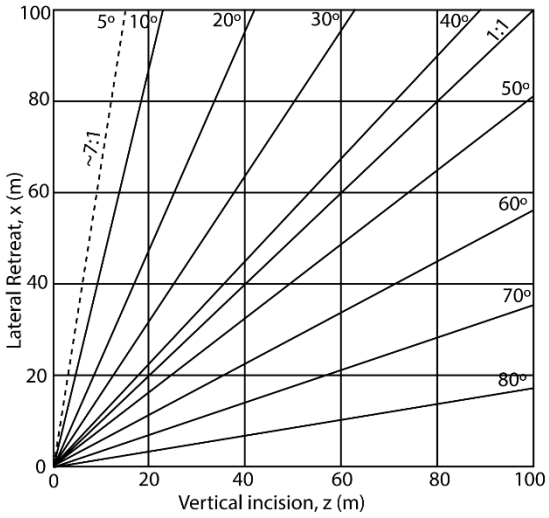

Figure 3.2. Ratios of lateral retreat to vertical incision as a function of bedrock dip as predicted by Eq. 2 with average gradient of first-order piedmont-gully drainages being 3°. The 5° bedrock-dip line (dashed) characterizes the Book Cliffs study area, with an expected retreat-to-denudation ratio of ~7:1.

Setting

This research focuses on the Book Cliffs of central Utah, which features four generations of Pleistocene talus flatiron (Figure 3.3 and Figure 3.4) (Koons, 1955; Schumm and Chorley, 1966). The escarpment is situated between the Laramide structural dome of the San Rafael Swell to the southwest and the Uinta Basin to the northeast. The Book Cliffs lie along the limb between these structures and the Cretaceous beds of the cliffs dip to the northeast toward the Uinta Basin, a 5-10°.

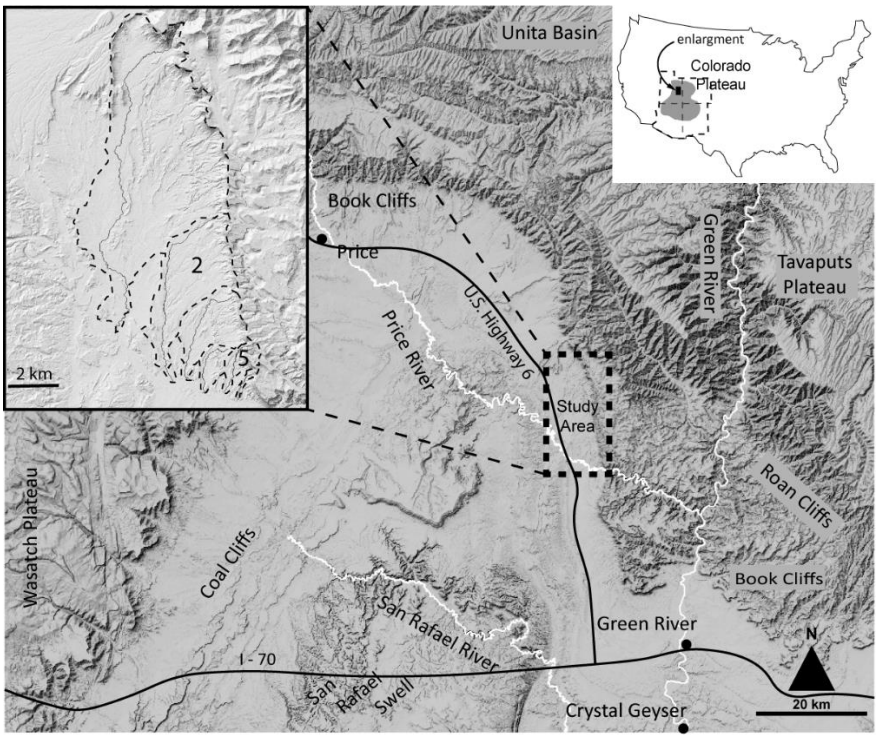

Figure 3.3. Regional map with the study section of the Book Cliffs enlarged.

Figure 3.4. Example of a Book Cliffs C_2 talus flatiron and partially abandoned C_1 deposit. Visible basal strath of colluvial remnants on Mancos Shale (K_{ms}) is denoted by white lines. The lower sandstone unit of the cliffs is the Black Hawk Formation (K_{bh}).

The Book Cliffs begin near Price, Utah, and the escarpment terminates near Grand Junction Colorado (Figure 3.4.). The cliffs are 300-600 meters in height and extend ~400 kilometers. The base of the Book Cliffs is composed of the easily erodible Cretaceous Mancos Shale. This unit underlies the primary toeslope or plinth, and the piedmont extending down slope of the cliff. This shale is overlain by the Mesa Verde Group, which is composed in ascending order of the Black Hawk Fm. and the Castlegate Sandstone member of the Price River Formation (Richardson, 1909; Fisher et al., 1960).

The top of the cliffs is held up by the Castlegate Sandstone with less pronounced cliffs formed by lower sandstones (Figure 3.4).

Drainages of the Colorado Plateau are characterized by deeply incised canyons formed in response to the uplift of the Colorado Plateau and the late-Cenozoic integration of the Colorado River into the low Basin and Range. Late-Pleistocene incision rates of 450 m/my have been calculated at Crystal Geyser for the Green River, 50 km south of the Book Cliffs (Figure 3.3; Pederson et al., 2013b). However, upstream of Crystal Geyser at the head of Desolation Canyon where the Green River steepens and crosses both the Roan and Book Cliffs, rates of incision have been estimated at only 43m/my, a full magnitude less (Darling et al., 2012). This suggests a wave of incision is crossing the Desolation Canyon reach of the Green River (Pederson et al., 2013a), adjacent to our study area.

The 20-km transect of the Book Cliffs examined in this study lies between Price and Green River, Utah. This section of the escarpment was chosen due to the aspect and lithology being constant. The northern section is marked by an alluvial fan that extends out of Horse Canyon (Carter, 1981). The southern end of the study area is where the path of the Price River cuts through the Book Cliffs on its way to the meet the Green River. The study transect varies systematically in elevation and distance from the local base level of the Price River, with both increasing to the north.

RESEARCH DESIGN

Flatiron profile generation

A 1ft (0.3m) pixel resolution LiDAR data set was used as the base data set for the generation of topographic profiles in ArcGIS, and a 5m resolution autocorrelated DEM downloaded from the Utah Automated Geographic Reference Center was used in places the LiDAR was unavailable. DEMs were prepared for hydrologic analysis and drainages defined using standard *fill, flow direction,* and *flow accumulation* tools in ArcGIS. The flow accumulation data set was then reclassified to a specific threshold contributing area draining the Book Cliffs. The channel-head contributing area threshold was set to 2,000 m^2, based on observations in the study area. This raster was converted to a feature using the raster-to-polyline tool for later profile construction.

The *watershed delineation* tool was used to create drainage divides, and these divide lines were pieced together manually to compile a profile from the top of the cliff face, downslope over the crest of talus flatiron, and along the highest parts of Pleistocene deposits on the toe slope to at ≥~1 km onto the piedmont (Figure 3.5). Pourpoints, above which drainage areas are delineated, were placed above every confluence of ~2^{nd} –order channels, generally following the location of a resistant bed outcropping along piedmont, which acted as a distance guide for the length of profiles. Segments of drainage divides where selected to create a profile line along targeted, well preserved flatiron. Once all line segments were selected, the profile line was confirmed to be free of gaps, then

extracted using the dissolve tool. This process was repeated for stream profiles nearby targeted flatirons generated during hydrologic analysis.

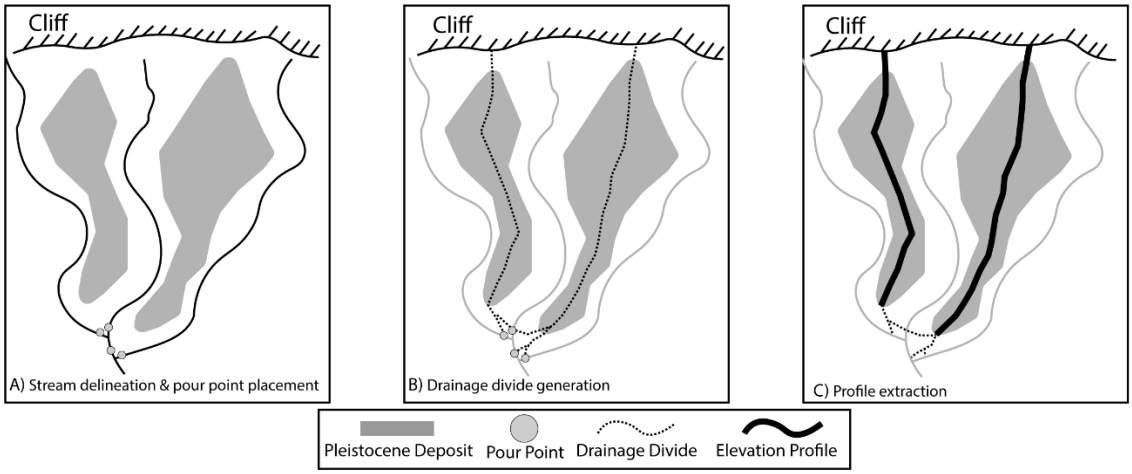

Figure 3.5. Steps in flatiron-profile generation and extraction. A) Follow GIS workflow for delineating drainages, pour points placed just above confluences; B) Drainage divides are generated following spines of Pleistocene flatirons; C) Portions of drainage divides are selected to extract elevation data profiles.

The *interpolate* shape tool in ArcGIS was then used to extract elevation data from the DEMs to the profile lines using a 10-meter sampling distance. Through a visual inspection, elevation profiles were classified into quality categories of poor, intermediate, and good as a function of, presence of flatiron apex, separation from cliff face, and continuity of piedmont. Point profiles designated "good" were exported to Microsoft Excel for slope analysis and flatiron profile fitting and projection

Measurement of lateral retreat and denudation distance calculations

For each talus-flatiron profile, slope was calculated in a 50 m moving window in Excel to locate where slope declines to 0.1 (~5 degrees) -- a threshold that approximates the slope break between talus and debris-flow alluvium of the toeslope. This was used as an objective way to delineate the true talus-flatiron profile to fit a curve to. Projection of

talus-flatiron profiles above this threshold was then performed in Matlab. Matlab code using the *polyfit* function was used to least-squares fit a power-law equation to each flatiron elevation profile. Each power-law fit was then used to project the profile upslope beyond remnant talus flatirons (Figure 3.6). This projected profile is then used to estimate the position of the cliff at the time the flatiron talus formed, and measure the subsequent retreat distance via two methods outlined below (Figure 3.6).

Previous studies have used polynomial and logarithmic curves for projection and lateral retreat calculation (Gutierrez et al., 1998; Sheehan and Ward, 2018). However, in the case of our study area we choose to use a power law for two reasons. First, due to its simplicity and applicability to drainage profiles. In the geomorphic sense, *a* is the steepness (k_s) and *b* the concavity (θ) in such a power-law function:

$$z = ax^b \qquad \text{Eq. 3.3}$$

Second, we found that polynomial curves would commonly projected into the modern escarpment, while power-law projections better represent paleo-cliffs necessary to deliver tock falls recorded in flatirons.

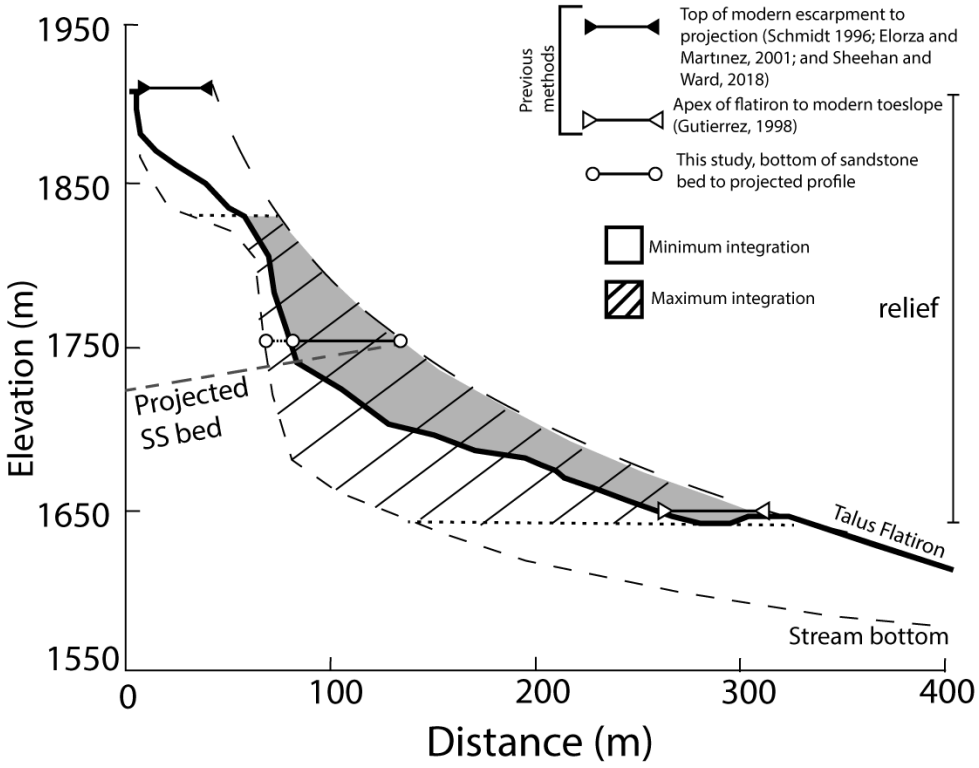

Figure 3.6. Approaches to determine retreat distance. The lines with triangle end points represent the approaches used by previous studies, where the apex of the preserved flatiron to modern toeslope distance is used or the top of the modern escarpment to projection. The line with circular end points represents the approach used in this study. The bottom of the lowest sandstone-bed cliff is projected out to intersect with the projected flatiron profile. Shaded and hashed areas illustrate the integrated difference in area used to calculate minimum retreat distance (grey) and maximum retreat distance from modern gully drainages (hashed). Both areas are divided by relief, with the upper bound defined by the lowest sandstone bench of the escarpment.

Lateral retreat measurements were done by two methods. The first is a modified version of the approach used in previous studies such as Gutierrez (1998), Elorza and Martínez (2001), and Sheehan and Ward (2018). These previous workers projected a horizontal line form the top of the cliff face to where it meets the projected flatiron profile or from the apex of the flatiron to the modern toeslope in order to measure lateral retreat (Figure 3.6). Our modified method projects the bottom of the lowest cliff-forming bed out to where it meets the projected flatiron profile, taking into account the dip of the

beds (Figure 3.6). A horizontal line is measured from the intersection on the projected profile to the modern cliff face.

The second and novel method we employ is based on integrating areas between projected elevation profiles and modern topography using the *trapz* function in Matlab. In order to get an integration with no missing area, the profiles z and x dimensions are transposed so that, effectively, the area between curves is calculated laterally (Figure 3.6). The average lateral distance of retreat for the cliff can be computed using the area between profiles, divided by the relief:

$$\Delta x = \frac{A_{projection} - A_{cliff\ profile}}{profile\ relief} \quad \text{Eq. 3.4}$$

For the area integration approach, we can calculate a minimum and maximum lateral distance. Using the minimum area integration approach, the distance is calculated exclusively from the elevation profile as it follows the drainage divide up a flatiron to the modern cliff face. A lateral retreat calculated from this profile are minimum distances due the drainage divides being the highest points in a landscape and thus may have not changed much in elevation since the time of talus deposition. The maximum area integration approach is calculated from the cliff face elevation profile as well as a single gully profile closest to flatiron profiles. Retreat distances calculated from a projected flatiron to the gully profile are maximum distance because measuring to a gully bottom represents maximum amount of erosion that has occurred since the deposition of the talus-flatiron. We then adopt the average of these minimum and maximum values as the best estimate for comparison.

Vertical incision distances were measured using the same integration approach. A single gully profile, same used in lateral retreat calculations, closest to flatiron profiles were extracted and the area between stream bottom and the nearby talus projection was found by integrating using the *trapz* function. The maximum downslope limit of this integration was set to the full length of the flatiron profile as was determined when divide lines were pieced together during profile construction in ArcGIS. Therefore, incision rates include not only the talus flatiron, but also the proximal piedmont.

Terrain Analysis

Drainage profiles were extracted for the six largest piedmont drainages to explore spatial patterns using k_{sn} and χ in Matlab (Wolfgang and Scherler, 2014). The stream power erosion law can be simplified such that gradient of the channel scales to drainage area for a channel profile in steady state with a constant uplift rate and uniform erodibility, (Hack, 1957; Flint, 1974). A common formulation of this scaling behavior is known as Flint's Law,

$$S = k_s A^{-\theta} \quad \text{Eq. 3.5}$$

where S is channel gradient, A is upstream contributing area, k_s is a channel steepness index, and θ is a concavity index. While k_s can be used to compare channel steepness along a single drainage, it unsuitable for comparison across drainages of different, sizes, shapes, and setting due to its value varying with drainage area and concavity. Therefore, a fixed, reference concavity (θ_{ref}) can be used for a normalized steepness index:

$$S = k_{sn} A^{-\theta \mathrm{ref}} \quad \text{Eq. 3.6}$$

(Whipple et al, 2013). k_{sn} can be used to identify reaches of fluvial systems that do not match the expected equilibrium profile with the concavity of θ_{ref}.

Another more direct method for analyzing stream profiles is plotting the elevation along the stream against another steepness index, χ. In this case elevation (z) is the dependent variable while χ is an integral of contributing drainage area function (Perron and Royden, 2013). χ is defined following the stream power erosion law as:

$$z(x) = z(x_b) + (\frac{U}{KA_O^m})^{\frac{1}{n}}\chi \qquad \text{Eq. 3.7}$$

with

$$\chi = \int_{x_b}^{x} (\frac{A_o}{A(x)})^{\frac{m}{n}} dx, \qquad \text{Eq. 3.8}$$

where $z(x_b)$ is the elevation at the stream base level, U is rock uplift or baselevel fall, K is an erodibility coefficient, m and n are empirical coefficients, and A_o is a reference drainage area. When plotted with consistent concavity (m/n), χ for an equilibrium profile is linear and its slope is a normalized steepness index, while breaks in slope identify knickpoints. Also, since χ is a representation of relative position in the drainage network independent of basin size, knickpoints with a common source should collapse to a common value on the χ axis for all tributaries in a catchment (Perron and Royden, 2013). χ can also be used to reveal contrasts in adjustment to baselevel fall and to predict migration of drainage divides by mapping the values in planform across the landscape (Willett et al., 2014). Although this latter analysis was conducted for the study area, it had no significant or pertinent results and is not presented here.

Error Propagation

The range in lateral retreat distances, the error in the LiDAR dataset, as well as the mean 2σ error of the mean depositional age of geomorphic units were incorporated in the retreat rate uncertainty through arithmetic error propagation:

$$x = a + b - c; \quad \sigma_x = \sqrt{\sigma_a^2 + \sigma_b^2 + \sigma_c^2}, \qquad \text{Eq. 3.9. a}$$

$$x = \frac{a * b}{c}; \quad \frac{\sigma_x}{x} = \sqrt{(\frac{\sigma_a}{a})^2 + (\frac{\sigma_b}{b})^2 + (\frac{\sigma_c}{c})^2} \qquad Eq. 3.9. b$$

Where *a*, *b*, and *c* are measured variables (such as luminescence age or lateral retreat distance) with associated uncertainty or variance of σ_a, σ_b, and σ_c, *x* is a value calculated form these variables (such as retreat rate), and σ_x is the corresponding uncertainty of that value (Cadwell and Vahidsafa, 2013). Using these equations, the cumulative uncertainty of lateral retreat rate is reported as its standard deviation. When considering the error associated with the high-quality nature of the LiDAR dataset, we assume it was near zero for purposes of propagating errors. Therefore, all of the error in our reported average rates is the result of the large variance in retreat distances and the error associated with the average OSL errors.

RESULTS

Retreat rates and incision

A total of 46 talus profiles of "good" quality were generated, projected, and used to calculate retreat distances and vertical incision across the Book Cliffs toeslope. Forty-one of those are from C2 landforms, C4/3 are represented by five. C1 landforms are still attached to the cliff face and so effectively have a retreat distance of 0 m. Therefore, the

most robust results are from C2 landforms. The two methods used to calculate retreat distances, bed projection and area integration, produced coherent results. Full results are in Appendix B, with summary statistics in Table 3.1. In fact, the bed projection and the minimum values for area integration results, both using the modern drainage divide profile, match well. However, the maximum values are much greater and average values for area-integrated retreat distances are approximately 2x greater than simple bed-projection results.

TABLE 3.1. AVERAGES AND STANDARD DEVIATIONS OF RETREAT DISTANCES FOR GEOMORPHIC UNITS MEASURED BY AREA-INTEGRATION METHOD

Geomorphic Unit	# of profiles	Bed-projection (m)	Min. Integrated area (m)	Max. Integrated area (m)	Ave. Integrated area (m)
C2	41*	47 ± 32	30 ± 0.5	212 ± 108	105 ± 63
C3/4	5	109 ± 22	110 ± 30	353 ± 81	228 ± 45

* 35 gully profiles were paired with the 41 flatiron profiles for maximum areas, due to some flatirons being adjacent to the same gully profile and certain gully profiles being corrupted by errors during extraction.

The average retreat distance from the 41 C2 flatirons is 105 ± 63 m with the area-integration method, and the average is 228 ± 45 m for C4/3. To convert distances to rates, we divide these average lateral retreat distances by the average OSL age of the deposit, 117 ± 9.4 ka for C4/3 and 57 ± 2.5 ka for C2 (Chapter 2) (Table 3.2). Due to the difficult nature of differentiating generation 3 and 4 flatirons without OSL chronology we use the older generation 4 average age in order to be conservative in our calculation of retreat rates. The resulting, average C2 retreat rate is 1.84 ± 1.1 m/ky and 1.9 ± 0.4 m/ky

for C4/3. The average rates of retreat for C2 and C4/3 match very closely when the area-integration approach is used.

TABLE 3.2. AVERAGE AND STANDARD DEVIATION OF RETREAT RATES FROM AREA-INTEGRATION APPROACH

Geomorphic Unit	Min. Retreat Rates (m/ky) *			Max Retreat Rates (m/ky) *			Ave Retreat Rates (m/ky) *		
C2	0.52	±	0.3	3.81	±	1.9	1.84	±	1.1
C3/4	0.93	±	0.3	2.97	±	0.7	1.92	±	0.4

*Using ages of 54ka (C2), and 117 ka (C3/4) based on chapter 2.

To explore any influence of baselevel proximity on rates of retreat, we plot the retreat rates for individual talus-flatirons by their upstream distance from the Price River along piedmont drainage lines. Figure 3.7A illustrates that there is no significant trend. The cliff, no matter how far from baselevel, is locally retreating between 1.25 m/ky and 3.5 m/ky across the entire study reach, with only one outlier at 4.5 m/ky.

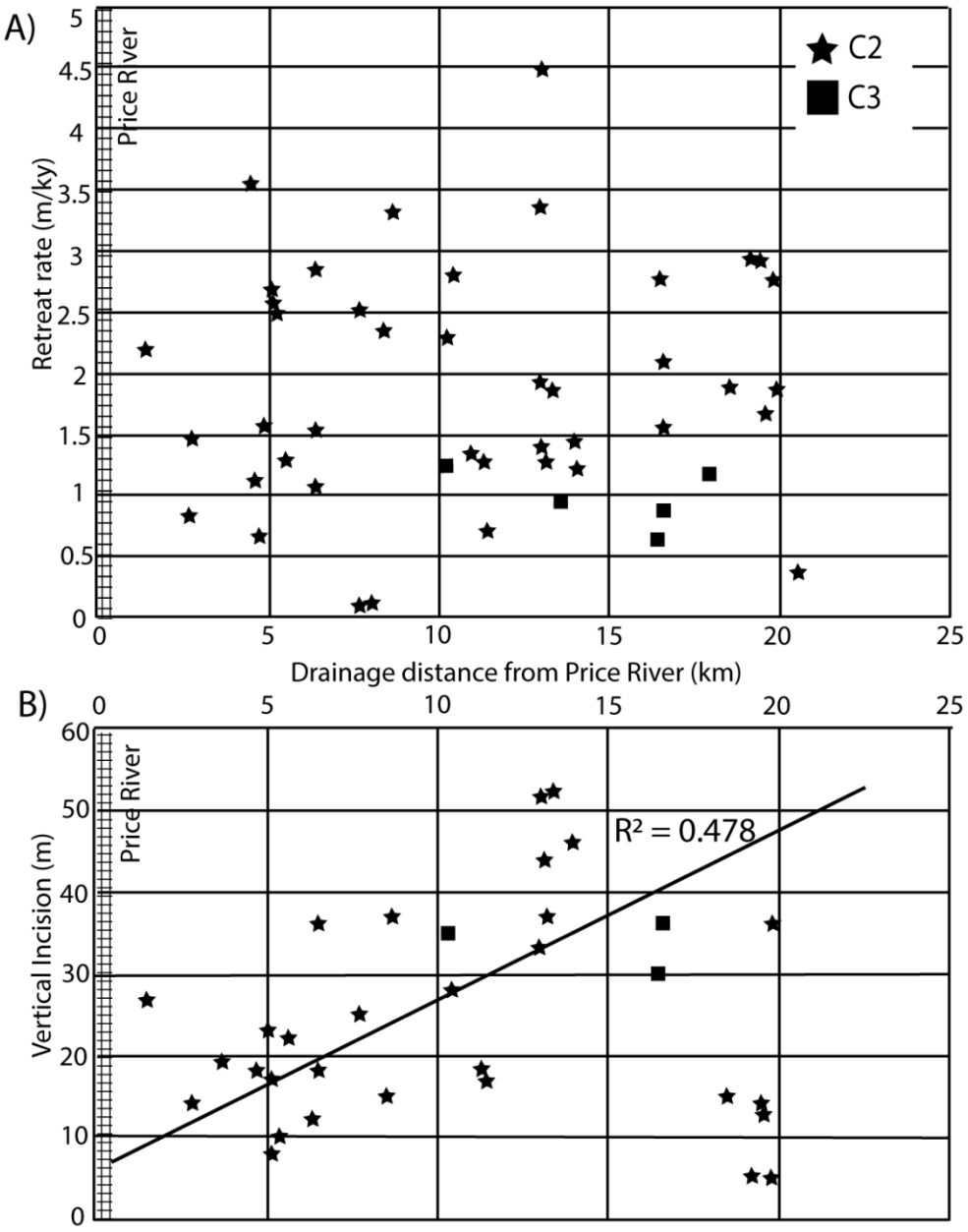

Figure 3.7. A) Retreat rates for individual C2 and C4/3 remnants using age for each generation plotted against distance upstream along tributary drainages of the Price River, illustrating no correlation. B) Vertical incision distances for C2 and C4/3 deposits plotted against distance upstream along piedmont drainages, indicating increasing values as you move away from baselevel. The best fit line is excluding the outlier population in the bottom right.

A total of 40 drainage-gully profiles were generated and used to calculate retreat and vertical incision across the Book Cliffs toeslope. Thirty-five of those are linked to P2 landforms, while P3/4 are represented by five (Table 3.3). Therefore, the most robust results are from P2 landforms. The number of vertical profiles for P2 (35) is less than lateral profiles for C2 (41) due to some individual P2 profiles being used with two C2 profiles or due to vertical profiles being confounded by LiDAR data gaps during extraction. For the similar exercise of calculating vertical incision by profile area-integration, full results are found in Appendix B and a summary of statistics in Table 3.3. Average incision for P3/4 is 40 ± 3.0 m and P2 is 22 ± 13 m. The study area average incision rate calculated from the 40 profiles, with errors propagated through, was calculated to be 0.4 ± 0.2 m/ka. To convert distances to rates, we divide these average lateral retreat distances by the average OSL age the landform, 57 ka ± 2.5 for P4/3 and 117 ± 9.4 ka for P2 (Chapter 2). The incision rate is calculated to 0.3 ± 0.17 m/ka for P4/3 and 0.4 ± 0.21 m/ka for P2 with errors propagated through using equations 10 and 11.

TABLE 3.3. AVERAGE AND STANDARD DEVIATION OF INCISION DISTANCES AND RATES

Geomorphic Unit	# profiles	Average vertical incision (m)			Vertical incision Rate (m/ky)		
C2	35	22	±	13	0.43	±	0.21
C4/3	5	40	±	3.0	0.31	±	0.17

*Using ages of 54ka (C2), and 117 ka (C3/4) based on chapter 2.

When comparing this proximal piedmont incision to distance from baselevel, as done with lateral retreat, a different result is evident. A rough trend of increasing incision with increasing distance from the Price River can be observed (Figure. 3.7.B). C2 values exhibit a small cluster of low incision outlier values far from baselevel, which do not follow the general trend of the remainder of the data (Figure 3.7B). These outliers correspond to a localized group of flatirons in the far-northern portion of the study area. Regardless, vertical incision if anything, actually increases away from local Price River baselevel, which is not consistent with baselevel controlling patterns of toeslope incision.

Geometric relations between lateral retreat and vertical incision

Focusing on the larger C2 dataset, we compare rates of lateral retreat to vertical incision and find that lateral retreat is consistently greater than vertical incision (Figure 3.8). A least-squares linear regression for these data is not significant, with data points falling in a broad envelope between 20:1 to 1:1 lateral to vertical rates. The 7:1 ratio predicted from geometry in the Book Cliffs study area lies in the heart of this envelope. Errors for the individual lateral and vertical retreat rate calculation is a propagated 9.25% uncertainty of the mean generation two OSL age calculated in Chapter 2.

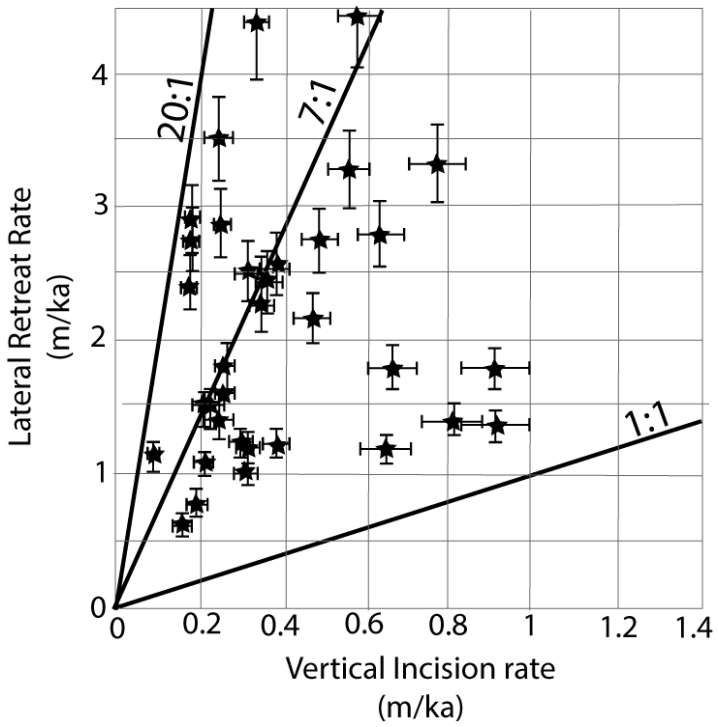

Figure 3.8. Lateral retreat rates for C2 as a function of corresponding incision rates. Points occur with great spread between 1:1 and 20:1. The geometric prediction of ~7:1 is show to be within the data cloud.

Drainage steepness, knickpoints, and baselevel

Six major drainages draining the Book Cliffs piedmont were analyzed using χ and k_{sn} steepness metrics as well as basic stream profiles using a reference m/n (concavity) value of 0.45 (piedmont-drainage concavity in the study area ranges form 0.3 – 0.9; full results in Appendix. C and D). With piedmont-drainages numbered from north to south across the study area (see Fig. 3.3 inset and Fig. 3.10 below), profiles 1, 2, and 3 exhibit evidence of knickpoints above steeper, lower drainages, with drainage 2 shown as an example in Figure 3.9A. Drainage profiles 4, 5, 6 show no clear evidence of steepened, lower reaches, however drainages 5 and 6 show steeper headwaters. Drainage 5 is shown

as an example in Figure 3.9. χ steepness profiles show similarly steep lower trunk streams across the entire study area with distinctively flatter contributing gully drainages across the piedmont (Figure 3.9, Appendix C). The profiles of trunk streams also change in slope with a knickpoint at ~2 χ (km) for all three northern drainages (Figure 3.9B and Appendix C). Drainage 5 exhibits a steep increase in gradient in upper reaches (Figure 3.9B) due to the upper gully running over a convergent colluvial hollow and then up the cliff face.

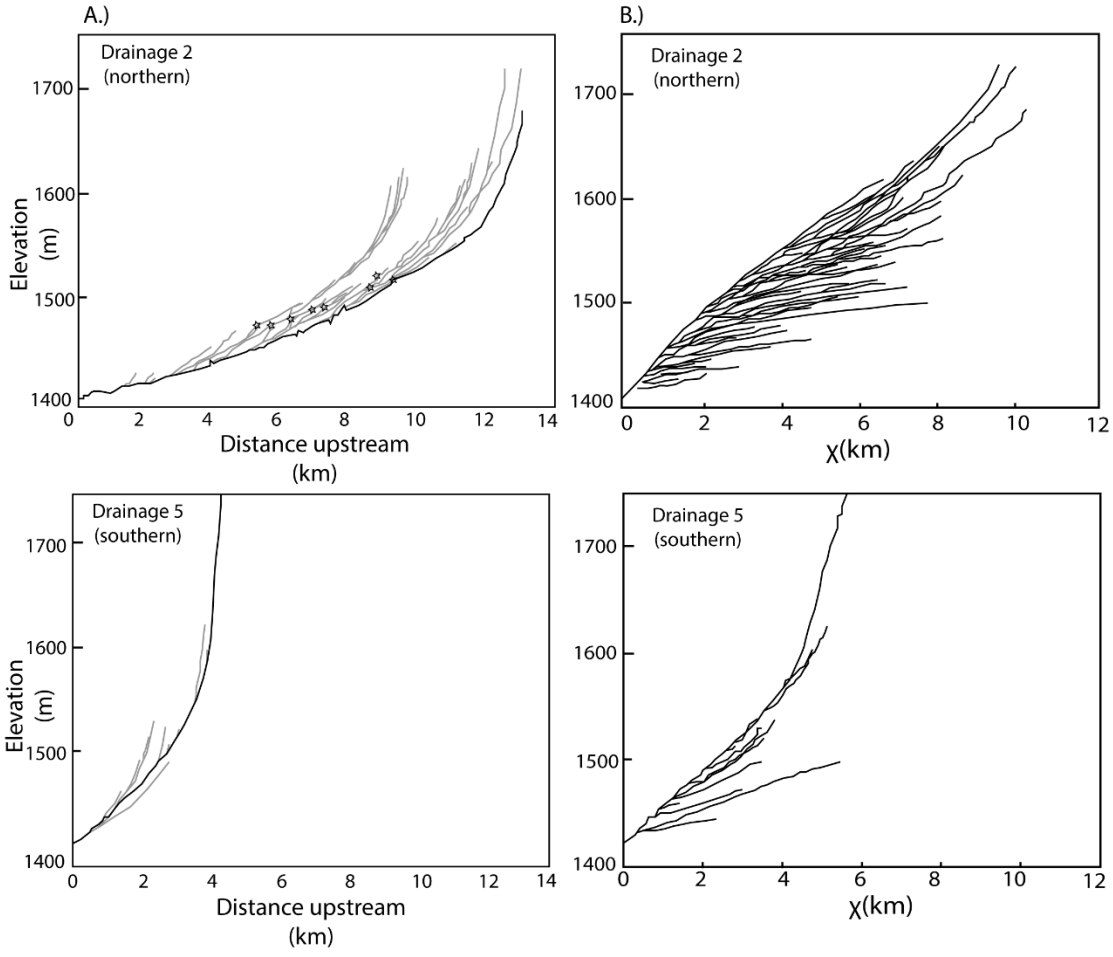

Figure 3.9. A.) Drainage profiles for two representative examples of the six study catchments of Book Cliffs study transect. Note in drainage 2 the presence of knickpoints, some highlighted by stars. B.) χ -plots for the same drainages using a m/n of 0.45. Note change in slope at approximately ~2 χ (km) and the distinctively flatter tributary streams.

When comparing the χ profiles of just the trunk drainages of those six tributaries, a north-south trend can be observed (Figure 3.10B). χ profiles become less steep to the south, with the largest northern drainage being steepest and the smallest southern drainage the shallowest. We hypothesize that this may reflect systematically coarser bed material derived from the increasingly higher cliffs of the northern catchments. An exception to this is the trunk stream of drainage 4, which is significantly shallower than its neighbors of comparable size. We attribute this to its catchment covering only low-lying piedmont areas (Fig. 3.10A), and therefore lacking large-caliber clasts in its channel bed from cliff mass-wasting.

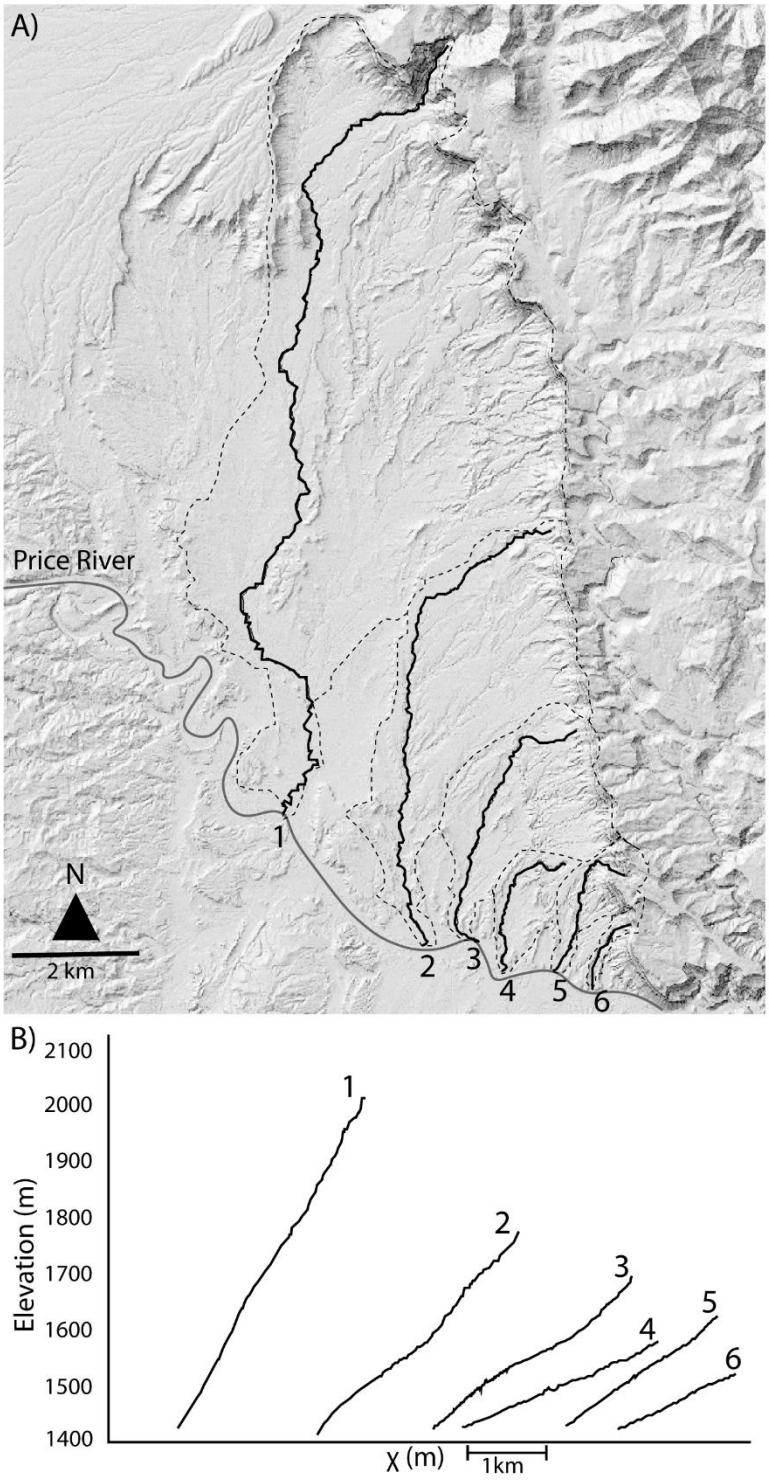

Figure 3.10. A) Drainages (solid back lines) of the six largest mainstem catchments (dashed lines) within the study transect. B) The corresponding χ profiles for each trunk stream, offset according to position of confluence with Price River to visually correspond with the trunk streams above.

K_{sn} maps using a reference steepness of 0.45 confirm the results of the χ analysis, with steeper, lower trunk drainages (Figure 3.10 and 3.11; Appendix C). This analysis likewise confirms that the southern drainage 5 has an extremely steep headwater reach in an area of converging toeslopes.

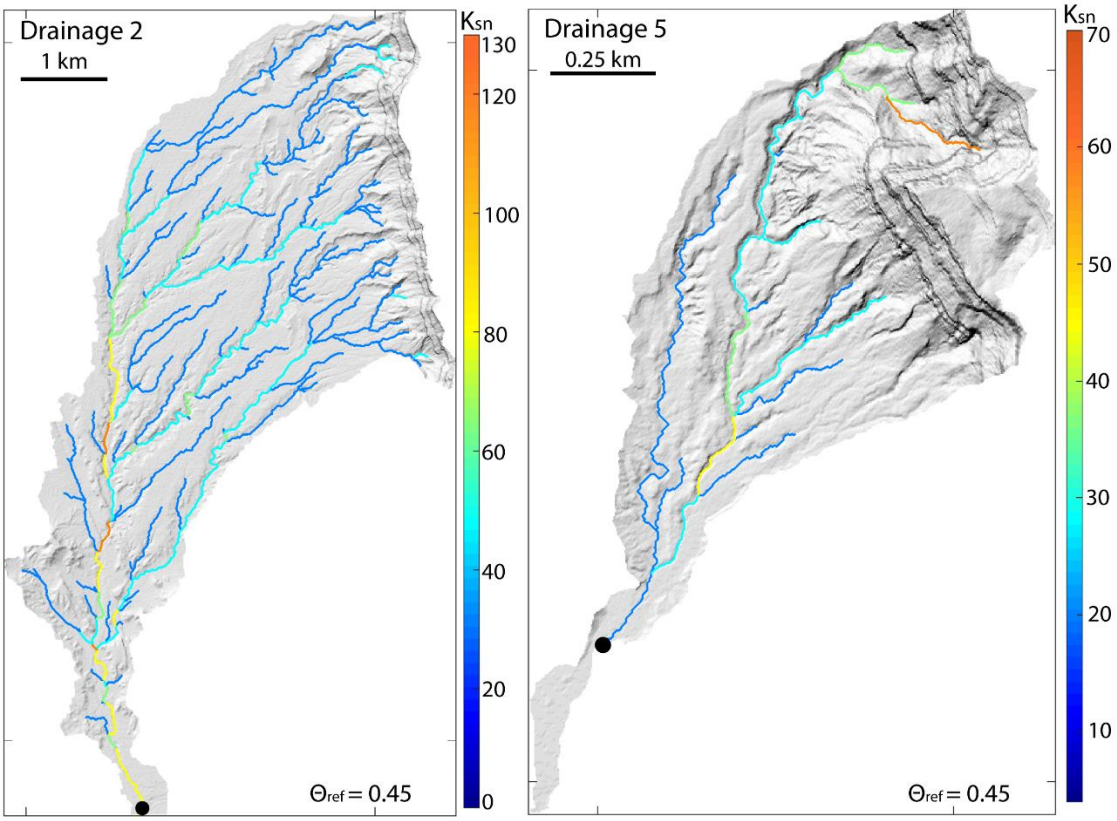

Figure 3.11. k_{sn} maps for two representative drainages of the Book Cliffs study transect. Note the low k_{sn} values in the headwaters and higher values in the steeper trunk of drainage 2, whereas in drainage 5 the headwaters in the toeslope are very steep and trunks are shallower compared to drainage 2.

DISCUSSION

Methods of measuring lateral retreat

Previous workers that measured lateral retreat used polynomial, logarithmic, or power-law profiles projected off flatiron treads, and they measured horizontal retreat distances from the top of the cliff face. We modified this approach by integrating the entire cliff face-toeslope region of an elevation profile and by taking into account dipping rocks in the lateral distance measurement. Through this area-integration approach, our minimum estimates match results following previous methods, yet our averages of maximum and minimum retreat distances produce significantly greater distances, which we suggest are more realistic. Our method estimate retreat across the length of an escarpment rather than just along modern gully-drainage-divides with minimum erosion. This area-integration method has three advantages. First, the drainage-divide profiles can be replicated independently and objectively, unlike previous studies that extract elevations from a subjectively drawn profile line. Second, the area-integration approach accounts for retreat for the majority of the cliff face and toe slope region, whereas previous methods rely on a single linear measurement at some point on the cliff face to projected profile. Third, previous methods assume that the cliff face is composed of nearly horizontal rocks for the lateral distance measurement.

Comparison of retreat rates to other local and global records

The combined use of a robust geochronology comprised of both colluvial and piedmont deposit ages as well as our new method of measuring lateral retreat coupled with the high-resolution LiDAR coverage has produced a high-quality measurements of

escarpment retreat. Furthermore because of these factors, we suggest this study provides the best constrained rates of escarpment retreat in the southwestern United States and perhaps globally.

For an independent, back-of-the-envelope, minimum estimate of the magnitude of retreat in the study area, we can roughly calculate the volume of material contained in Generation 2 deposits and then geometrically restore that to the cliff to derive the corresponding amount of retreat for just that deposit. The total area of catchments 2 through 5 is 35,750 km^2, and the Generation 2 deposits on average are ~5 m thick, therefore ~180 km^3 of material was stored along the piedmont of the Book Cliffs at the end of Generation 2 time. The cliff face in the study area is on average 250 m tall and is 18 km in length, covering an area of 4.5 km^2. Dividing the volume of stored material by this cliff-face area, results in a mean thickness of restored rock of 40 m. That is, 40 m of lateral retreat would account for the volume of sediment stored on the Generation 2 piedmont. However, this is only a minimum retreat estimate because we must assume that a significant portion of sediment produced in Pleistocene time escaped storage along the piedmont and was routed down the Price River. This back-of-the-envelope exercise suggests that every preserved deposit generation represents at least several 10's of meter of escarpment retreat. Furthermore, it also suggests that our average retreat distance of 105 meters and rate 1.8 m/ka, is a reasonable and consistent result for the study area.

Our lateral retreat rate for the Book Cliffs of ~1.9 m/ky falls between those of the eastern Grand Canyon, 0.18 – 0.72 m/ky, and the nearby Coal Cliffs, 3.2 – 18.1 m/ky. Considering how these previous measurements were produced, it may explain why they are significantly different than our values. The Grand Canyon rate was calculated by an

indirect, probabilistic estimation based on the position of packrat middens from the cave entrance. This probabilistic method used due to a combination of middens age and position that when modeled produce a retreat rate solution that is smaller than expected. The Coal cliffs rate is misleading due to being calculated from a short record and exposure ages that rely on in situ weathering estimates which together can lead to overestimations. Finally, Schmidt's (1996) strictly geometric estimated retreat rates of 2-3.5 m/ky for the Book Cliffs, is only slightly greater than our estimate. In fact, Schmidt's assumption that talus deposition is linked to glacial-interglacial transitions approximately matches our dataset.

Book Cliff retreat rates are much greater than those calculated in the Negev, Israel, 0.006-0.012 m/ky. The low rates of found in Israel are most likely related to one of the conclusions of Boroda et al. (2011) -- that continual hyper-arid conditions over the Pleistocene resulted in slow retreat. In the Ebro Basin, Spain, retreat rates of 0.5 – 1.5 m/ky are slightly slower than rates for the Book Cliffs. The similar Spanish rates may be due to similar semi-arid climate histories. Other controls such as lithology and baselevel-fall rate may contribute to the differences between the Book Cliffs and global rates.

Comparison of incision rates regionally

Incision rates for the Green River of 0.45 m/ky have been calculated at Crystal Geyser, 50 km south of the Book Cliffs (Figure 3.3; Pederson et al., 2013b). However, upstream of Crystal Geyser at the head of Desolation Canyon where the Green River steepens and crosses both the Roan and Book Cliffs, rates of incision have been calculated to 0.043 m/ky, an order of magnitude less (Darling et al., 2012). Our 0.4-0.5 m/ky rates of incision of Generation 2 and 3 toeslopes match those at Crystal Geyser.

However, our rates are calculated from the upper toeslope areas, not from trunk streams and therefore are measure of the rate of gully incision rather than river incision. Still, this is evidence that Pederson et al.'s (2013a) interpreted wave of incision passing through regional drainage systems has already reached the Book Cliffs study area.

Steepness trends and baselevel

Steepness profiles show that piedmont drainages #1-3 have knickpoints and steep, lower reaches whereas drainage #5 and 6 have less evidence of such. Drainage #4 since it is not connected to escarpment is shallower since it is not receiving large-caliber sediment. The presence of steep trunk reaches in northern drainages support the hypothesis that a wave of incision is currently working its way up through northern drainages. In Chapter 2 we propose that cycles of aggradation and incision of the Price lead to bottom-up local transient incision. Our terrain analysis furthers strengthens our conclusion that the Price River, driven by climate, can create local waves of transience that propagate up piedmont drainages. The lack of clear knickpoints in southern drainages 4, 5, and 6 suggest two possible explanations. The first, local transience has not yet propagated up from the Price due to a lack of stream power, or second, the transience has already worked its way all the way up to the cliff face in southern drainages.

Study-area wide, drainages have steep trunk streams and significantly flatter tributary catchments (Figure 3.9). Based on field observations, modern trunk streams have incised down through piedmont sediments, whereas small tributary streams of low gradient are stuck upon the piedmont due to lack of stream power. This is the simplest explanation for the unique steepness pattern we observe in the χ profiles (Figure 3.9 and Appendix C).

Landscape evolution of the Book Cliffs

The ratio of lateral retreat to vertical incision for Generation 2 landforms has a large scatter but conforms to our geometric prediction of ~7:1. Also our study shows, for the first time via direct measurement, that lateral retreat rates are greater than the pace of vertical incision (Figure 3.8). Furthermore, the large scatter of retreat to incision ratios may be due that topography and erosion are naturally variable and do not simply follow idealized relationships. Our results also show that the pace of lateral retreat and toeslope incision show no pattern in relation with distance from baselevel (Figure 3.7B). This suggests that the retreat of the Book Cliffs is at least somewhat decoupled from bottom-up incisional processes, and is consistent with top-down processes triggered by climate being drivers of retreat (Chapter 2). Given the relatively large amount of lateral retreat compared to incision, it can be logically concluded that significant material can be removed from the landscape by lateral retreat as Clarence Dutton (1884) Lester King (1953) initially championed.

Zooming out regionally, Clarence Dutton envisioned lateral retreat as a primary mechanism of valley and canyon widening. He suggested it would take "millions of centuries" (100's of millions of years) for cliffs to retreat a hundred miles or more. Assuming that the cliffs are retreating constantly at the pace of rounded rate of ~2 m/ky the cliffs would retreat 2 km in a million years. This would be approximately half the distance from the cliff face to U.S. Route 6 presently (Figure 3.3). When we consider the Cretaceous age of the rocks that compose the cliffs and that the Cenozoic has been a time of uplift and erosion in the region we can project this thought experiment back to the beginning of the Cenozoic. If the cliffs have been retreating at a similar rate since 65 Ma,

the cliffs would have retreated 130 km (80 miles), which falls in line with the magnitude of retreat Dutton was envisioning.

REFERENCES

Aslan, Andres, William C. Hood, Karl E. Karlstrom, Eric Kirby, Darryl E. Granger, Shari Kelley, Ryan Crow, Magdalena S. Donahue, Victor Polyak, and Yemane Asmerom. "Abandonment of Unaweep Canyon (1.4–0.8 Ma), Western Colorado: Effects of Stream Capture and Anomalously Rapid Pleistocene River Incision." *Geosphere* 10, no. 3 (June 2014): 428–46.

Boroda, R., R. Amit, A. Matmon, R. Finkel, N. Porat, Y. Enzel, Y. Eyal, and ASTER Team. "Quaternary-Scale Evolution of Sequences of Talus Flatirons in the Hyperarid Negev." *Geomorphology* 127, no. 1–2 (2011): 41–52.

Bryan, Kirk. "Gully Gravure-a Method of Slope Retreat." *Journal of Geomorphology*, no. 3 (1940): 89–107.

Caldwell, Jarred, and Alex Vahidsafa. "Propagation of Error." Chemistry LibreTexts, October 2, 2013.

Cole, Kenneth L., and Larry Mayer. "Use of Packrat Middens to Determine Rates of Cliff Retreat in the Eastern Grand Canyon, Arizona." *Geology* 10, no. 11 (1982): 597–599.

Cook, Kristen L., Kelin X. Whipple, Arjun M. Heimsath, and Thomas C. Hanks. "Rapid Incision of the Colorado River in Glen Canyon–Insights from Channel Profiles, Local Incision Rates, and Modeling of Lithologic Controls." *Earth Surface Processes and Landforms* 34, no. 7 (2009): 994–1010.

Darling, Andrew L., Karl E. Karlstrom, Darryl E. Granger, Andres Aslan, Eric Kirby, William B. Ouimet, Gregory D. Lazear, David D. Coblentz, and Rex D. Cole. "New Incision Rates along the Colorado River System Based on Cosmogenic Burial Dating of Terraces: Implications for Regional Controls on Quaternary Incision." *Geosphere* 8, no. 5 (October 2012): 1020–41.

Dutton, Clarence Edward. *Tertiary History of the Grand Canon District*. U.S. Geologic Survey, 1882.

Elorza, M. Gutiérrez, and VH Sesé Martínez. "Multiple Talus Flatirons, Variations of Scarp Retreat Rates and the Evolution of Slopes in Almazán Basin (Semi-Arid Central Spain)." *Geomorphology* 38, no. 1–2 (2001): 19–29.

Fisher, D. Jerome, Charles Edgar Erdmann, and John Bernard Reeside. *Cretaceous and Tertiary Formations of the Book Cliffs, Carbon, Emery, and Grand Counties, Utah, and Garfield and Mesa Counties, Colorado*. US Government Printing Office, 1960.

Flint, Jean-Jacques. “Stream Gradient as a Function of Order, Magnitude, and Discharge.” *Water Resources Research* 10, no. 5 (1974): 969–973.

Forte, Adam M., Brian J. Yanites, and Kelin X. Whipple. “Complexities of Landscape Evolution during Incision through Layered Stratigraphy with Contrasts in Rock Strength.” *Earth Surface Processes and Landforms* 41, no. 12 (2016): 1736–57.

Gerson, Ran, and Sari Grossman. “Geomorphic Activity on Escarpments and Associated Fluvial Systems in Hot Deserts.” *Climate, History, Periodicity, Predictability*, 1987, 300–322.

Gutiérrez, Mateo, Carlos Sancho, and Tomás Arauzo. “Scarp Retreat Rates in Semiarid Environments from Talus Flatirons (Ebro Basin, NE Spain).” *Geomorphology* 25, no. 1–2 (1998): 111–121.

Hack, John Tilton. *Studies of Longitudinal Stream Profiles in Virginia and Maryland*. U.S. Government Printing Office, 1957.

Jochems, Andrew P., and Joel L. Pederson. “Active Salt Deformation and Rapid, Transient Incision along the Colorado River near Moab, Utah.” *Journal of Geophysical Research: Earth Surface* 120, no. 4 (2015): 730–44.

King, Lester C. “Canons of Landscape Evolution.” *Geological Society of America Bulletin* 64, no. 7 (1953): 721–752.

Koons, Edwin Donaldson. “Cliff Retreat in the Southwestern United States.” *American Journal of Science* 253, no. 1 (1955): 44–52.

Lucchitta, Ivo, Garniss H. Curtis, Marie E. Davis, Sidney W. Davis, and Brent Turrin. “Cyclic Aggradation and Downcutting, Fluvial Response to Volcanic Activity, and Calibration of Soil-Carbonate Stages in the Western Grand Canyon, Arizona.” *Quaternary Research* 53, no. 1 (January 2000): 23–33.

Pederson, Joel, Neil Burnside, Zoe Shipton, and Tammy Rittenour. “Rapid River Incision across an Inactive Fault—Implications for Patterns of Erosion and Deformation in the Central Colorado Plateau.” *Lithosphere* 5, no. 5 (October 1, 2013b): 513–20.

Pederson, Joel L., Matt D. Anders, Tammy M. Rittenhour, Warren D. Sharp, John C. Gosse, and Karl E. Karlstrom. “Using Fill Terraces to Understand Incision Rates and Evolution of the Colorado River in Eastern Grand Canyon, Arizona.” *Journal of Geophysical Research: Earth Surface* 111, no. F2 (2006).

Pederson, Joel L., W. Scott Cragun, Alan J. Hidy, Tammy M. Rittenour, and John C. Gosse. "Colorado River Chronostratigraphy at Lee's Ferry, Arizona, and the Colorado Plateau Bull's-Eye of Incision." *Geology* 41, no. 4 (April 1, 2013a): 427–30.

Perron, J. Taylor, and Leigh Royden. "An Integral Approach to Bedrock River Profile Analysis." *Earth Surface Processes and Landforms* 38, no. 6 (2013): 570–76.

Pinheiro, Marcos Roberto, and José Pereira de Queiroz Neto. "From the Semiarid Landscapes of Southwestern USA to the Wet Tropical Zone of Southeastern Brazil: Reflections on the Development of Cuestas, Pediments, and Talus." *Earth-Science Reviews* 172 (2017): 27–42.

Richardson, George Burr. "Reconnaissance of the Book Cliffs Coal Field, between Grand River, Colorado and Sunnyside, Utah." Goverment Print. U.S. Geological Survey, 1909.

Schmidt, Karl-Heinz. "Talus and Pediment Flatirons-Indicators of Climatic Change on Scarp Slopes on the Colorado Plateau, USA." *Zeitschrift Fur Geomorphologie Supplementband*, 1996, 135–58.

Schumm, Stanely Alfred, and R.J. Chorely. "Talus Weathering and Scarp Recession in the Colorado Plateaus." *US Geological Survey*, 1966, 11–36.

Schwanghart, Wolfgang, and Dirk Scherler. "TopoToolbox 2–MATLAB-Based Software for Topographic Analysis and Modeling in Earth Surface Sciences." *Earth Surface Dynamics* 2, no. 1 (2014): 1–7.

Sheehan, Christopher E., and Dylan J. Ward. "Late Pleistocene Talus Flatiron Formation below the Coal Cliffs Cuesta, Utah, USA." *Earth Surface Processes and Landforms* 43, no. 9 (2018): 1973–1992.

Tucker, Gregory, Stephen Lancaster, Nicole Gasparini, and Rafael Bras. "The Channel-Hillslope Integrated Landscape Development Model (CHILD)." In *Landscape Erosion and Evolution Modeling*, edited by Russell S. Harmon and William W. Doe, 349–88. Boston, MA: Springer US, 2001.

Ward, D. J., M. M. Berlin, and R. S. Anderson. "Sediment Dynamics below Retreating Cliffs." *Earth Surface Processes and Landforms* 36, no. 8 (2011): 1023–43.

Whipple, K. X., Roman Alexander Dibiase, and B. T. Crosby. "Bedrock Rivers." *Treatise on Geomorphology*, March 1, 2013, 550–73.

Willett, Sean D., Scott W. McCoy, J. Taylor Perron, Liran Goren, and Chia-Yu Chen. "Dynamic Reorganization of River Basins." *Science* 343, no. 6175 (March 7, 2014): 1248765.

CHAPTER 4

SUMMARY

This Thesis includes two core chapters exploring focusing on aspects of escarpment retreat along the Book Cliffs of central Utah. Chapter 2 focuses on the chronostratigraphic record preserved along the cliff as talus flatirons and piedmont terraces. Chapter 3 constrains rates and patterns of cliff retreat through computational terrain analysis.

Cliff retreat as controlled by climate

Pairs of remnant colluvial, talus flatiron, and piedmont terrace deposits preserve a record spatially of the retreat history of the Book Cliffs escarpment. Four generations of these features were identified through both mapping and OSL chronology, dating to 115.9 ± 10.8 to 119.2 ± 12.8 ka, 90.3 ± 9.8 to 75.6 ± 7.5 ka, 69.1 ± 6.7 to 44.3 ± 4.0 ka, and 10.7 ± 1.0 to 1.6 ± 0.2 ka. These depositional episodes mark transitions between glacial and interglacial epochs or periods of high climatic variability. This goes against the classical assumption that depositional episodes in arid piedmonts are tied to glacial maxima. A decrease in age with increasing upstream distance from the Price River reveals the presence of transient incision related to incision of the Price River. Taken in sum, Book Cliff escarpment erosion follows a conceptual model where first, cliff failure and retreat is triggered by glacial-interglacial transitions or periods of climate instability, then second, once sediment supply significantly decreases, top-down gully incision and bottom-up transience incision proceeds across the piedmont. Additional studies are required to better understand the spatial extent as well as the timing of the deposition of

the oldest two generations of deposits along the larger Book Cliff region as well as the relationship between escarpment related deposits and those of the nearby Price River.

Measurements of the retreat of the Book Cliffs

Measurements of lateral retreat and vertical incision were performed through a novel profile-area-integration approach. Results confirm the geometric prediction that lateral cliff retreat proceeds at 1 -3 m/ky, several times faster than vertical incision of toeslopes at ~0.5 m/ky, with the ratio of lateral retreat to vertical incision for given deposits ranging widely between 20:1 to 1:1. These measurements are in line with early, unconstrained estimates of retreat rates in the Colorado Plateau as well as rates from similar studies in Spain. Drainage-steepness analysis provides evidence for transient incision in kickzones in northern three drainage. This result suggests that a recent baselevel fall of the Price River has triggered a wave of transience up cliff drainages, however this is likely the result of periodic climate-controlled aggradation and incision proposed in Chapter 2, rather than the larger regional transience working its way through the Colorado Plateau. Although we show that cliffs move laterally faster than canyons are cut, that is not the same thing as hillslope processes accounting for more mass removal than fluvial processes, which will require further analysis and future studies.

APPENDICES

Appendix A. Luminescence sample data and D_e Distribution

TABLE A1. SAMPLE LOCATION AND CHEMISTRY DATA

USU#	Field Designation	Latitude	Longitude	Location	K %	Rb ppm	Th ppm	Ur ppm	Sample depth (m)	wt. % H2O[$]
280	P3_horsecanyonfan	39.39403	-110.42038	Mid-Horse Canyon Fan Northern Piedmont	1.72	72.4	7.5	2.3	8	1.59%
1128	P2_studyarea	39.33032	-110.35006	Piedmont Northern	0.81	36.4	4.5	2.2	2.5	0.00%
1129	P2_studyarea	39.33051	-110.35003	Piedmont Northern	0.84	36.9	4.6	2.2	2	0.00%
1130	M3_price river	39.30347	-110.4061	Price River Terrace	0.66	31.2	4.7	2.2	20.4	0.00%
1131	M3_price river	39.30347	-110.4061	Price River Terrace	0.71	29.6	4.7	1.8	3.1	0.00%
1132	P2_beckwith	39.02526	-110.28859	Beckwith piedmont Southern	1.1	46.9	4.9	2.5	2.2-3	0.00%
1151	P3_horsecanyonfan	39.39918	110.42229	Upper Horse Canyon Fan Northern Piedmont	1.69	83.1	9.3	3	2.2	3.23%

USU#	Field Designation	Latitude	Longitude	Location	K %	Rb ppm	Th ppm	Ur ppm	Sample depth (m)	wt. % H2O[$]
1173	P2_beckwith	39.0444	-110.27628	Beckwith piedmont Southern	1.37	52.7	6	1.2	6	0.21%
2764	C3_01	39.44517	-110.36013	Colluvium Northern	1.04	44.80	4.76	1.70	8.5	1.12%
2765	C2_02	39.44091	-110.362	Colluvium Northern	1.10	56.00	6.25	3.40	3.75	0.94%
2766	C1_03	39.44015	-110.36201	Colluvium Northern	0.93	43.70	4.66	1.90	1.3	0.41%
2767	P3_04	39.41750	-110.35080	Piedmont Northern	0.94	44.45	4.70	1.80	7.5	0.83%
2769	P2_06	39.41374	-110.34710	Piedmont Northern	0.88	41.60	4.42	1.80	~4	0.63%
2770	P2_07	39.41442	-110.34710	Piedmont (Northern)	1.10	53.90	5.57	2.60	1.4	3.74%
2771	C3_08	39.41470	-110.34040	Colluvium Northern	0.91	42.86	4.71	1.95	3.25	0.57%
2818	C2_09	39.31389	-110.31280	Piedmont Southern	0.82	36.20	3.66	1.70	4	0.37%
2819	P1_10	39.31062	-110.31390	Piedmont Southern	0.81	37.30	4.50	1.80	1.3	0.44%
2820	C1_11	39.29861	-110.30810	Colluvium Southern	1.06	50.30	5.09	1.90	1.5	0.08%
2821	P2_12	39.26199	-110.30332	Piedmont Southern	0.78	36.00	4.23	1.90	4.75	0.40%
2822	P3_13	39.33942	-110.3244	Piedmont South-Central	0.88	42.80	4.90	2.10	6.0	0.67%
2824	P1_15	39.41997	-110.3532	Piedmont Northern	0.75	32.10	3.58	1.50	1.5	5.65%

USU#	Field Designation	Latitude	Longitude	Location	K %	Rb ppm	Th ppm	Ur ppm	Sample depth (m)	wt. % H2O[$]
2984	C1_16	39.26037	-110.2998	colluvium (Southern)	1.25	66.2	6.7	3	0.5 -1	0%

$ Uniform moisture content of 5+/- 2% used in the dose rate calculation.

TABLE A2. PLEISTOCENE LUMINESCENCE CHRONOLOGY WITH 2σ ERRORS

Deposit*	USU #	# Aliquots (total)	Dose Rate (Gy/ka)			Equivalent dose (Gy)#			OSL age (ka)$			Model
C1	USU-2766	12 (29)	1.85	±	0.08	2.91	±	0.4	1.6	±	0.3	CAM
C1	USU-2820	15 (30)	1.98	±	0.08	8.28	±	2.6	4.2	±	1.3	MAM
P1	USU-2824	17 (33)	1.39	±	0.06	8.41	±	1.2	5.7	±	0.9	CAM
P1	USU-2819	18 (29)	1.69	±	0.07	10.00	±	2.7	5.9	±	1.5	MAM
C1	USU-2984	12 (22)	2.56	±	0.11	27.52	±	2.2	10.7	±	1.2	CAM
C2	USU-2765	17 (25)	2.39	±	0.10	105.90	±	8.3	44.3	±	5.0	CAM
P2	USU-1132	26 (66)	2.14	±	0.12	99.52	±	14.0	47.2	±	7.7	CAM
P2	USU-2770	17 (19)	2.22	±	0.09	106.56	±	9.6	48.0	±	5.9	CAM
P2	USU-2769	17 (22)	1.67	±	0.07	80.85	±	5.9	48.1	±	5.3	CAM
P2	USU-1128	25 (53)	1.82	±	0.10	99.91	±	8.3	55.8	±	6.5	CAM
C2	USU-2818	18 (21)	1.58	±	0.06	91.43	±	4.9	58.3	±	5.7	CAM
P2	USU-1173	23 (67)	1.80	±	0.10	104.05	±	13.7	58.8	±	9.1	CAM
P2	USU-1129	20 (32)	1.88	±	0.10	112.54	±	16.2	61.0	±	10.1	CAM
P2	USU-2821	20 (24)	1.58	±	0.07	107.91	±	12.9	68.3	±	9.9	CAM
M3	USU-1130	16 (33)	1.45	±	0.06	112.91	±	14.9	78.1	±	12.2	CAM
M3	USU-1131	34 (52)	1.55	±	0.07	88.49	±	8.2	57.1	±	7.07	CAM
C3	USU-2764	19(21)	1.78	±	0.07	134.68	±	15.6	75.6	±	10.7	CAM
C3	USU-258	28 (33)	2.92	±	0.12	231.00	±	19.1	79.1	±	9.5	CAM
P3	USU-280	26 (45)	2.85	±	0.15	252.9	±	22.2	84.3	±	11.8	CAM
P3	USU-257	20 (25)	2.65	±	0.11	227	±	78.0	85.8	±	10.5	CAM
P3	USU-1151	18 (37)	3.21	±	0.17	258.7	±	22.1	85.9	±	13.1	CAM
P3	USU-1152	21 (34)	2.10	±	0.08	189.34	±	23.8	90.3	±	13.4	CAM
C4	USU-2771	18 (23)	1.79	±	0.07	211.36	±	19.1	115.9	±	14.1	CAM
P4	USU-2767	15 (22)	1.70	±	0.07	213.34	±	20.7	118.5	±	14.9	CAM
P4	USU-2822	16 (23)	1.65	±	0.07	203.18	±	28.8	119.2	±	19.5	CAM

*Organized by stratigraphic position, plus age results with in map units

Equivalent dose (DE) calculated using the CAM or MAM model of Galbraith and Roberts (2012) Reported with 2σ errors. All samples use 5 +/- 2% H2O in the dose rate calculation.

$ Age analysis using the single-aliquot regenerative-dose procedure of Murray and Wintle (2000) on 1-mm small aliquot of quartz sand. Reported with 2σ errors. All samples use 5 +/- 2% H2O in the dose rate calculation.

Figure A3. Equivalent Dose (D_E) Radial Plots and Probability Density Functions

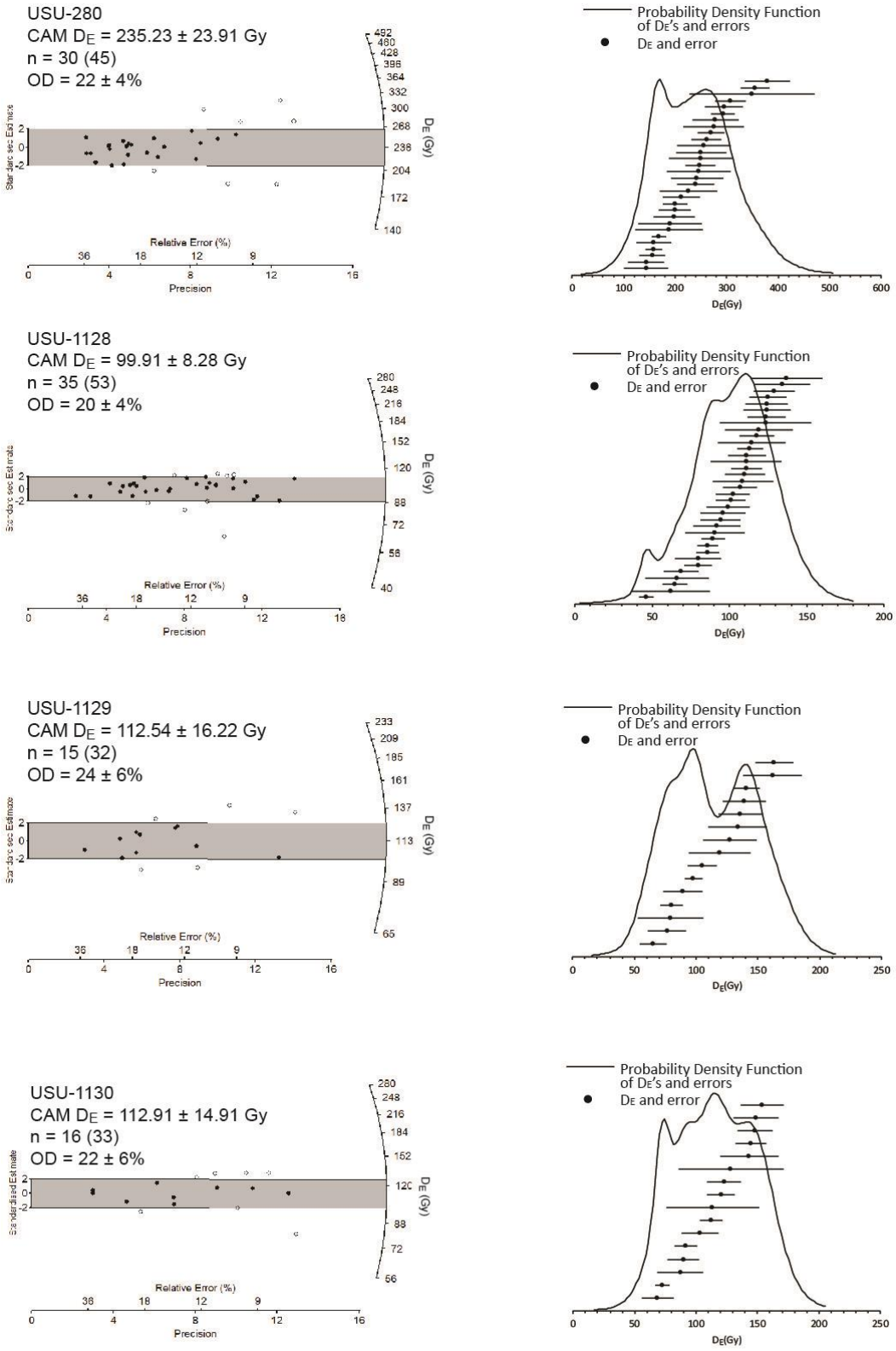

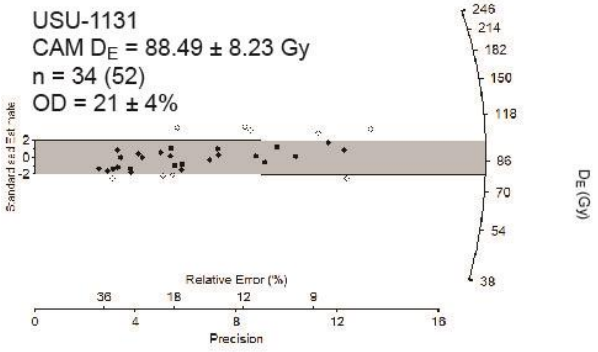
USU-1131
CAM D_E = 88.49 ± 8.23 Gy
n = 34 (52)
OD = 21 ± 4%
Standardised Estimate
Relative Error (%)
Precision
D_E (Gy)

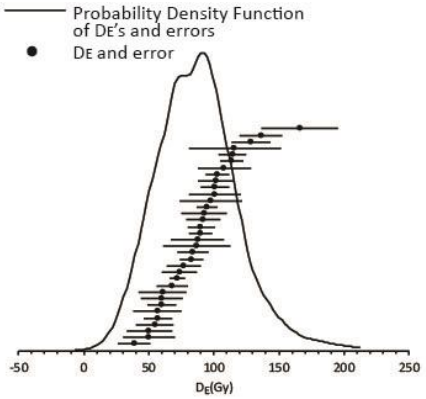
Probability Density Function
of DE's and errors
DE and error
DE(Gy)

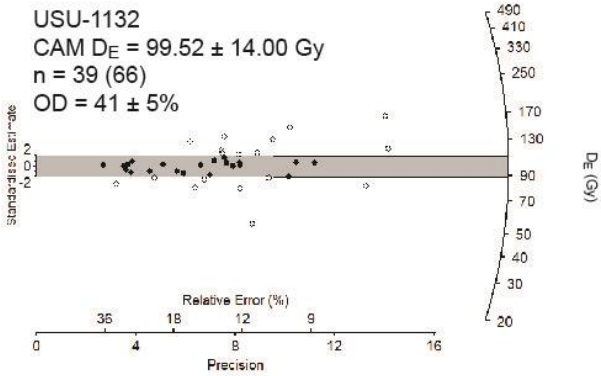
USU-1132
CAM D_E = 99.52 ± 14.00 Gy
n = 39 (66)
OD = 41 ± 5%
Standardised Estimate
Relative Error (%)
Precision
D_E (Gy)

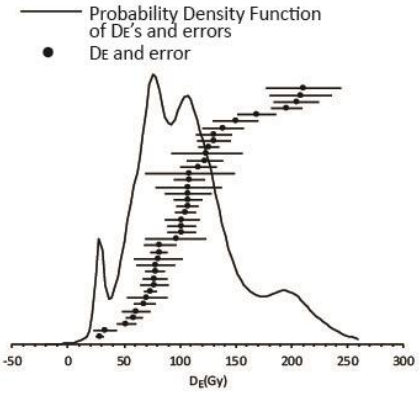
Probability Density Function
of DE's and errors
DE and error
DE(Gy)

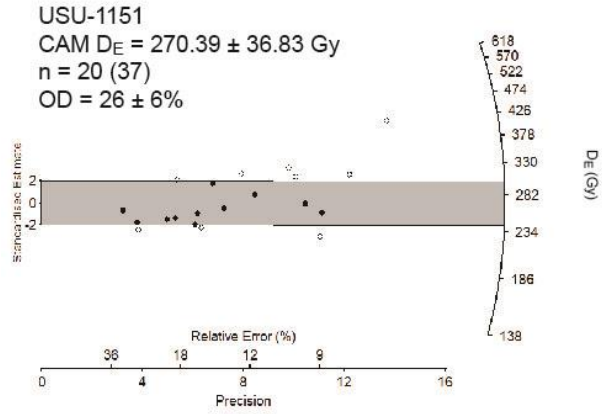
USU-1151
CAM D_E = 270.39 ± 36.83 Gy
n = 20 (37)
OD = 26 ± 6%
Standardised Estimate
Relative Error (%)
Precision
D_E (Gy)

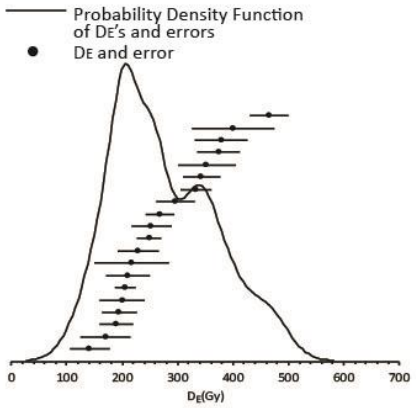
Probability Density Function
of DE's and errors
DE and error
DE(Gy)

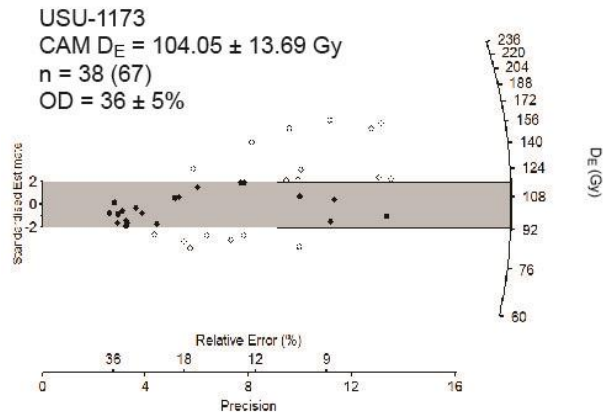
USU-1173
CAM D_E = 104.05 ± 13.69 Gy
n = 38 (67)
OD = 36 ± 5%
Standardised Estimate
Relative Error (%)
Precision
D_E (Gy)

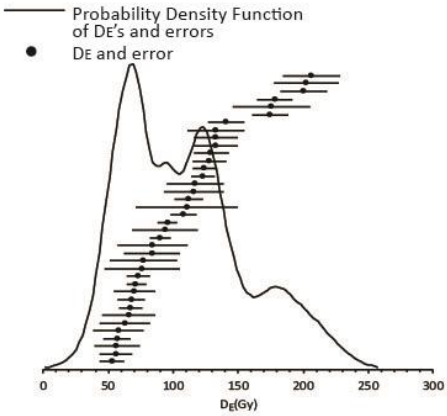
Probability Density Function
of DE's and errors
DE and error
DE(Gy)

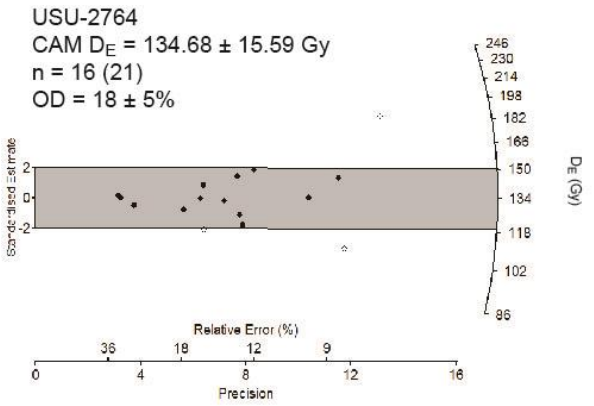
USU-2764
CAM D_E = 134.68 ± 15.59 Gy
n = 16 (21)
OD = 18 ± 5%
Standardised Estimate
Relative Error (%)
Precision
D_E (Gy)

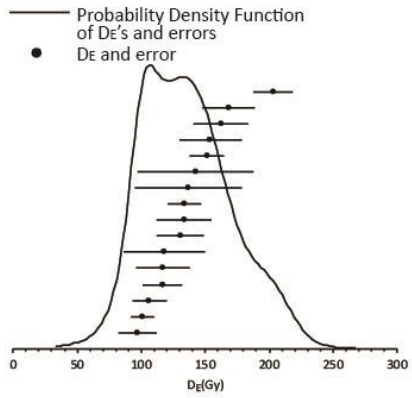
Probability Density Function of DE's and errors
DE and error
DE(Gy)

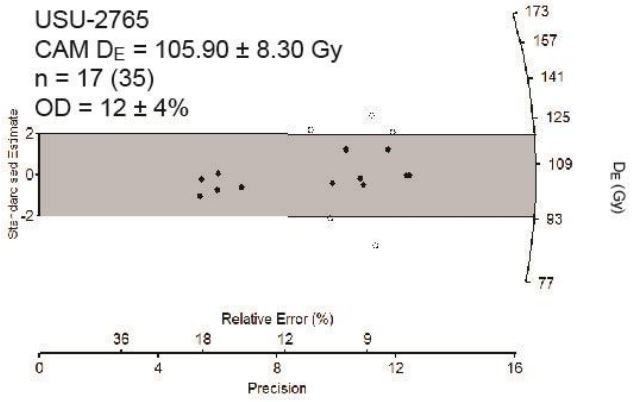
USU-2765
CAM D_E = 105.90 ± 8.30 Gy
n = 17 (35)
OD = 12 ± 4%
Standardised Estimate
Relative Error (%)
Precision
D_E (Gy)

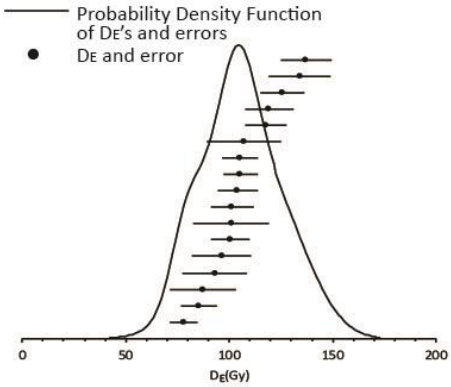
Probability Density Function of DE's and errors
DE and error
DE(Gy)

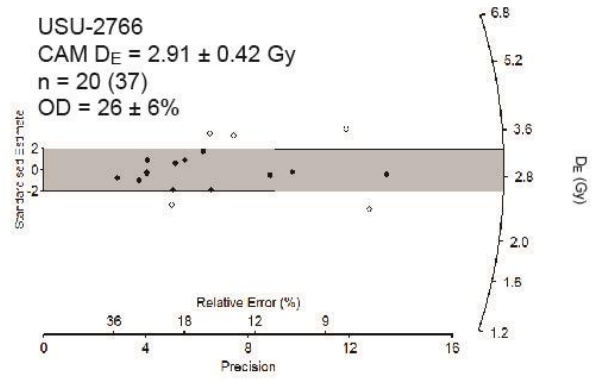
USU-2766
CAM D_E = 2.91 ± 0.42 Gy
n = 20 (37)
OD = 26 ± 6%
Standardised Estimate
Relative Error (%)
Precision
D_E (Gy)

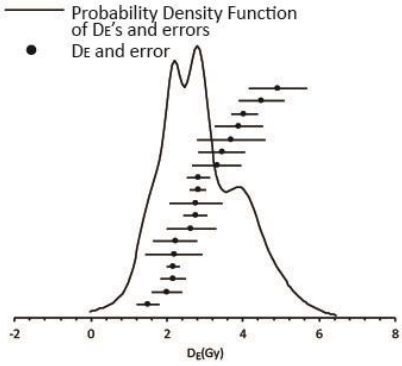
Probability Density Function of DE's and errors
DE and error
DE(Gy)

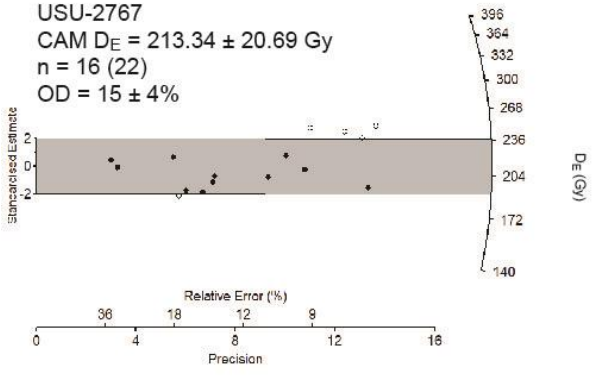
USU-2767
CAM D_E = 213.34 ± 20.69 Gy
n = 16 (22)
OD = 15 ± 4%
Standardised Estimate
Relative Error (%)
Precision
D_E (Gy)

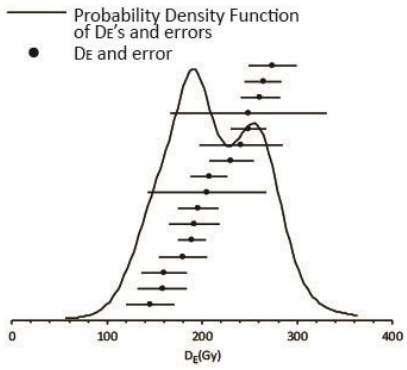
Probability Density Function of DE's and errors
DE and error
DE(Gy)

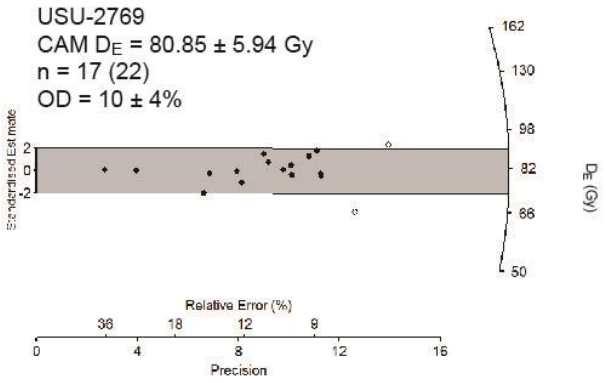
USU-2769
CAM D_E = 80.85 ± 5.94 Gy
n = 17 (22)
OD = 10 ± 4%
Standardised Estimate
Relative Error (%)
Precision
D_E (Gy)

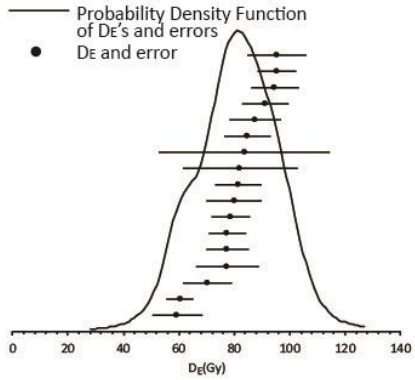
Probability Density Function of D_E's and errors
D_E and error
D_E(Gy)

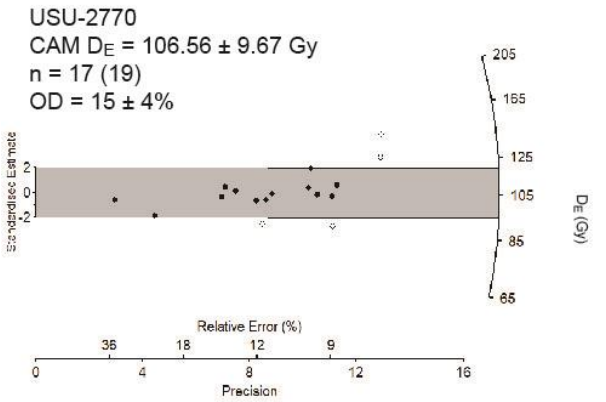
USU-2770
CAM D_E = 106.56 ± 9.67 Gy
n = 17 (19)
OD = 15 ± 4%
Standardised Estimate
Relative Error (%)
Precision
D_E (Gy)

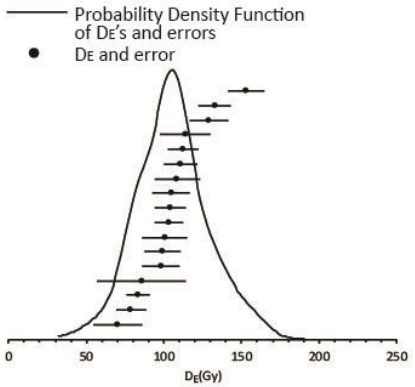
Probability Density Function of D_E's and errors
D_E and error
D_E(Gy)

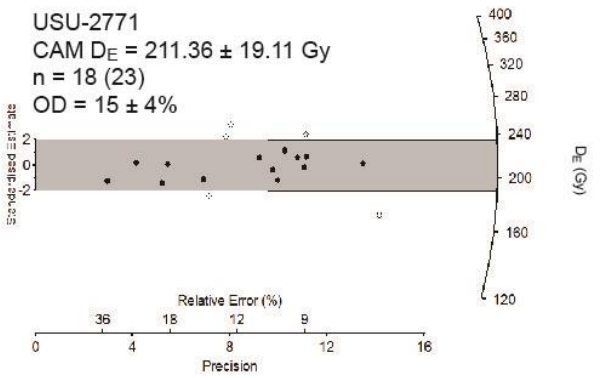
USU-2771
CAM D_E = 211.36 ± 19.11 Gy
n = 18 (23)
OD = 15 ± 4%
Standardised Estimate
Relative Error (%)
Precision
D_E (Gy)

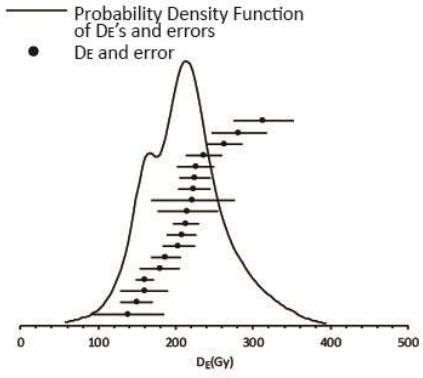
Probability Density Function of D_E's and errors
D_E and error
D_E(Gy)

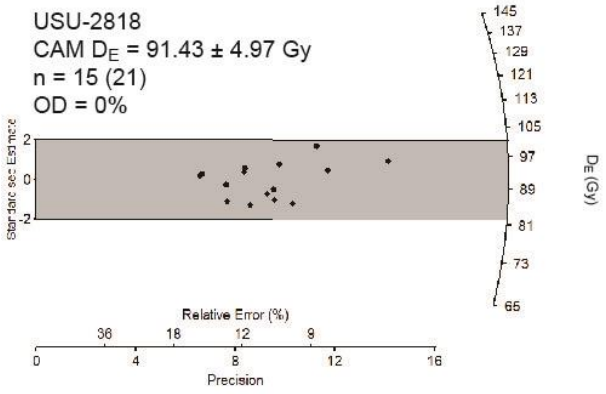
USU-2818
CAM D_E = 91.43 ± 4.97 Gy
n = 15 (21)
OD = 0%
Standardised Estimate
Relative Error (%)
Precision
D_E (Gy)

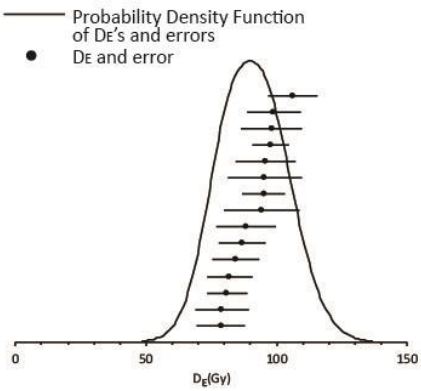
Probability Density Function of D_E's and errors
D_E and error
D_E(Gy)

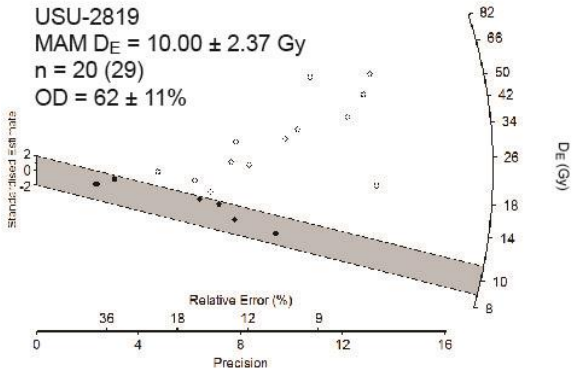
USU-2819
MAM D_E = 10.00 ± 2.37 Gy
n = 20 (29)
OD = 62 ± 11%
Standardised Estimate
D_E (Gy)
Relative Error (%)
Precision

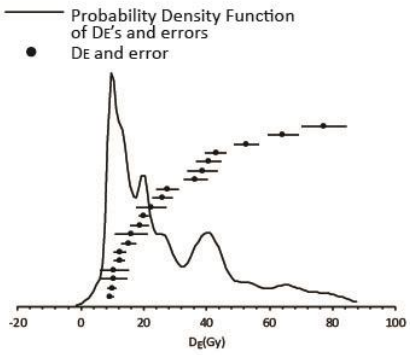
Probability Density Function
of DE's and errors
DE and error
DE(Gy)

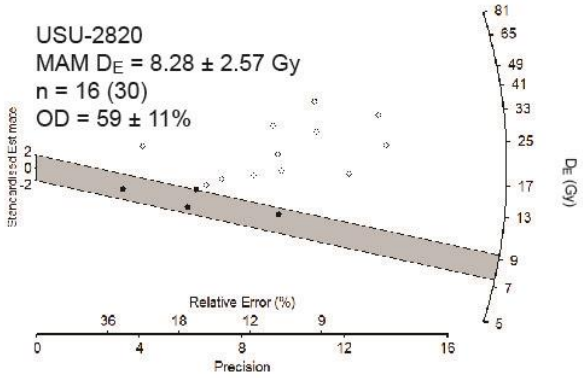
USU-2820
MAM D_E = 8.28 ± 2.57 Gy
n = 16 (30)
OD = 59 ± 11%
Standardised Estimate
D_E (Gy)
Relative Error (%)
Precision

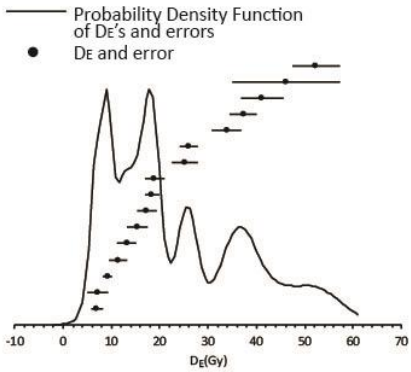
Probability Density Function
of DE's and errors
DE and error
DE(Gy)

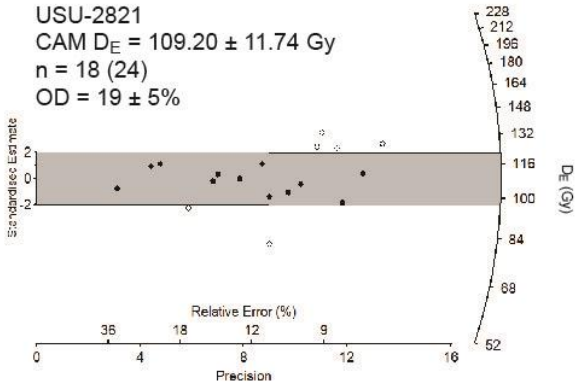
USU-2821
CAM D_E = 109.20 ± 11.74 Gy
n = 18 (24)
OD = 19 ± 5%
Standardised Estimate
D_E (Gy)
Relative Error (%)
Precision

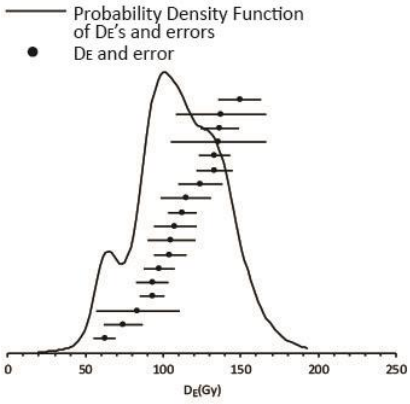
Probability Density Function
of DE's and errors
DE and error
DE(Gy)

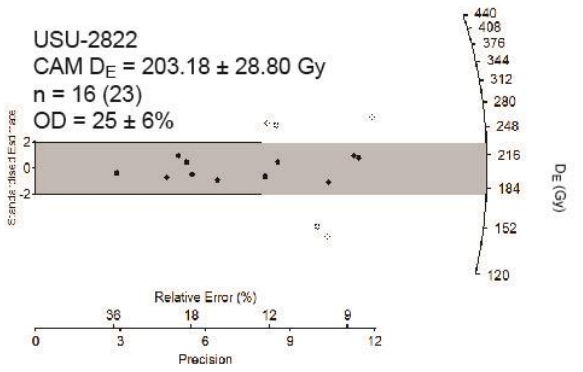
USU-2822
CAM D_E = 203.18 ± 28.80 Gy
n = 16 (23)
OD = 25 ± 6%
Standardised Estimate
D_E (Gy)
Relative Error (%)
Precision

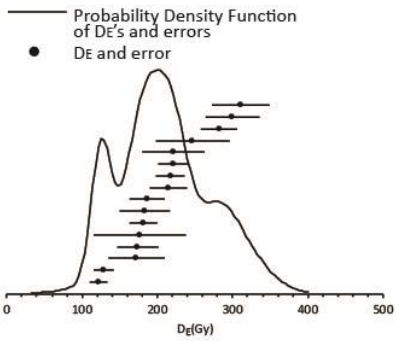
Probability Density Function
of DE's and errors
DE and error
DE(Gy)

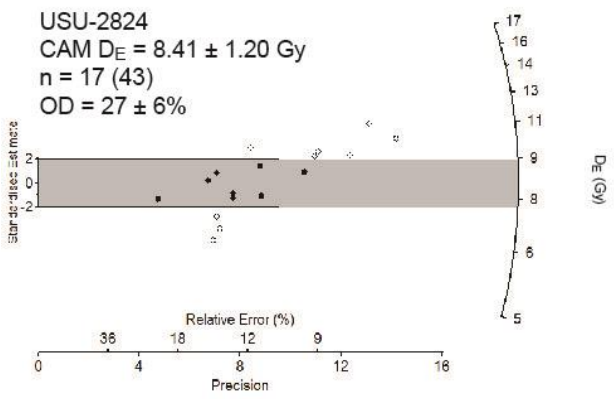
USU-2824
CAM D_E = 8.41 ± 1.20 Gy
n = 17 (43)
OD = 27 ± 6%
Standardised Estimate
Relative Error (%)
36
18
12
9
Precision
D_E (Gy)

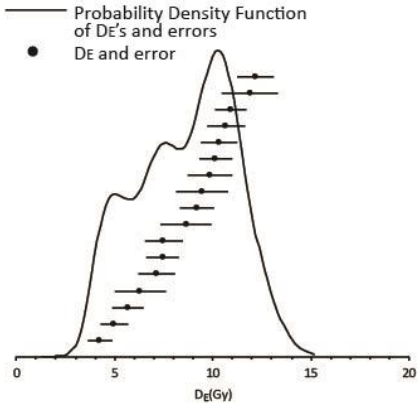
Probability Density Function
of DE's and errors
DE and error
D_E(Gy)

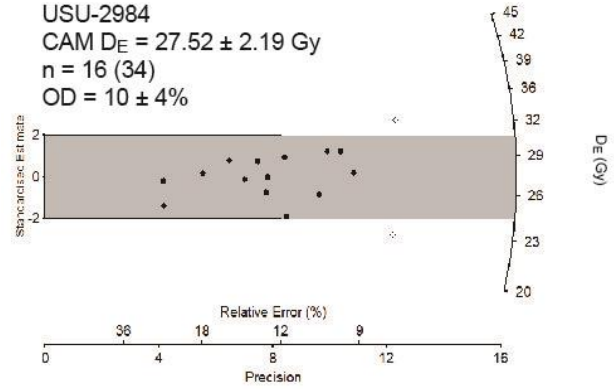
USU-2984
CAM D_E = 27.52 ± 2.19 Gy
n = 16 (34)
OD = 10 ± 4%
Standardised Estimate
Relative Error (%)
36
18
12
9
Precision
D_E (Gy)

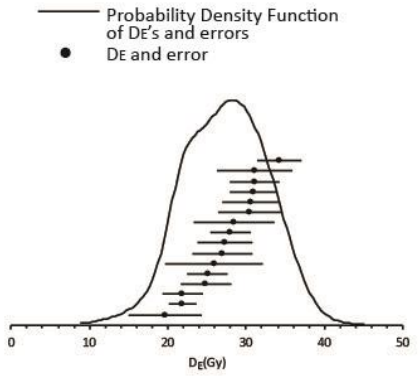
Probability Density Function
of DE's and errors
DE and error
D_E(Gy)

Appendix B. Talus flatiron projection and measurement of erosion

Figure B1. Map of Watersheds

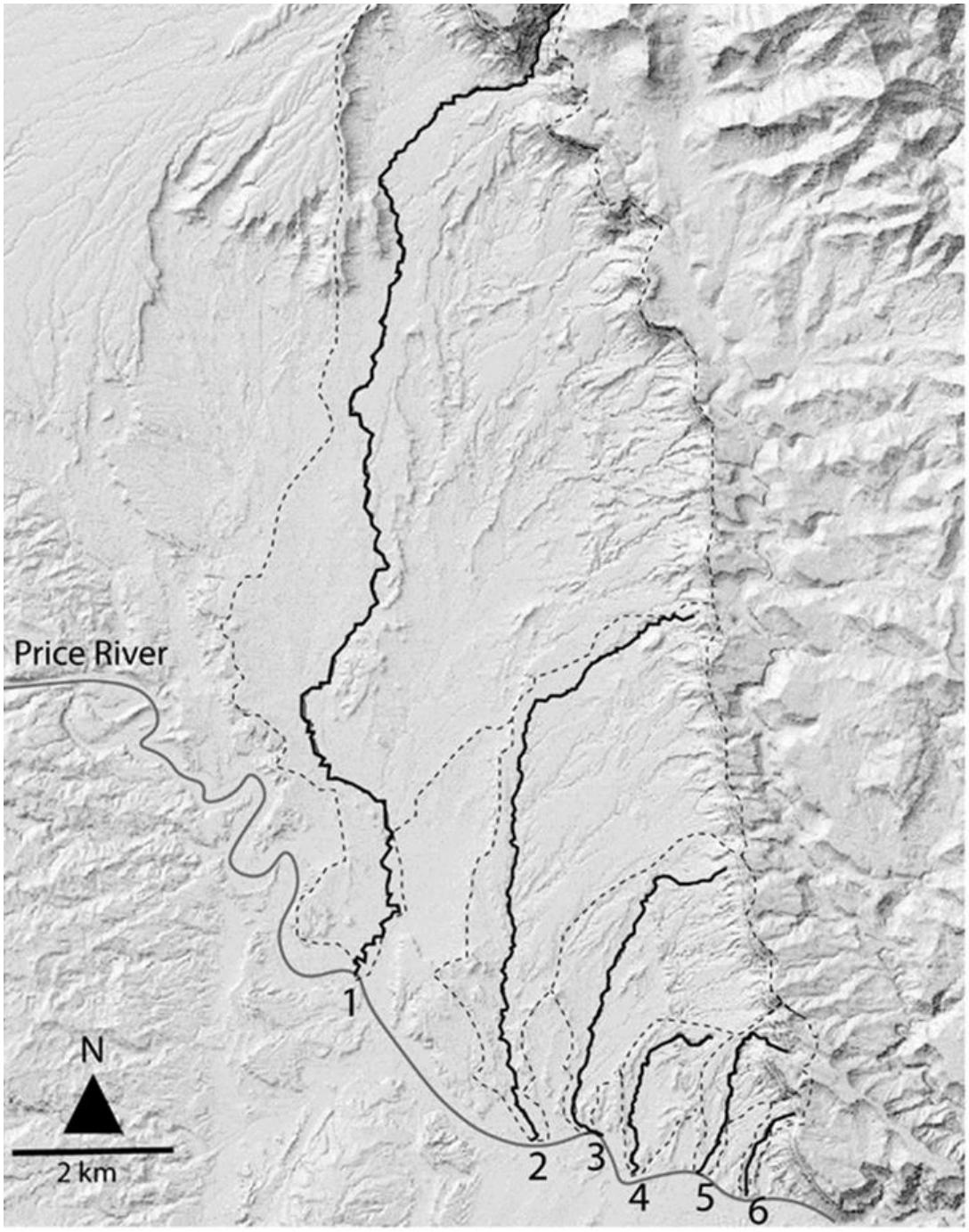

Figure B2. Profile Lines Map

A) Northern Study Area

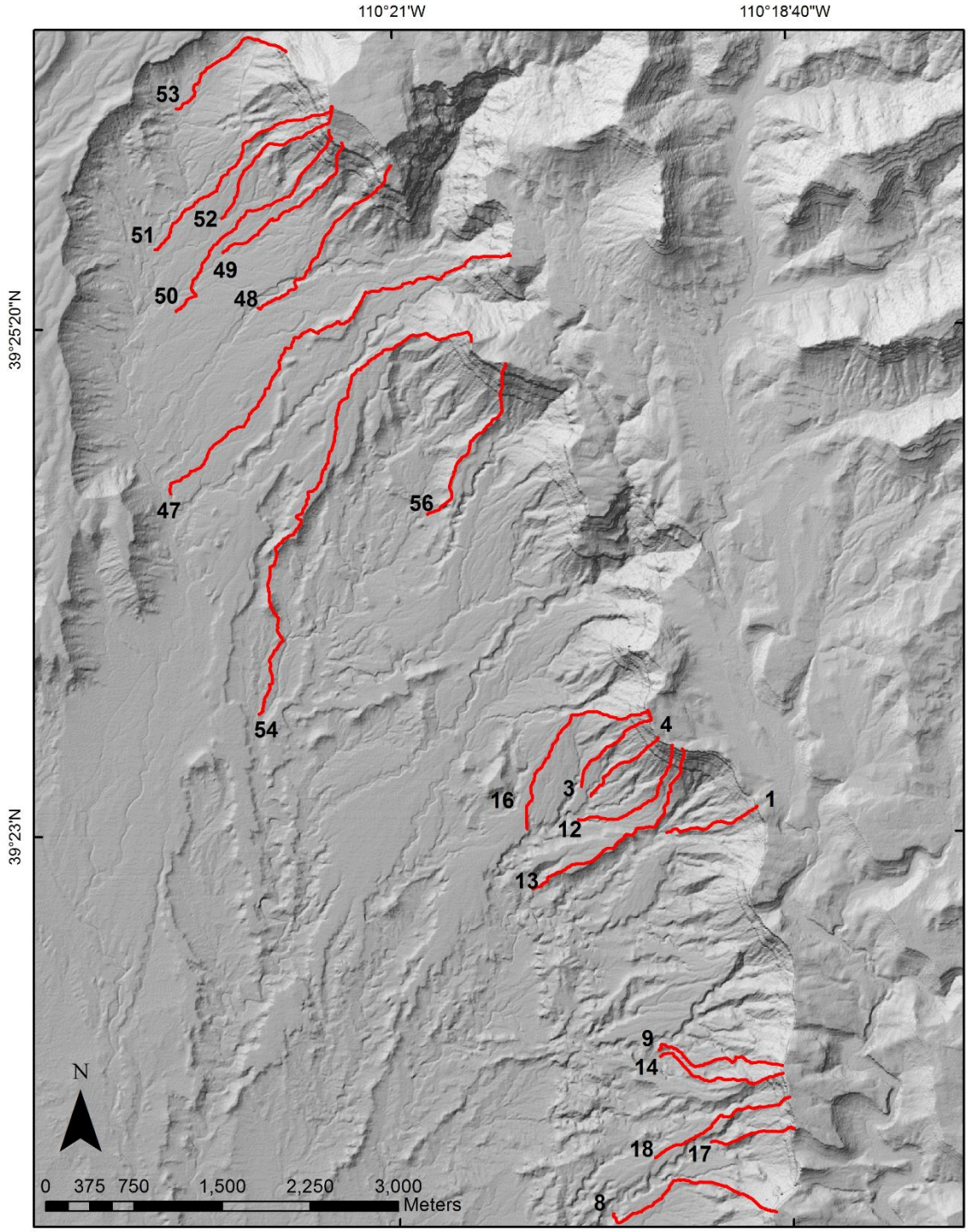

B) Southern Study Area

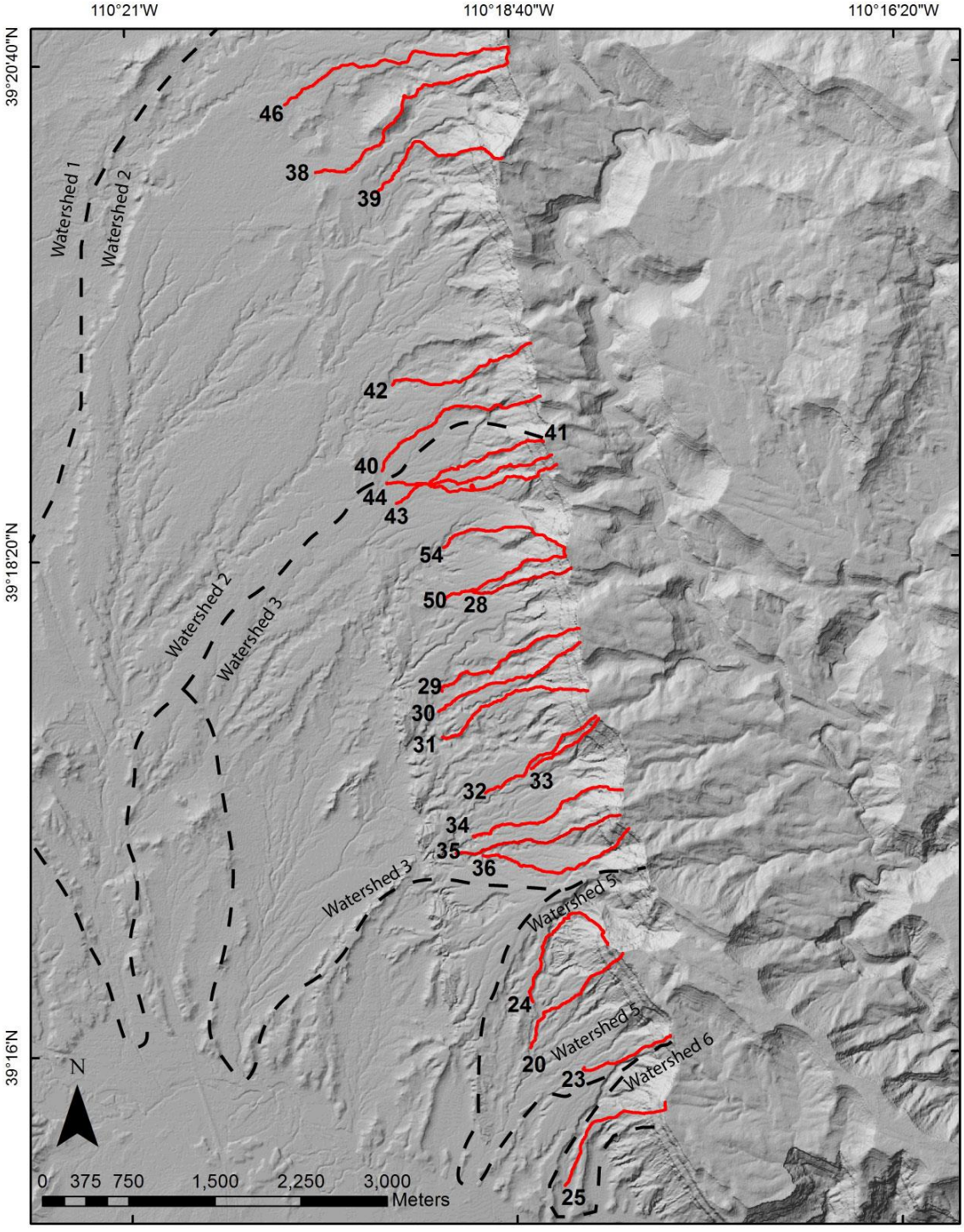

Figure B3. Talus Flatiron Projection Plots

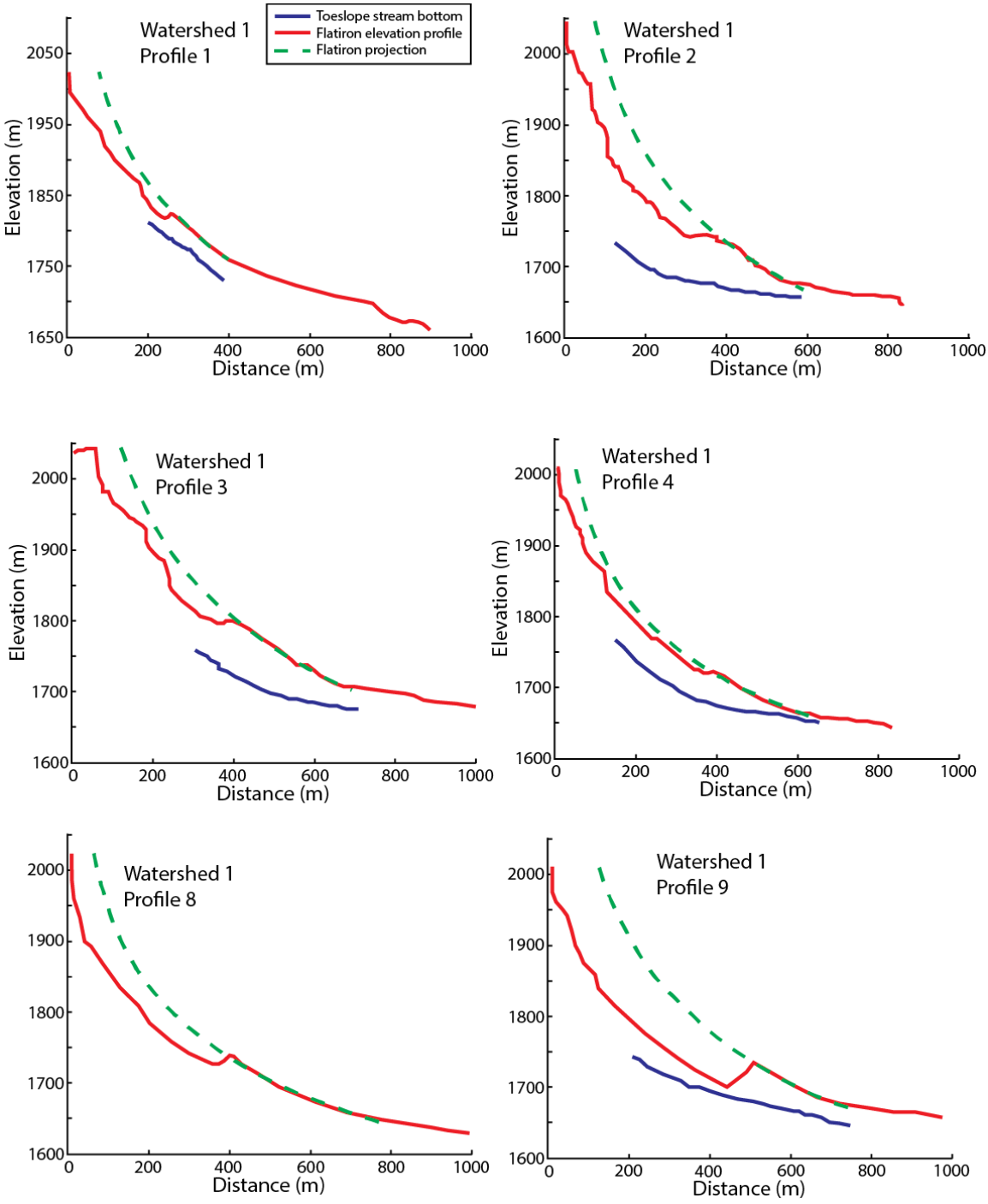

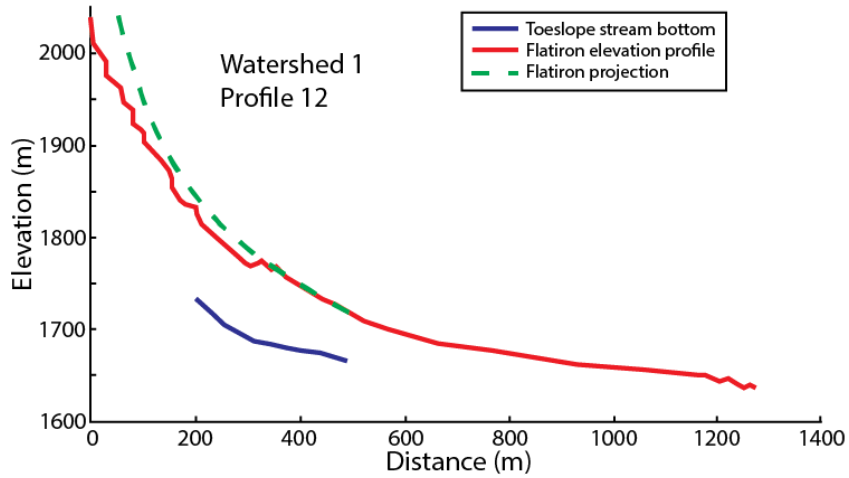
Toeslope stream bottom
Flatiron elevation profile
Flatiron projection
Watershed 1
Profile 12
Elevation (m)
2000
1900
1800
1700
1600
0
200
400
600
800
1000
1200
1400
Distance (m)

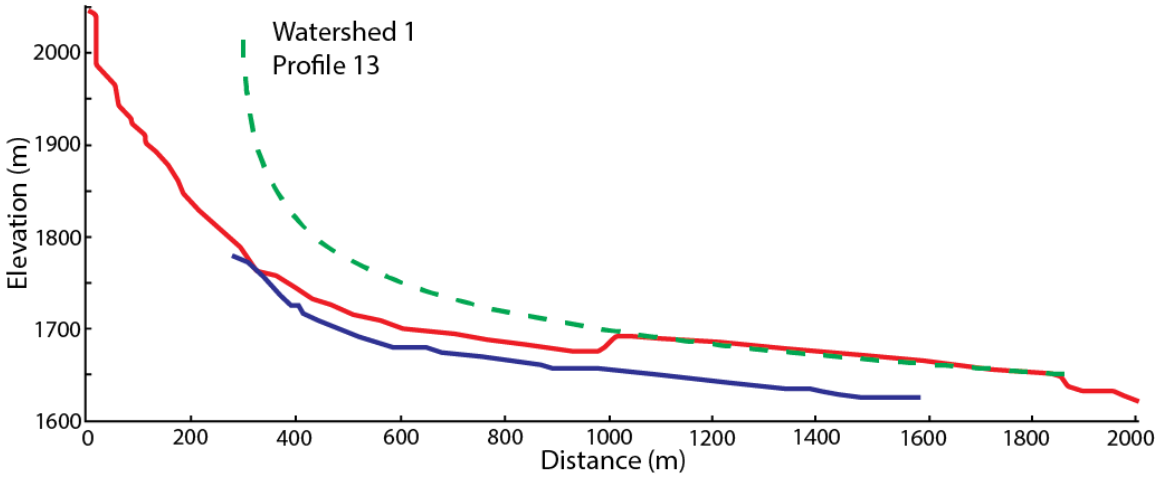
Watershed 1
Profile 13
Elevation (m)
2000
1900
1800
1700
1600
0
200
400
600
800
1000
1200
1400
1600
1800
2000
Distance (m)

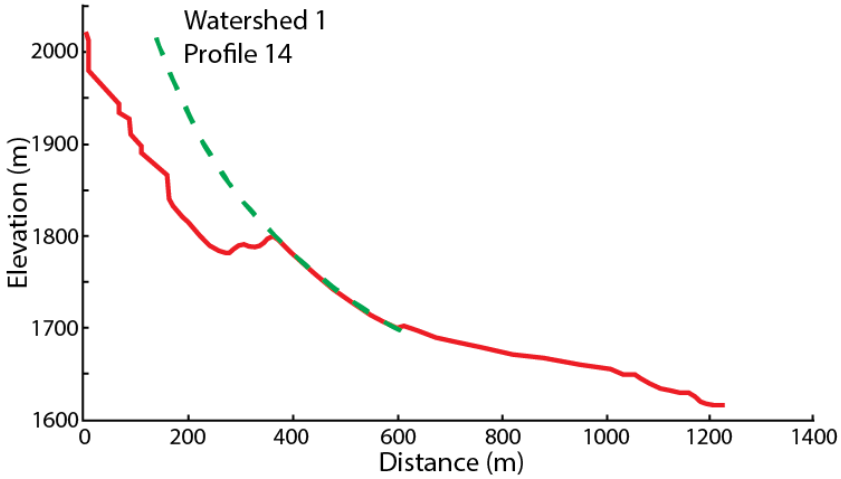
Watershed 1
Profile 14
Elevation (m)
2000
1900
1800
1700
1600
0
200
400
600
800
1000
1200
1400
Distance (m)

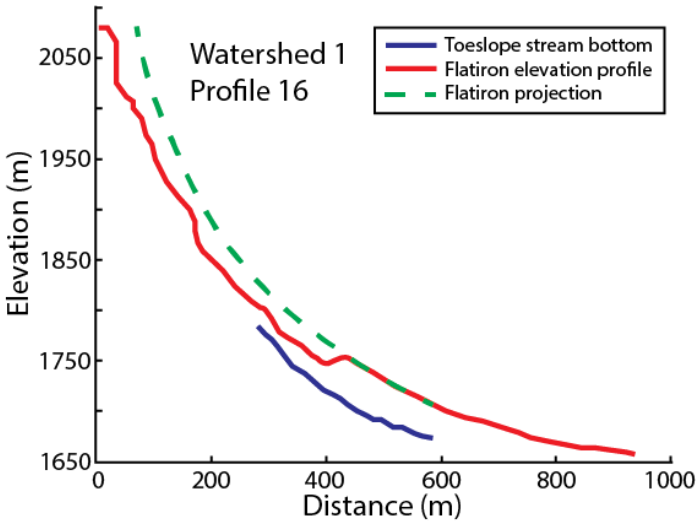
Watershed 1
Profile 16
Toeslope stream bottom
Flatiron elevation profile
Flatiron projection
Elevation (m)
2050
1950
1850
1750
1650
0
200
400
600
800
1000
Distance (m)

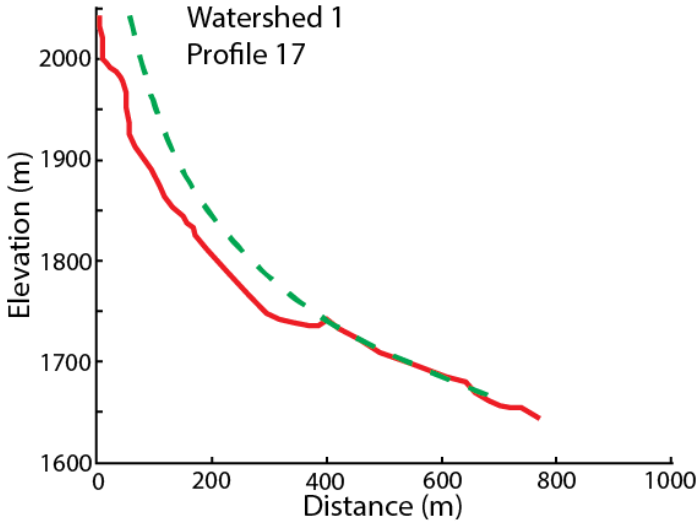
Watershed 1
Profile 17
Elevation (m)
2000
1900
1800
1700
1600
0
200
400
600
800
1000
Distance (m)

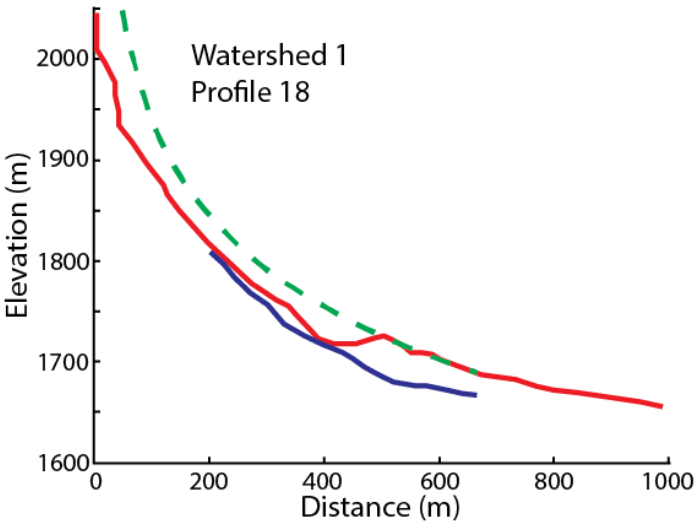
Watershed 1
Profile 18
Elevation (m)
2000
1900
1800
1700
1600
0
200
400
600
800
1000
Distance (m)

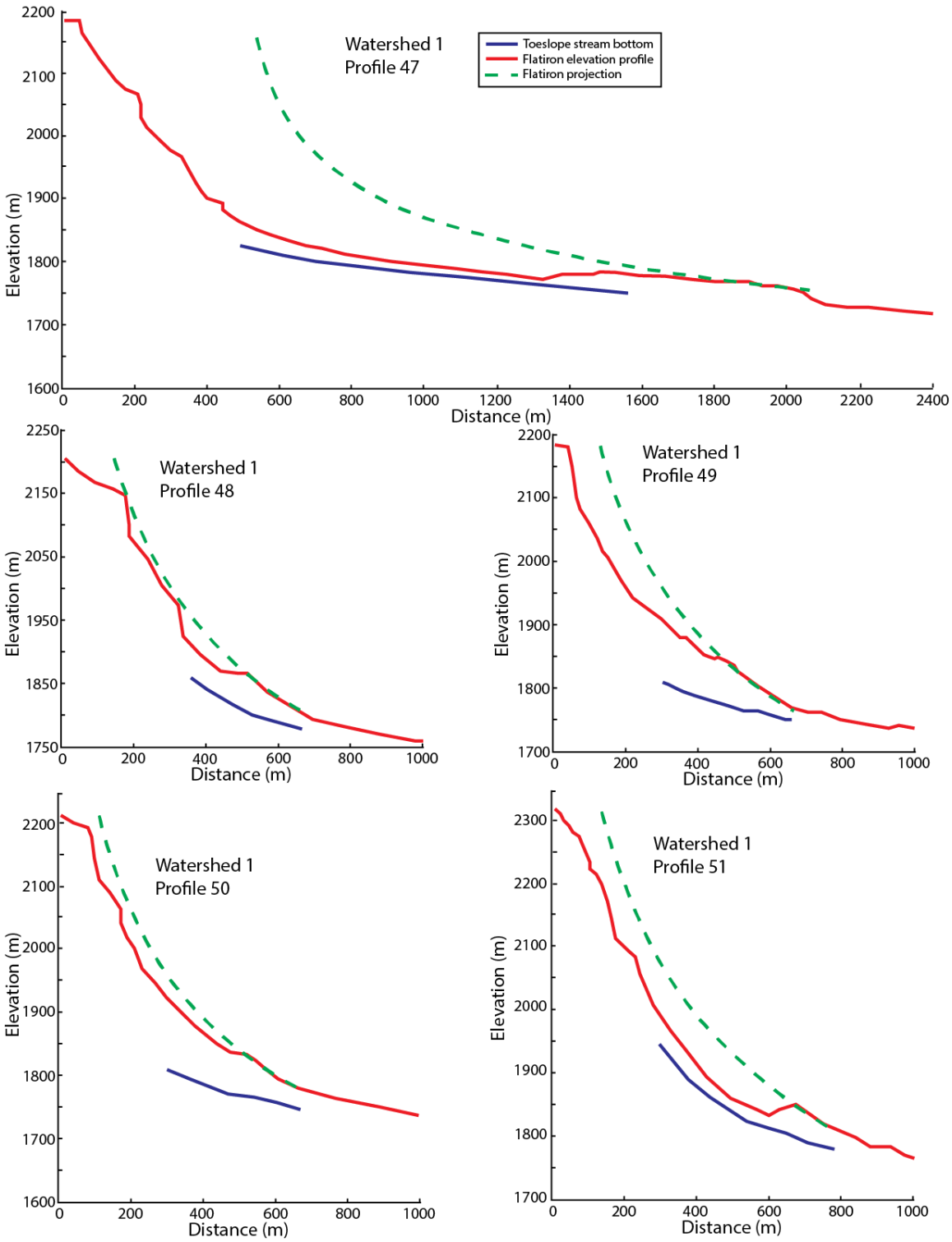
Watershed 1
Profile 47
Toeslope stream bottom
Flatiron elevation profile
Flatiron projection
Elevation (m)
Distance (m)
Watershed 1
Profile 48
Watershed 1
Profile 49
Watershed 1
Profile 50
Watershed 1
Profile 51

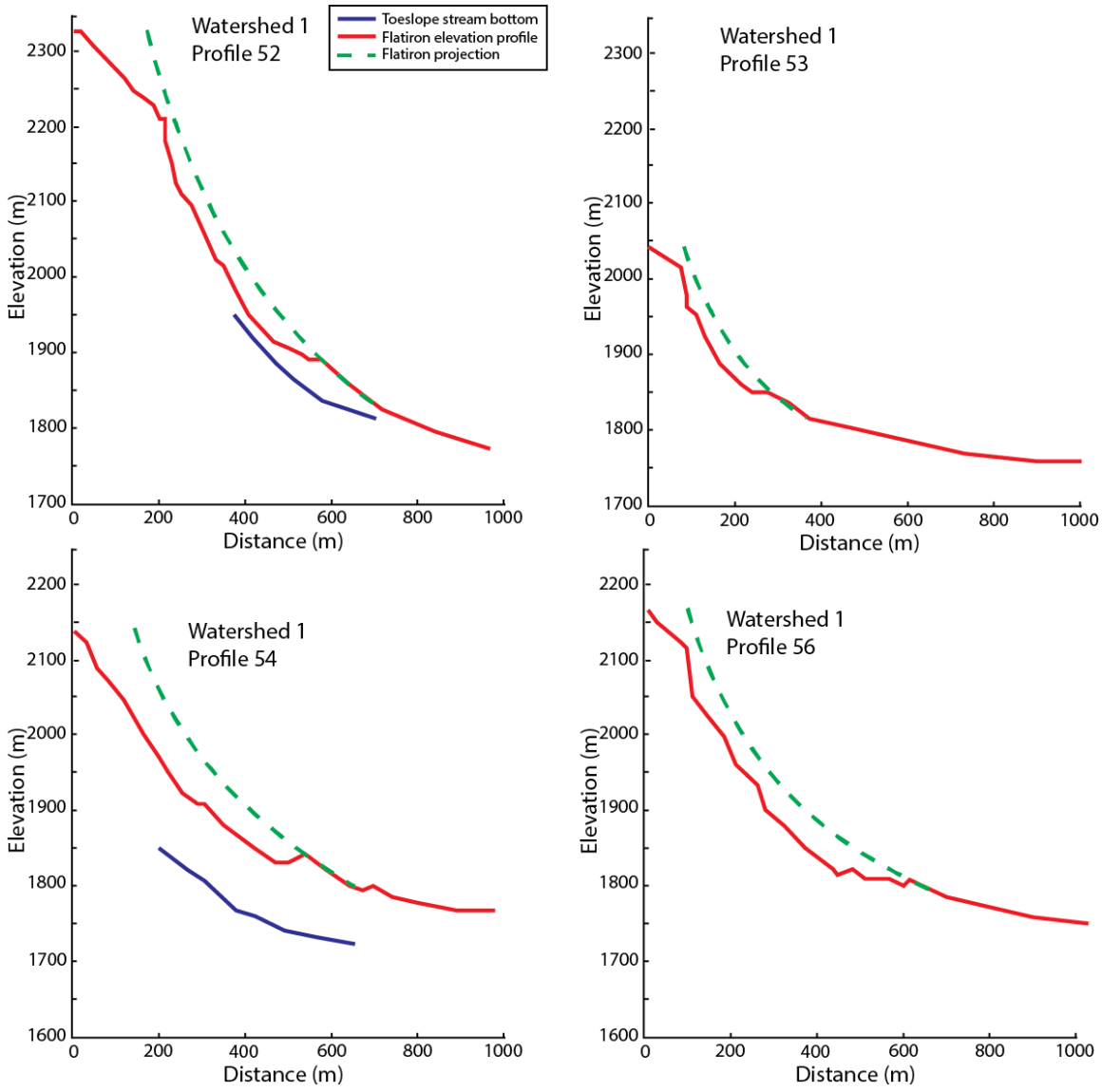
Watershed 1
Profile 52
Toeslope stream bottom
Flatiron elevation profile
Flatiron projection
Elevation (m)
Distance (m)
Watershed 1
Profile 53
Watershed 1
Profile 54
Watershed 1
Profile 56

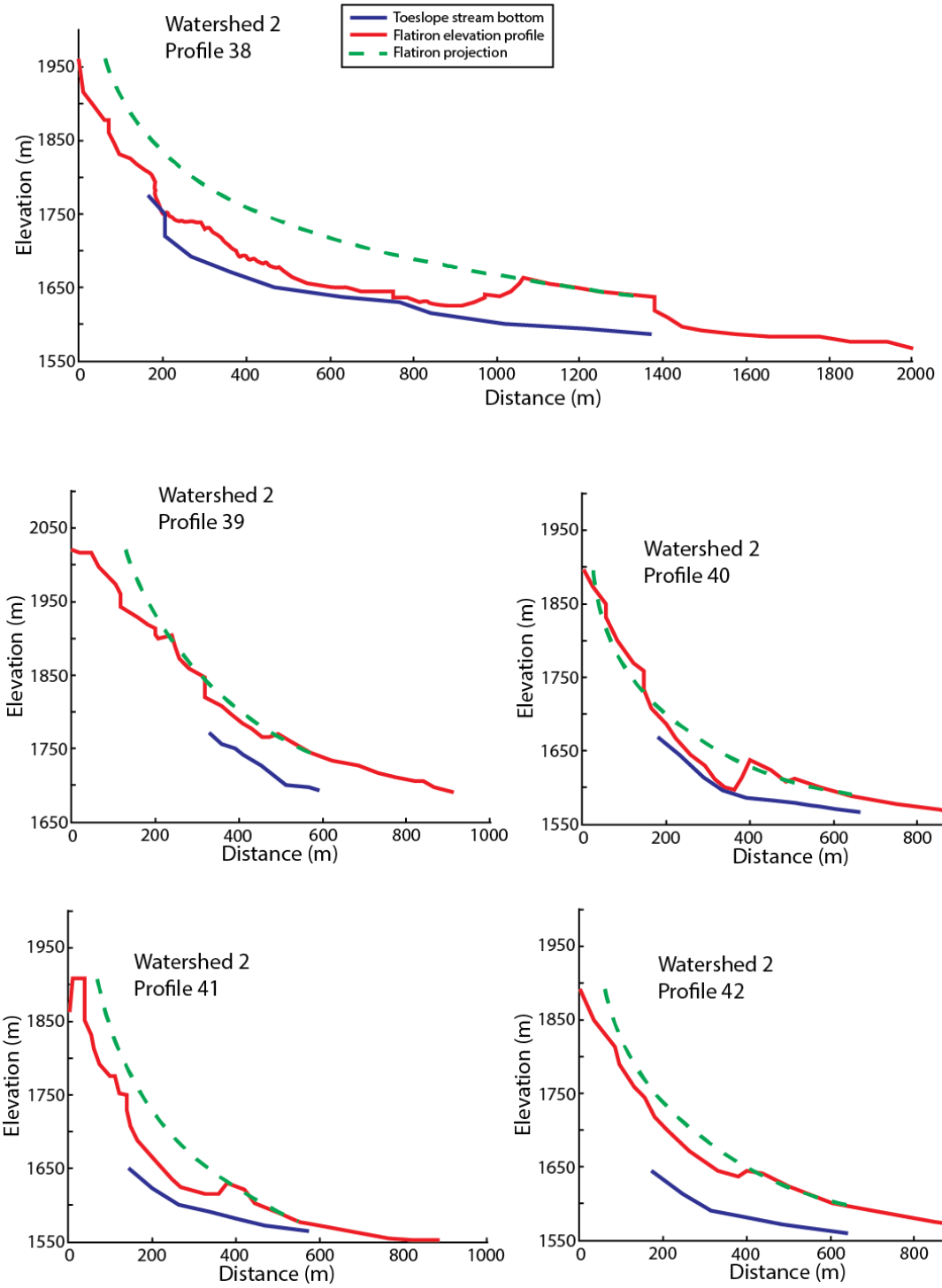
Watershed 2
Profile 38
Toeslope stream bottom
Flatiron elevation profile
Flatiron projection
Elevation (m)
Distance (m)
Watershed 2
Profile 39
Watershed 2
Profile 40
Watershed 2
Profile 41
Watershed 2
Profile 42

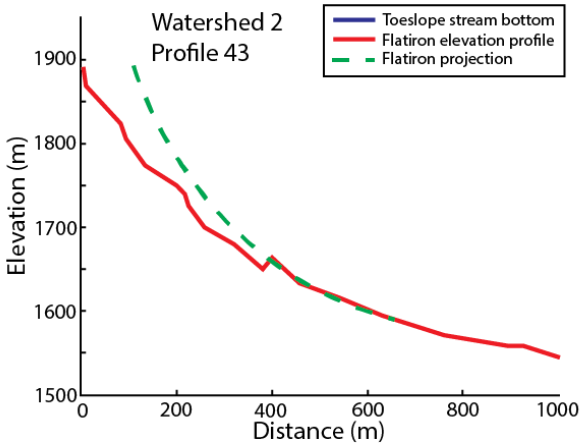
Watershed 2
Profile 43
Toeslope stream bottom
Flatiron elevation profile
Flatiron projection
Elevation (m)
1900
1800
1700
1600
1500
0
200
400
600
800
1000
Distance (m)

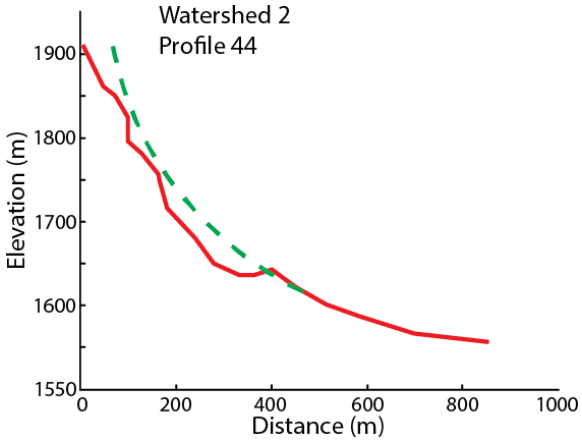
Watershed 2
Profile 44
Elevation (m)
1900
1800
1700
1600
1550
0
200
400
600
800
1000
Distance (m)

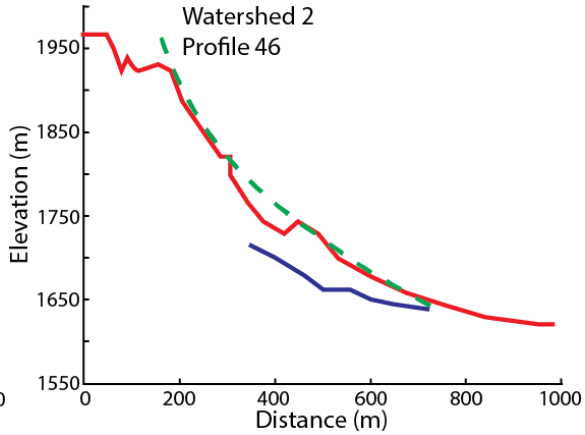
Watershed 2
Profile 46
Elevation (m)
1950
1850
1750
1650
1550
0
200
400
600
800
1000
Distance (m)

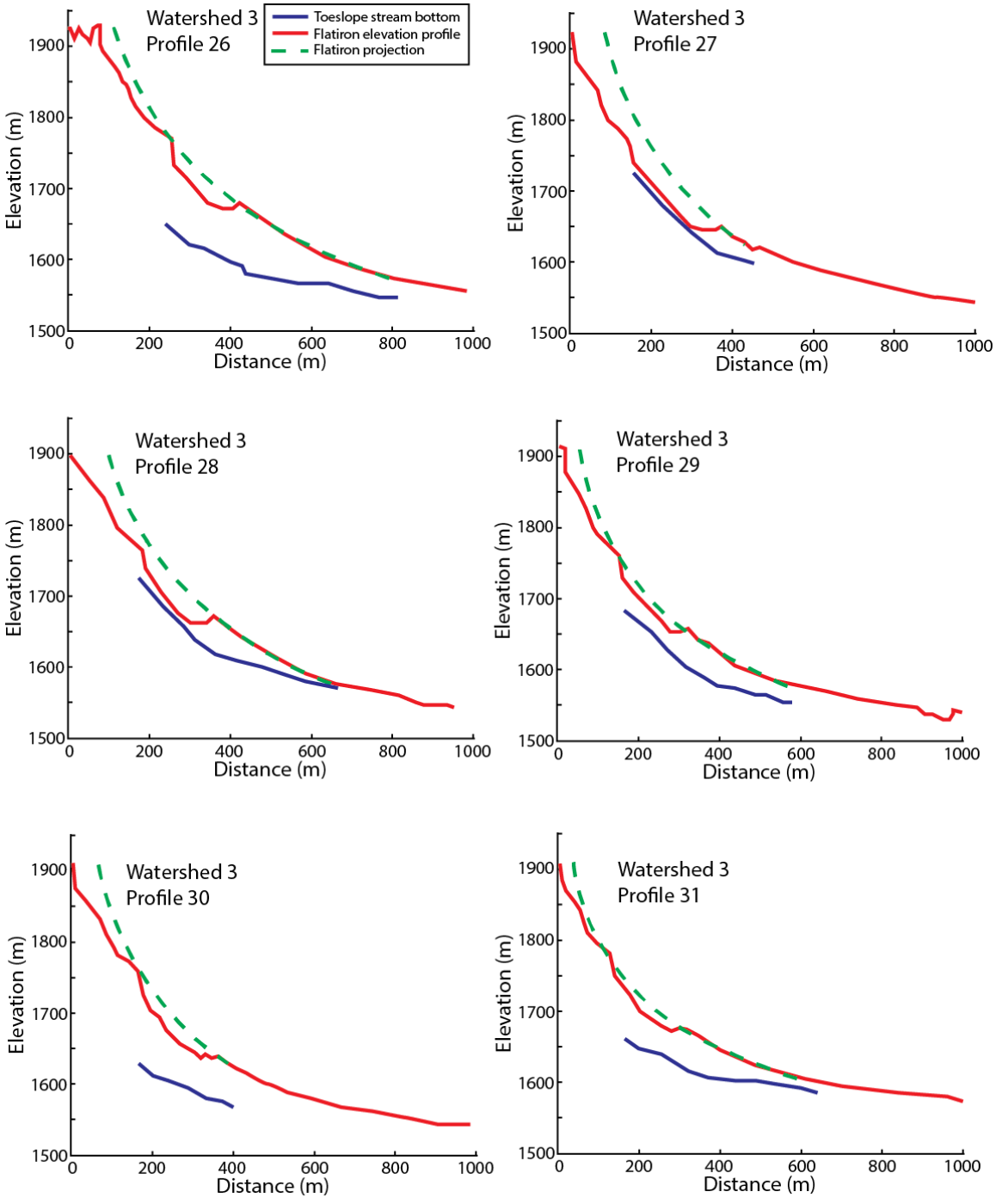
Watershed 3
Profile 26
Toeslope stream bottom
Flatiron elevation profile
Flatiron projection
Watershed 3
Profile 27
Watershed 3
Profile 28
Watershed 3
Profile 29
Watershed 3
Profile 30
Watershed 3
Profile 31
Elevation (m)
Distance (m)
1500
1600
1700
1800
1900
0
200
400
600
800
1000

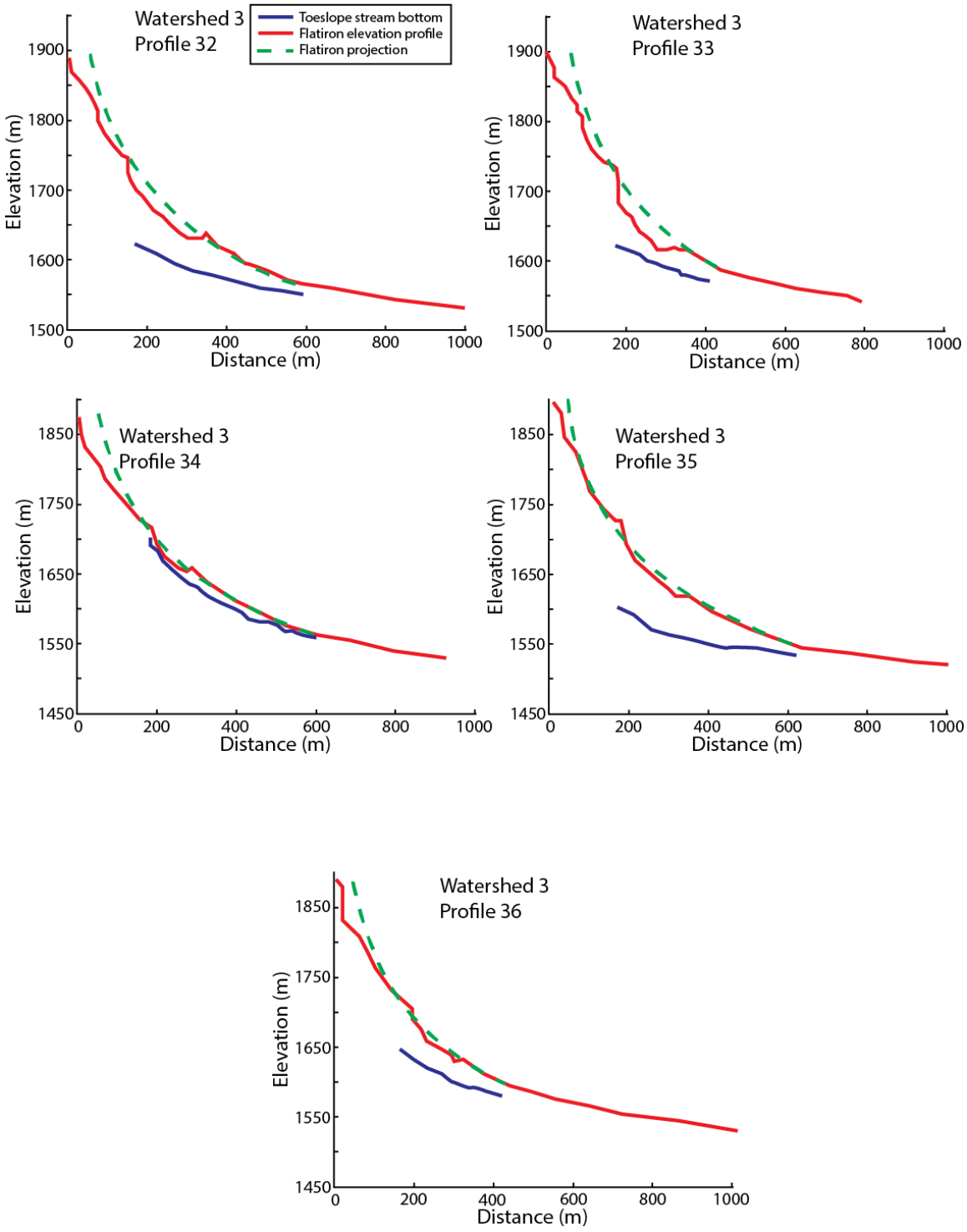
Watershed 3
Profile 32
Toeslope stream bottom
Flatiron elevation profile
Flatiron projection
Elevation (m)
Distance (m)
Watershed 3
Profile 33
Watershed 3
Profile 34
Watershed 3
Profile 35
Watershed 3
Profile 36

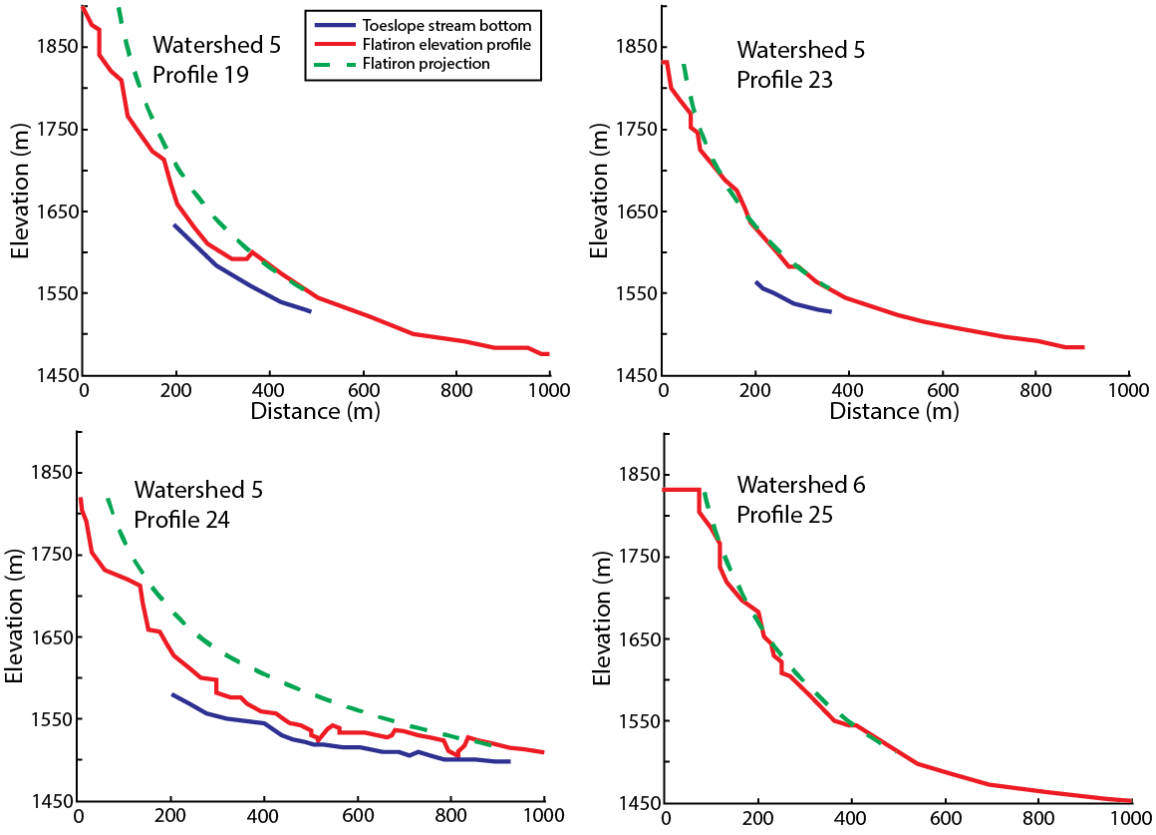
Toeslope stream bottom
Flatiron elevation profile
Flatiron projection
Watershed 5
Profile 19
Watershed 5
Profile 23
Watershed 5
Profile 24
Watershed 6
Profile 25
Elevation (m)
Distance (m)
1850
1750
1650
1550
1450
0
200
400
600
800
1000

TABLE B4. INDIVIDUAL RETREAT STATISTICS AND VALUES FROM PROFILES

Drainage	Line #	Stratigraphic Unit	Latitude	Longitude	Steepness (k_s)$	Concavity (θ)$	Retreat Distance: Bed-projection (m)	Retreat Distance: Min. Integration (m)	Retreat Distance: Max. Integration (m)	Retreat Distance: Ave. Integration (m)	Average vertical incision (m)	Min. Retreat Rates (m/ky)*	Max Retreat Rates (m/ky)*	Ave Retreat Rates (m/ky)*	Vertical incision Rate (m/ky)*
Wshd_1	1	C2	39.387399	-110.316624	2670.5	-0.0691	15.3	24.1	105.0	64.6	5.0	0.4	1.8	1.1	0.1
Wshd_1	2	C2	39.388362	-110.325752	3199.0	-0.1012	95.9	29.3	126.0	77.6	52.0	0.5	2.1	1.4	0.9
Wshd_1	3	C2	39.3912	-110.333692	3623.2	-0.1146	58.1	42.1	117.0	79.5	46.0	0.7	2.3	1.4	0.8
Wshd_1	4	C2	39.388824	-110.326981	2877.2	-0.0847	30.2	6.9	130.0	68.5	37.0	0.1	2.3	1.2	0.6
Wshd_1	8	C2	39.355384	-110.315417	2974.7	-0.0897	67.6	50.8	n/a	n/a	n/a	0.9	n/a	n/a	n/a
Wshd_1	9	C2	39.365799	-110.317249	3828.2	-0.1254	166.2	59.8	450.0	254.9	33.0	1.0	7.9	4.5	0.6
Wshd_1	12	C2	39.384689	-110.32745	2732.2	-0.0745	24.5	43.0	337.0	190.0	44.0	0.8	5.9	3.3	0.8
Wshd_1	13	C3	39.38315	-110.326995	2247.0	-0.0407	n/a	106.3	n/a	n/a	42.0	0.9	n/a	n/a	0.4
Wshd_1	14	C2	39.364332	-110.316488	3599.1	-0.1158	113.2	90.7	n/a	n/a	n/a	1.6	n/a	n/a	n/a
Wshd_1	16	C2	39.389216	-110.330058	3040.0	-0.0904	20.2	19.3	184.0	101.7	52.0	0.3	3.2	1.8	0.9
Wshd_1	17	C2	39.359497	-110.317539	2766.9	-0.0774	54.7	56.0	n/a	n/a	n/a	1.0	n/a	n/a	n/a
Wshd_1	18	C2	39.360143	-110.320431	2735.6	-0.0739	24.6	18.6	123.0	70.8	17.0	0.3	2.2	1.2	0.3
Wshd_1	47	C3	39.42756	-110.341705	2592.0	-0.0510	n/a	136.0	n/a	n/a	40.0	1.1	n/a	n/a	0.3
Wshd_1	48	C2	39.432062	-110.352714	4281.3	-0.1329	45.2	48.8	160.0	104.4	15.0	0.9	2.8	1.8	0.3
Wshd_1	49	C2	39.43551	-110.35548	4129.1	-0.1308	88.2	30.2	301.0	165.6	10.0	0.5	5.3	2.9	0.2
Wshd_1	50	C2	39.436065	-110.356612	3870.4	-0.1195	45.3	25.1	303.0	164.0	14.0	0.4	5.3	2.9	0.2
Wshd_1	51	C2	39.438617	-110.356743	4649.6	-0.1410	108.8	45.8	268.0	156.9	10.0	0.8	4.7	2.8	0.2
Wshd_1	52	C2	39.437583	110.357306	4805.4	-0.1465	41.0	41.3	142.0	91.6	15.0	0.7	2.5	1.6	0.3
Wshd_1	53	C2	39.443851	-110.361353	2636.7	-0.0628	25.6	10.4	n/a	n/a	n/a	0.2	n/a	n/a	n/a
Wshd_1	54	C2	39.421306	-110.345205	3623.2	-0.1146	13.5	35.0	169.0	102.0	38.0	0.6	3.0	1.8	0.7
Wshd_1	54	C3	39.421306	-110.345205	3283.1	-0.0950	130.3	98.6	260.0	179.3	36.0	0.8	2.2	1.5	0.3

Wshd_1	56	C3	39.415569	-110.339516	6565.6	-0.1970	86.1	68.5	406.0	237.3	40.0	0.6	3.4	2.0	0.3
Wshd_2	38	C3	39.340685	-110.322041	2498.0	-0.0585	111.8	142.8	394.0	268.4	44.0	1.2	3.3	2.3	0.4
Wshd_2	39	C2	39.337282	-110.317915	2633.1	-0.0779	21.1	20.6	294.0	157.3	28.0	0.4	5.2	2.8	0.5
Wshd_2	40	C2	39.317332	-110.313359	2641.2	-0.0800	56.6	41.5	220.0	130.8	20.0	0.7	3.9	2.3	0.4
Wshd_2	41	C2	39.314114	-110.312172	3617.5	-0.1198	65.2	39.2	242.0	140.6	21.0	0.7	4.2	2.5	0.4
Wshd_2	42	C2	39.319747	-110.31573	2942.3	-0.0885	40.6	17.4	356.0	186.7	32.0	0.3	6.2	3.3	0.6
Wshd_2	43	C2	39.311079	-110.313871	2283.1	-0.0559	43.9	22.0	n/a	n/a	n/a	0.4	n/a	n/a	n/a
Wshd_2	44	C2	39.311645	-110.315613	2801.1	-0.0912	38.5	32.0	n/a	n/a	n/a	0.6	n/a	n/a	n/a
Wshd_2	46	C2	39.345506	-110.314122	2557.1	-0.0728	40.9	25.4	113.0	69.2	18.0	0.4	2.0	1.2	0.3
Wshd_3	26	C2	39.308033	-110.31081	3176.8	-0.1056	37.1	27.4	292.0	159.7	36.0	0.5	5.1	2.8	0.6
Wshd_3	27	C2	39.304902	-110.310441	2463.2	-0.0684	57.1	31.5	85.0	58.2	18.0	0.6	1.5	1.0	0.3
Wshd_3	28	C2	39.303896	-110.309753	3004.2	-0.0996	51.6	16.5	154.0	85.2	12.0	0.3	2.7	1.5	0.2
Wshd_3	29	C2	39.298435	-110.309937	2629.6	-0.0802	27.1	23.5	118.0	70.8	22.0	0.4	2.1	1.2	0.4
Wshd_3	30	C2	39.296436	-110.309082	2520.0	-0.0732	18.4	14.4	263.0	138.7	10.0	0.3	4.6	2.4	0.2
Wshd_3	31	C2	39.295258	-110.305747	2530.1	-0.0749	21.2	23.9	272.0	147.9	22.0	0.4	4.8	2.6	0.4
Wshd_3	32	C2	39.291057	-110.306649	2657.1	-0.0833	30.3	23.0	267.0	145.0	18.0	0.4	4.7	2.5	0.3
Wshd_3	33	C2	39.290658	-110.306103	2463.2	-0.0720	32.8	28.6	144.0	86.3	13.0	0.5	2.5	1.5	0.2
Wshd_3	34	C2	39.286692	-110.305484	2588.2	-0.0789	51.6	18.7	51.0	34.8	9.0	0.3	0.9	0.6	0.2
Wshd_3	35	C2	39.28342	-110.307141	2555.1	-0.0776	20.7	17.5	384.0	200.8	14.0	0.3	6.7	3.5	0.2
Wshd_3	36	C2	39.281213	-110.305166	2447.4	-0.0697	21.6	9.2	114.0	61.6	12.0	0.2	2.0	1.1	0.2
Wshd_5	20	C2	39.273763	-110.301423	2398.0	-0.0671	31.0	20.3	140.0	80.2	14.0	0.4	2.5	1.4	0.2
Wshd_5	23	C2	39.271895	-110.30427	2779.1	-0.0937	28.3	3.6	85.0	44.3	11.0	0.1	1.5	0.8	0.2
Wshd_5	24	C2	39.276319	-110.307254	2200.1	-0.0588	82.6	31.9	466.0	248.9	19.0	0.6	8.2	4.4	0.3
Wshd_6	25	C2	39.26166	-110.30177	2962.8	-0.1081	17.0	21.4	224.0	122.7	27.0	0.4	3.9	2.2	0.5

$ Least squares best fit steepness (a) and concavity (b) values calculated by Matlab Code during power law paleo-surface profile fitting and projection from flatiron apexes using Eq. 3.3

*Using ages of 54ka (C2), and 117 ka (C3/4) based on chapter 2.

Appendix C. Piedmont drainage long-profile analysis

Figure C1. Map of drainages

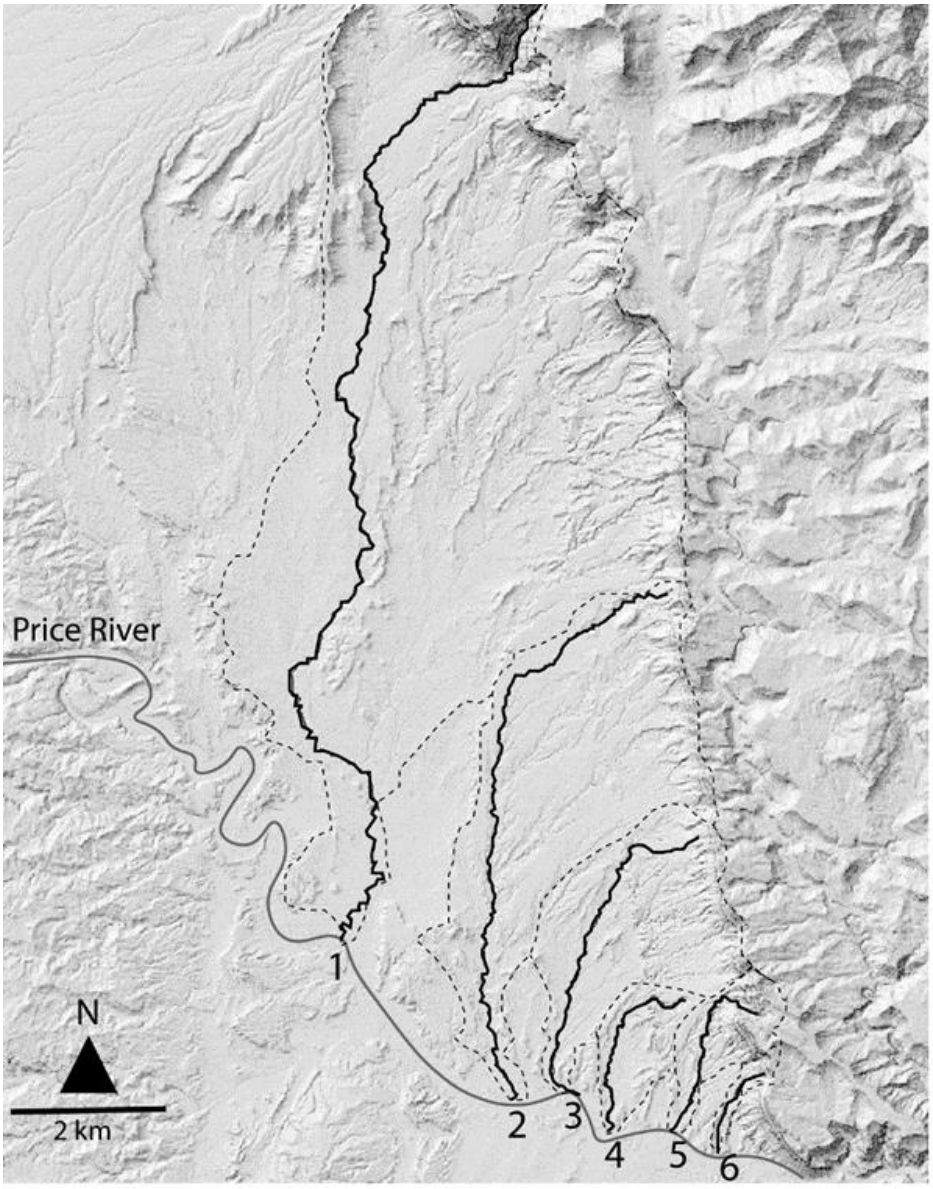

Figure C2. A) Long profiles; B) χ transformed profiles

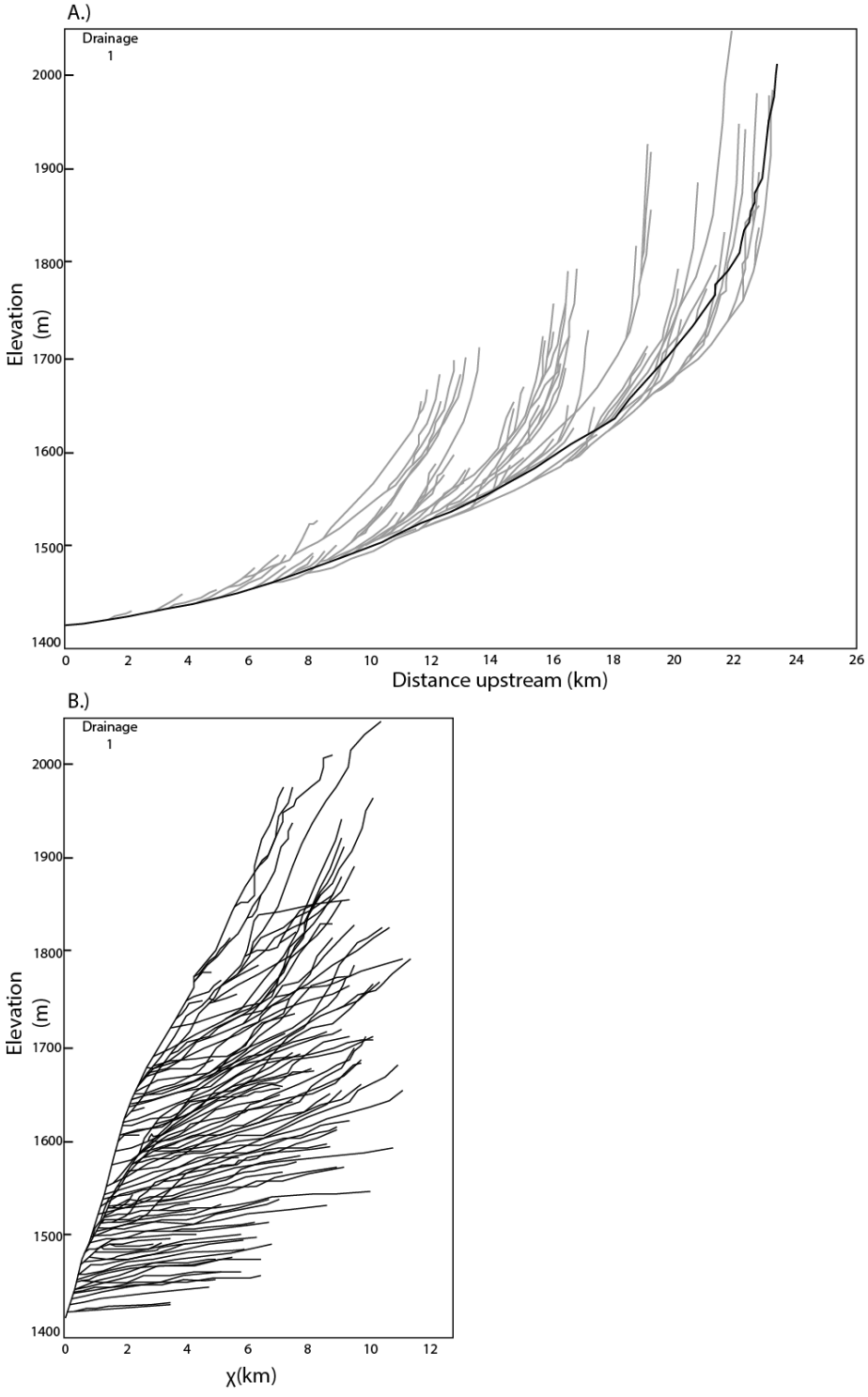

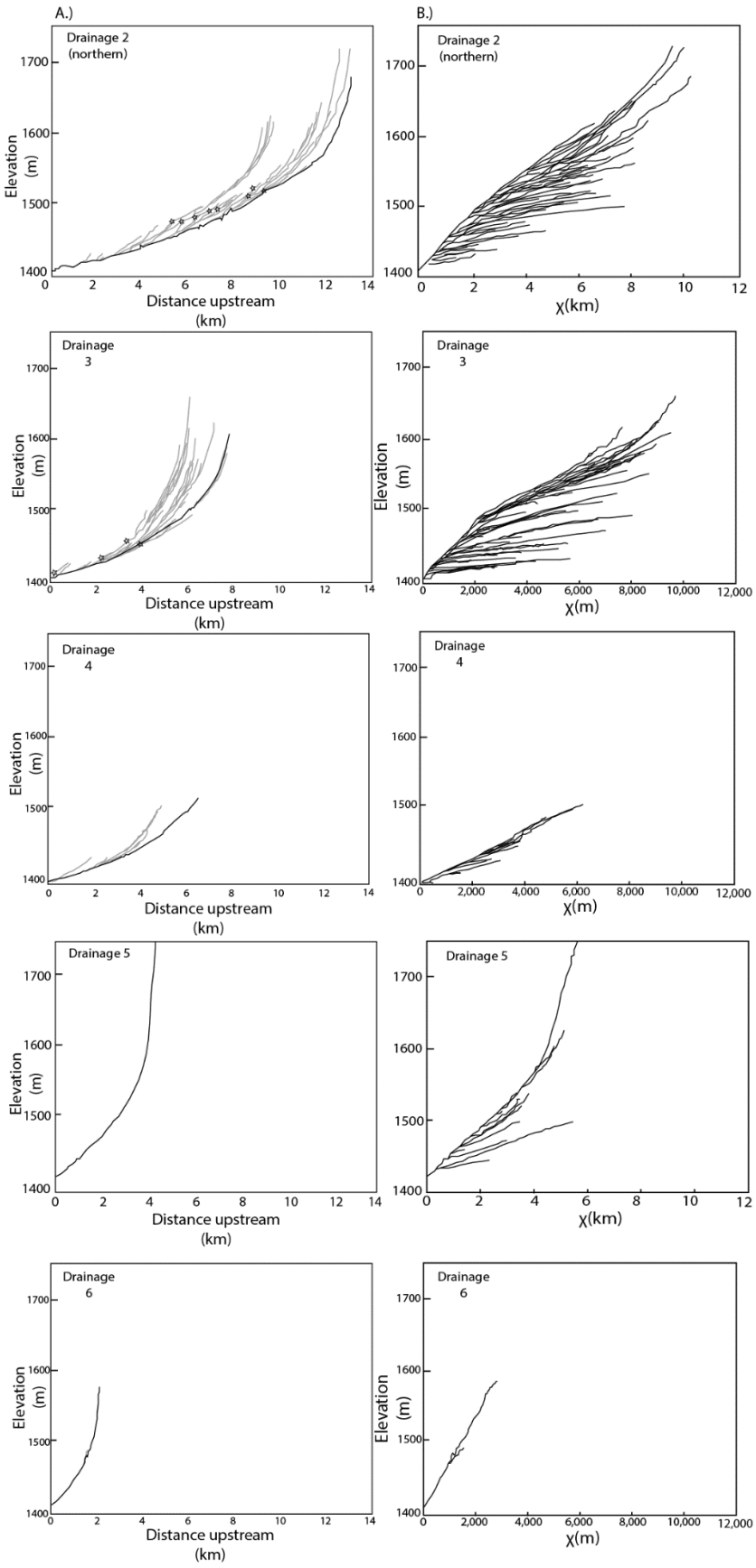
A.)
B.)
Drainage 2
(northern)
Drainage 2
(northern)
Drainage
3
Drainage
3
Drainage
4
Drainage
4
Drainage 5
Drainage 5
Drainage
6
Drainage
6
Elevation
(m)
Distance upstream
(km)
χ(km)
χ(m)

Figure C3. K_{sn} in map-view

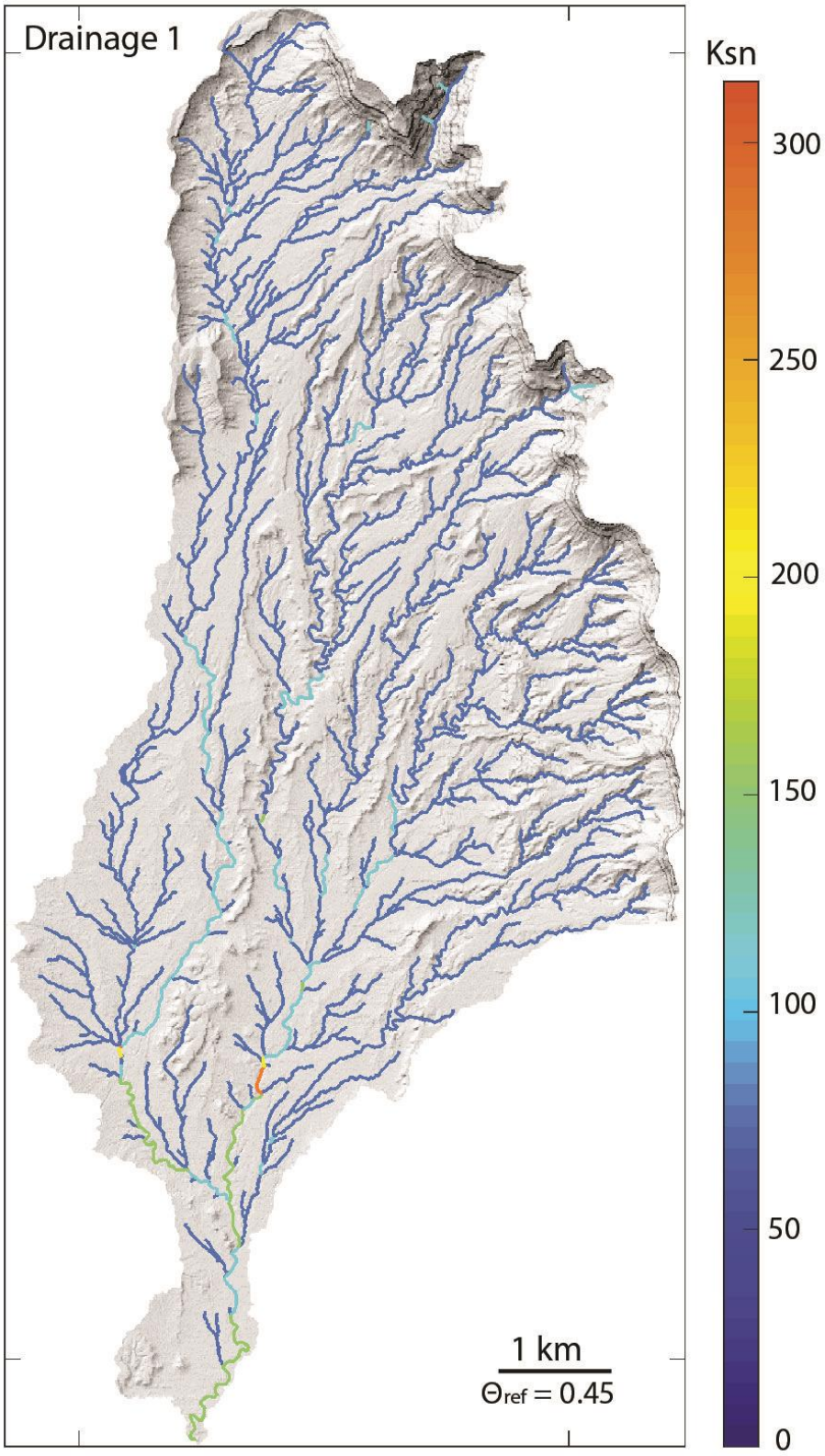

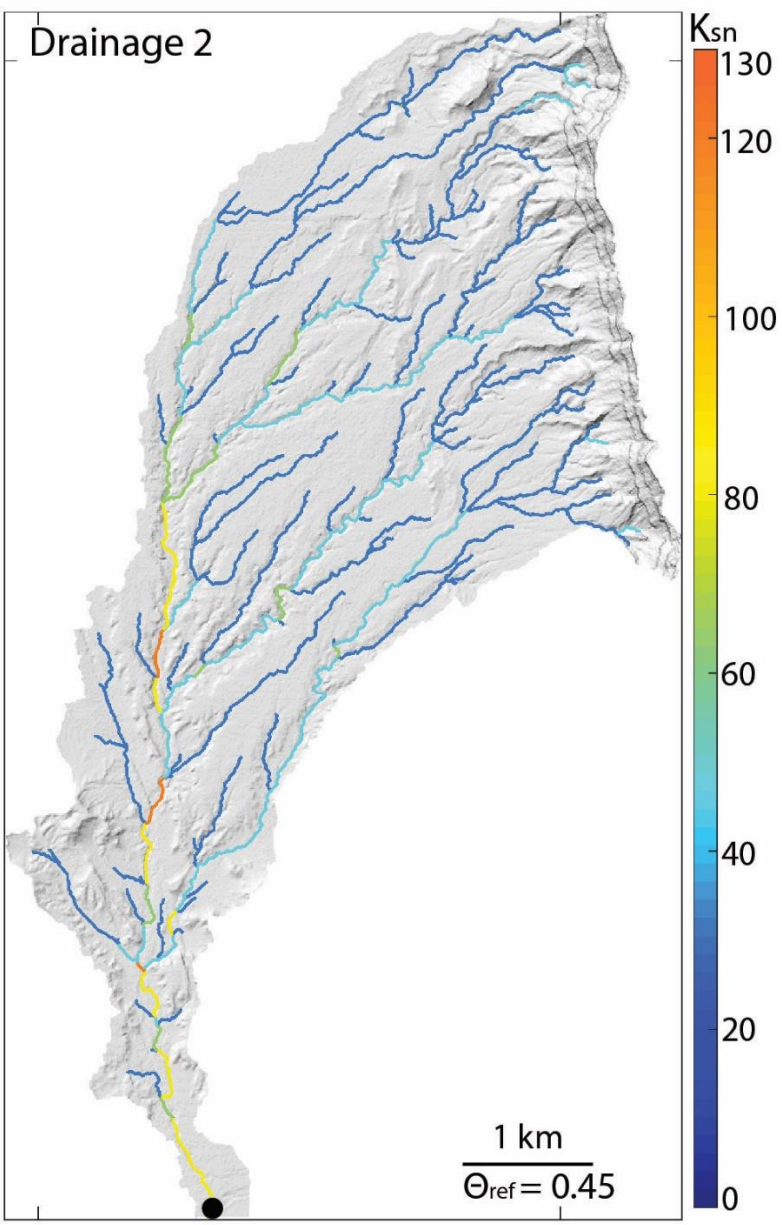
Drainage 2
Ksn
130
120
100
80
60
40
20
0
1 km
Θref = 0.45

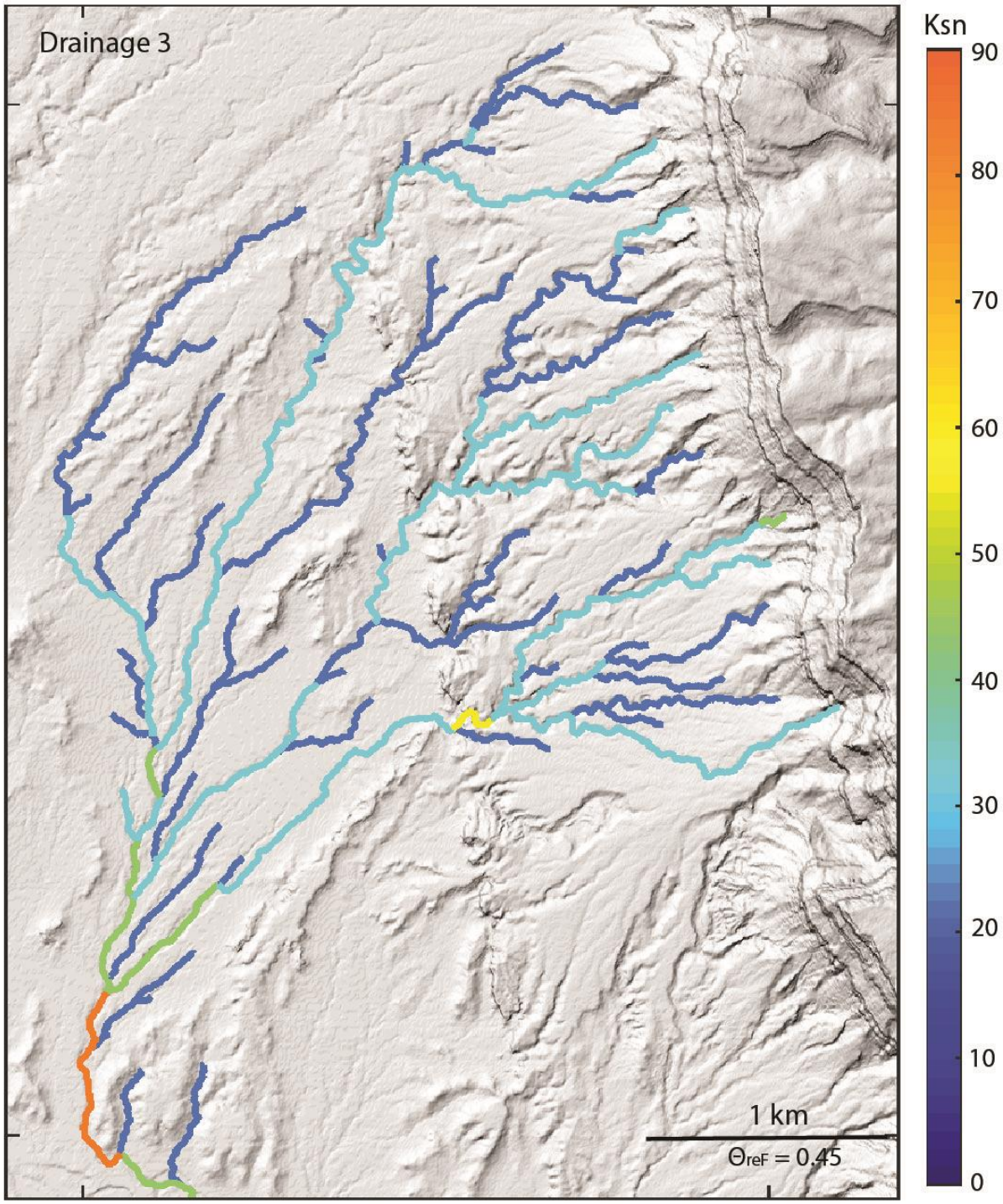
Drainage 3
Ksn
90
80
70
60
50
40
30
20
10
0
1 km
Θref = 0.45

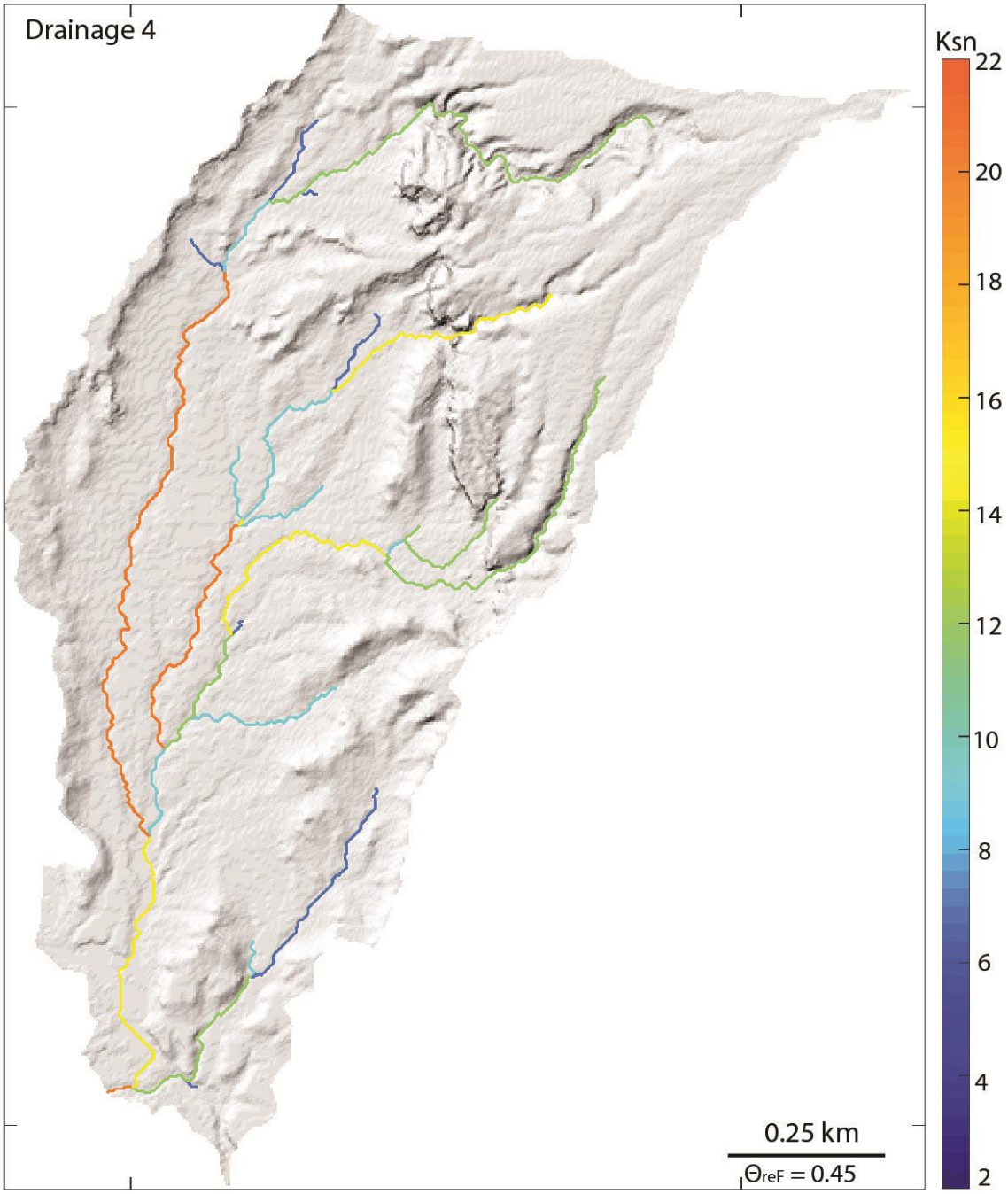
Drainage 4
Ksn
22
20
18
16
14
12
10
8
6
4
2
0.25 km
ΘreF = 0.45

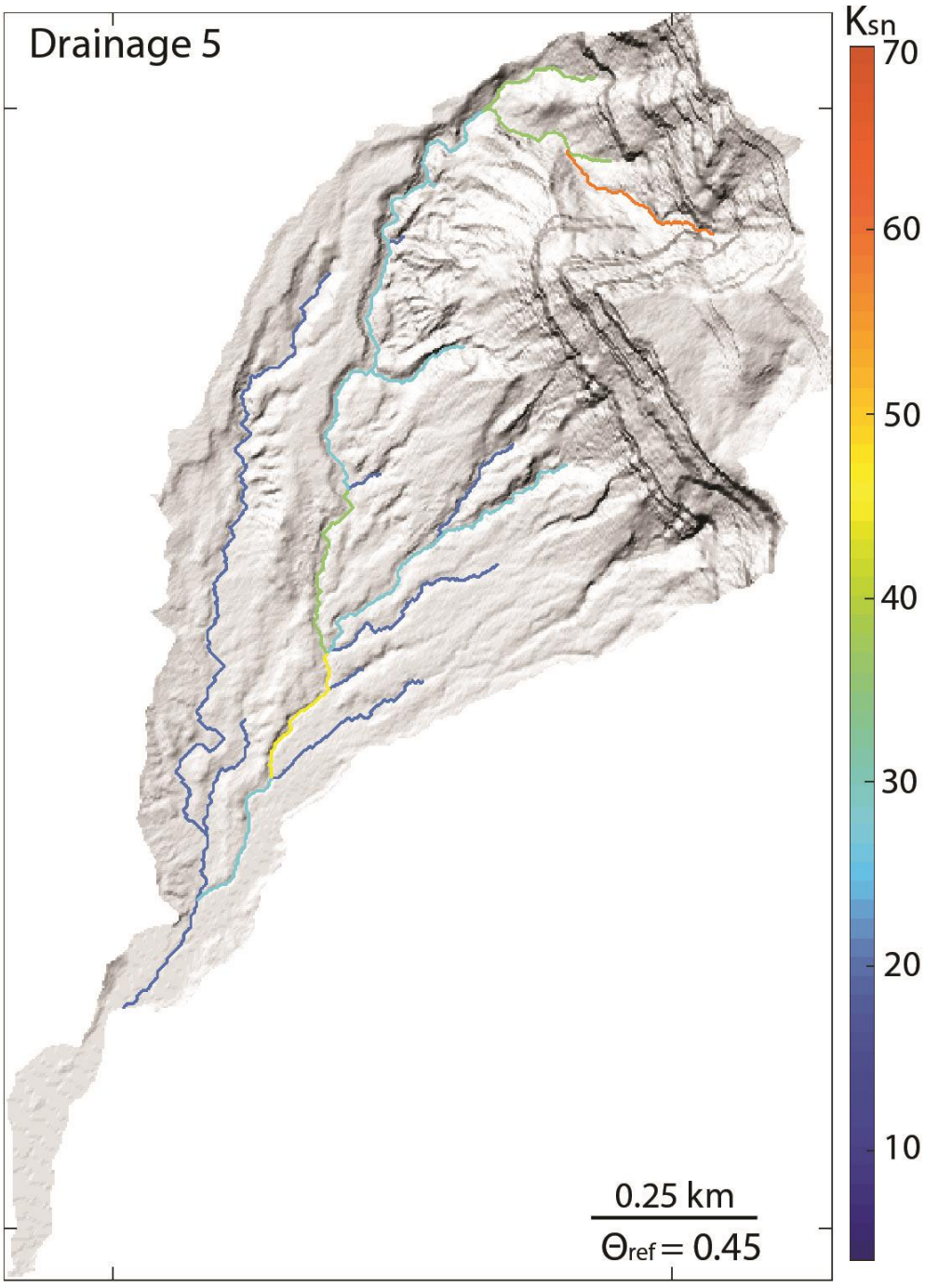
Drainage 5
Ksn
70
60
50
40
30
20
10
0.25 km
Θref = 0.45

Figure C4. Slope-area plots

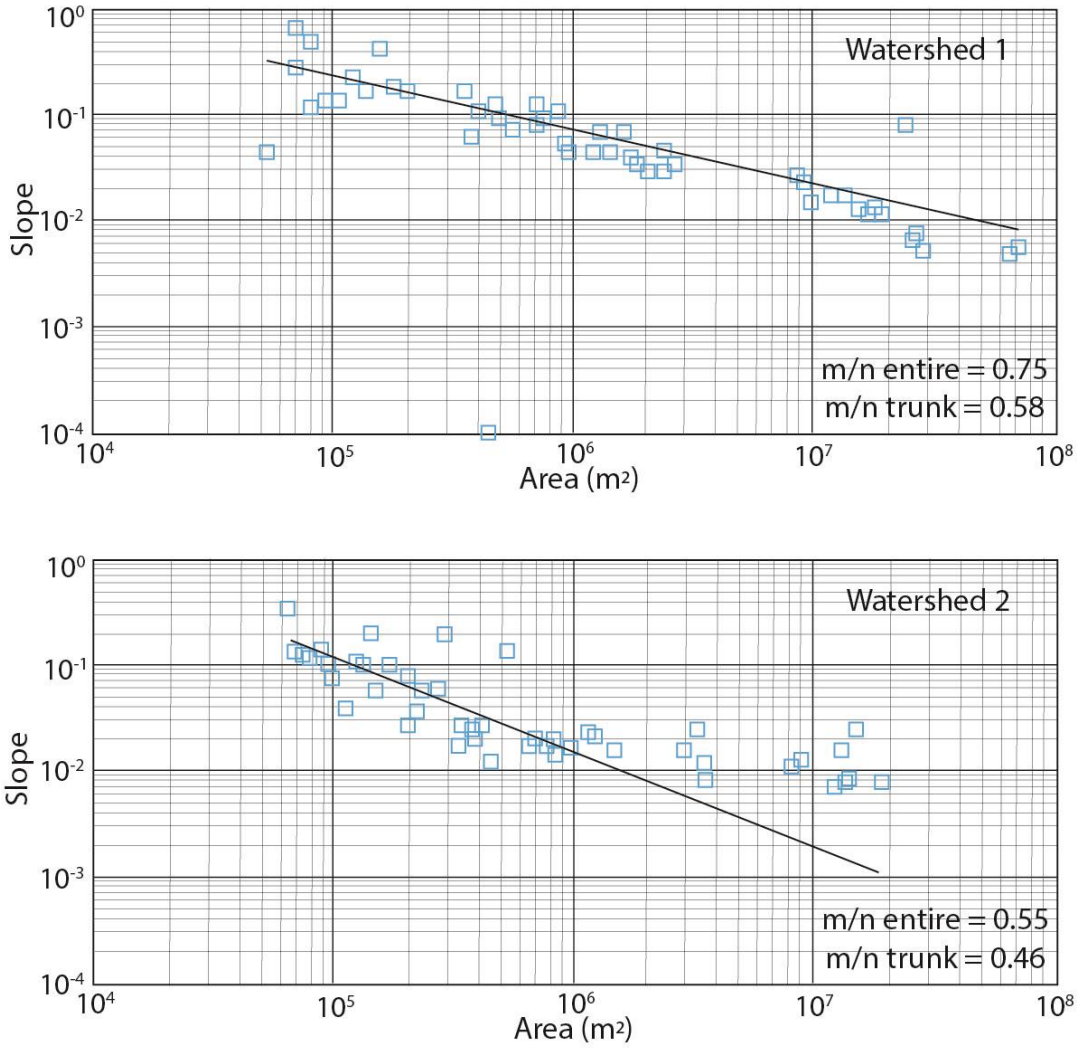

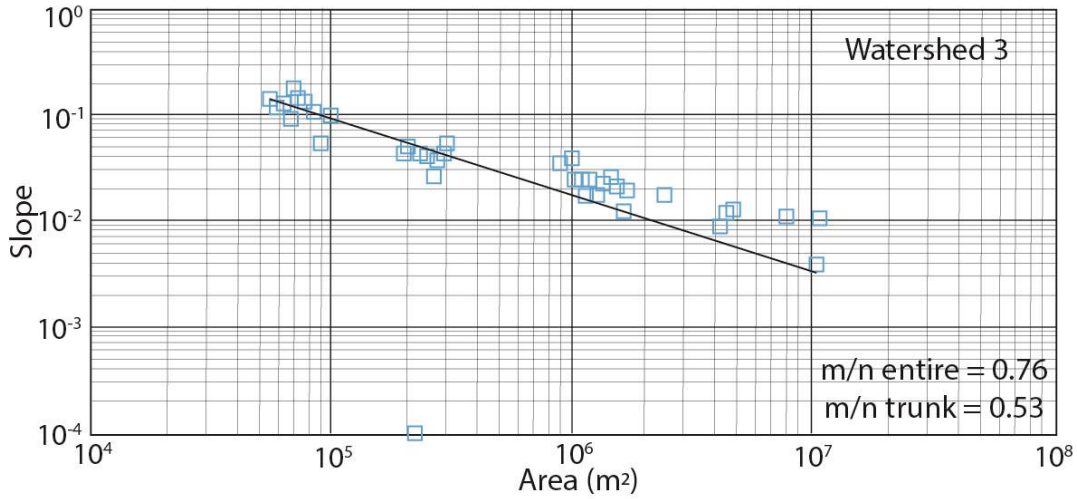
Watershed 3
m/n entire = 0.76
m/n trunk = 0.53
Slope
Area (m²)
10⁰
10⁻¹
10⁻²
10⁻³
10⁻⁴
10⁴
10⁵
10⁶
10⁷
10⁸

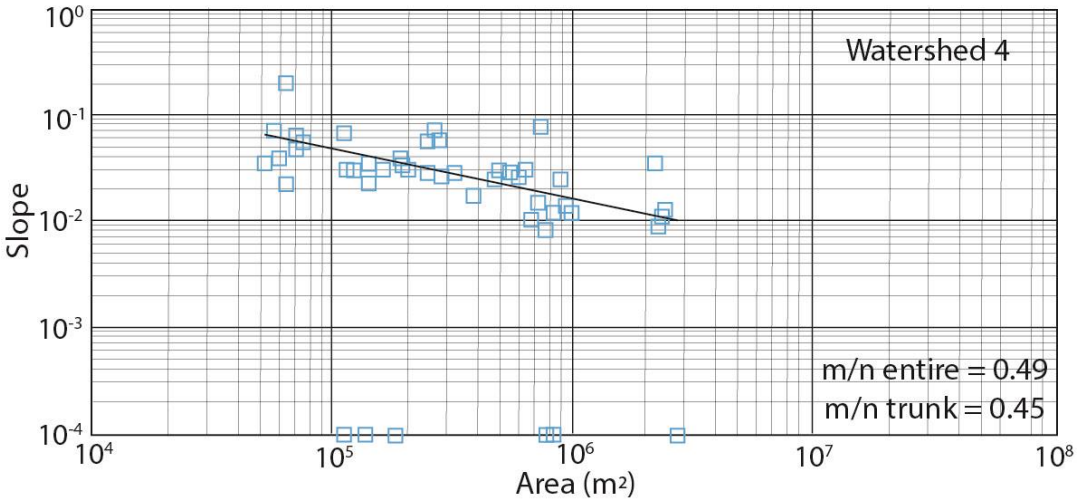
Watershed 4
m/n entire = 0.49
m/n trunk = 0.45
Slope
Area (m²)
10⁰
10⁻¹
10⁻²
10⁻³
10⁻⁴
10⁴
10⁵
10⁶
10⁷
10⁸

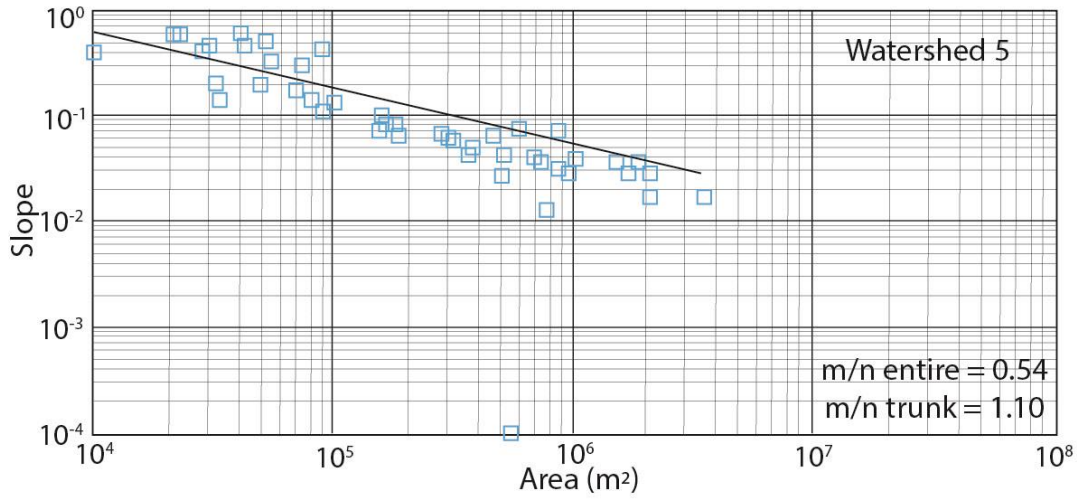
Watershed 5
m/n entire = 0.54
m/n trunk = 1.10
Slope
Area (m²)
10⁰
10⁻¹
10⁻²
10⁻³
10⁻⁴
10⁴
10⁵
10⁶
10⁷
10⁸

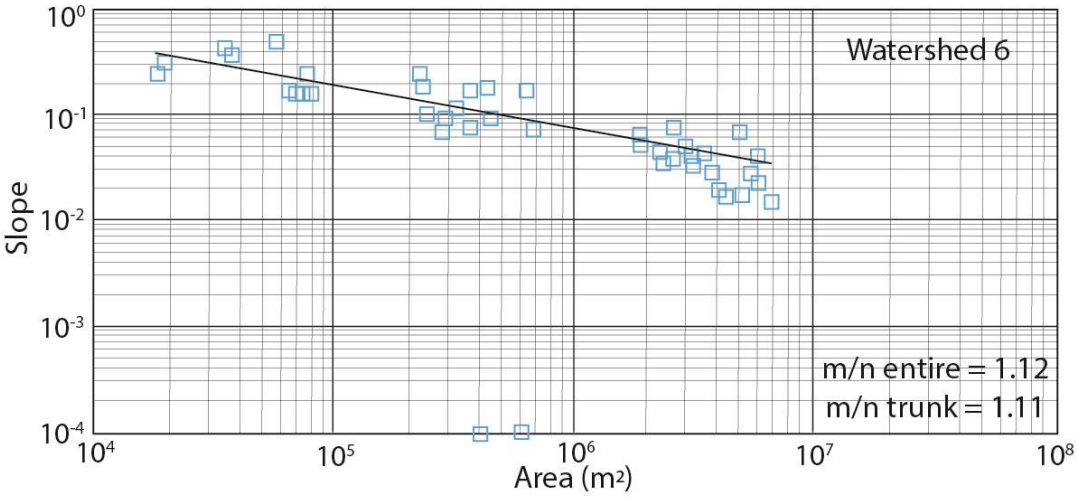
Watershed 6
m/n entire = 1.12
m/n trunk = 1.11
Slope
Area (m²)
10⁰
10⁻¹
10⁻²
10⁻³
10⁻⁴
10⁴
10⁵
10⁶
10⁷
10⁸

Appendix D. Pictures of the Book Cliffs

Figure D1. Southern view from northern end of study area

Figure D2. Northern view from center of study area

Figure D3. Close up of generation 2 proximal piedmont and southern section of book cliffs

Figure D1. Southern view from northern end of study area

Figure D2. Northern view from center of study area

Figure D3. Close up of generation 2 proximal piedmont and southern section of book cliffs